April 2009

Catapults, Corked Bats, and Tesla Coils: Finding the Truth

Amanda Marie Pesce
Worcester Polytechnic Institute

Jessica Ann LaGoy
Worcester Polytechnic Institute

Thomas E. MacDonald
Worcester Polytechnic Institute

Project Number: GSI 0802

Catapults, Corked Bats, and Tesla Coils: Finding the Truth

A Major Qualifying Project Report

submitted to the Faculty

of the

WORCESTER POLYTECHNIC INSTITUTE

in partial fulfillment of the requirements for the

Degree of Bachelors of Science

by

_____

Amanda Cox

_____

Jessica LaGoy

_____

Thomas MacDonald

Date: 4/28/09

Approved:

_____

Professor Germano S. Iannacchione, Major Advisor

1. Catapult
2. Corked Bats
3. Solid State Tesla Coil

Abstract

This project is a collection of smaller projects that are brought together under the unifying theme of using the scientific method to further understand observed phenomena. These phenomena include catapults with an emphasis on projectile motion and the range equation, understanding the physics of corking a bat and if it has any effect, and further understanding resonance by constructing a solid state Tesla coil.

Acknowledgements

There are many people who helped us greatly along the way to make this project not only be the best that it could be but highly special to all of us. For this, we would specifically like to thank our advisor, Professor Germano Iannachionne, who was there for us at each step along the way. On the construction side of our project, Mr. Roger Steele was an exceptional resource of information, technique, and overall wisdom, with which we have been lost without. Other contributing faculty who assisted us along the way that we would like to thank are: Mr. Jack Ferraro, Mrs. Jackie Malone, Mr. Fred Hudson, Professor Rafael Garcia, and Professor Frank Dick, Mr. Gregory Artim.

Finally we would like to thank our family and friends, who provided immeasurable support throughout the year.

Table of Contents

List of Figures

List of Equations

List of Tables

Overall Introduction

Any scientific inquiry has begun with an initial curiosity to find the truth of a certain phenomena. Whether it was Newton and his inkling of constant gravity or Einstein with his theory of general relativity, it began with that initial interest. This Major Qualifying Project was inspired by this curiosity. Each member of the group, however motivated, was stirred by a certain physical concept and wanted to research it further. The project is entitled "Catapults, Corked Bats, and Tesla Coils: Finding the Truth" as this encompasses all concepts that each member wanted to research further and find the truth much like popular television program *Mythbusters*. In this show, they begin with a question and use the scientific method to either prove or disprove their question. In the following sections, we will use a similar method and "find the truth" to our own questions about catapults, corked bats, and tesla coils.

Introduction – Catapult Projectile Motion

Equipment Background

Catapults are a piece of medieval engineering that demonstrate and work by using basic principles of physics. A catapult is a large category of "military machines for hurling missiles, such as large stones or spears, used in ancient and medieval times." (Catapult Definition)

Two machines that fall under this category and that are particularly common are the torsion catapult and the trebuchet. The Torsion catapult uses a torsion spring or uses torsional pressure, generally from twisted rope, to store energy for the shot. That energy is then used to hurl the projectile at its target. "The Greek engineers who introduced science into the design of torsion catapults based the catapult's proportions on the diameter of the torsion spring; they gave a formula for the size of the torsion spring required,

$D = 130m^{1/3}$." (Cotterel and Kamminga)

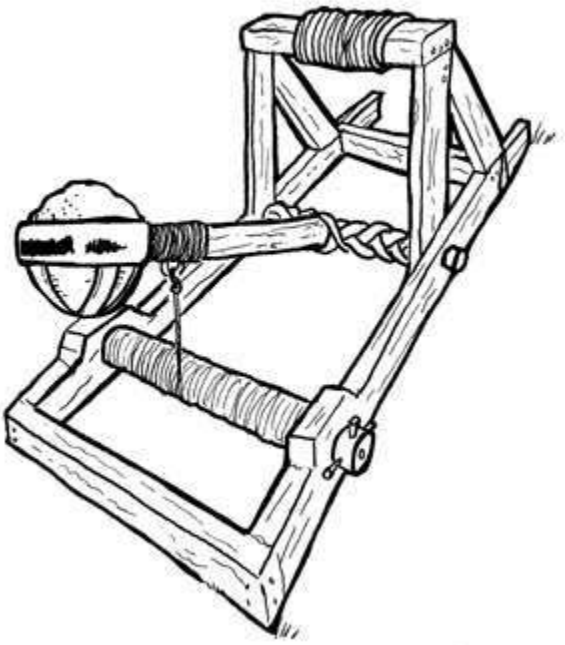

Figure 1: Example of medieval torsion catapult (Catapult Picture)

The trebuchet is a catapult that uses the force of gravity to launch a projectile. The trebuchet has a counterweight that is tied in a fixed position. Then when the projectile is ready for launch, the tie is severed and the counterweight is forced to fall to the ground by gravity. This causes the projectile to be launched. It is a redirection of force, just as the torsion catapult is.

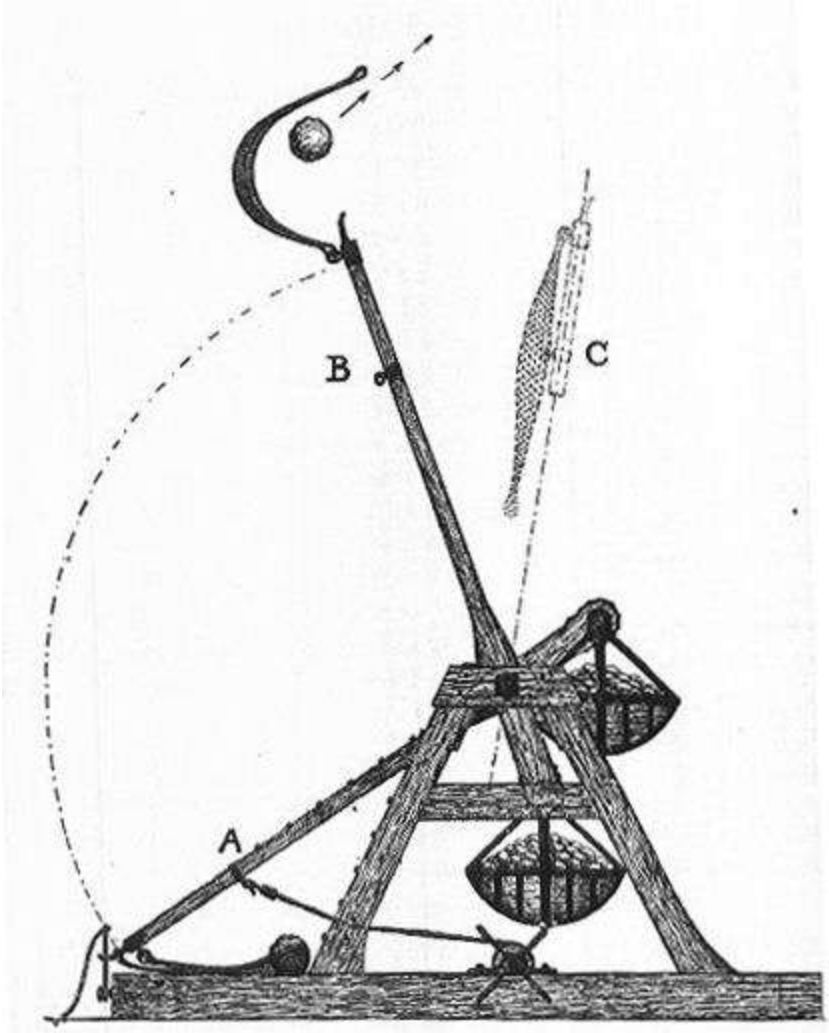

Figure 2: Example of medieval trebuchet (Trebuchet Picture)

One major difference between the two engines is the fact that the trebuchet is a much more powerful machine. It is much more accurate with its launches and travels a much further difference. This is based on the fact the trebuchet uses a sling to hold the projectile. This sling provides a longer arc without having a taller apparatus, as it tucked underneath.

Educational Background

It is a proven fact that students of all ages learn and understand educational material in different ways. (Cox, McGill and Spremulli) There are many different categories of learning that

students can be divided into but the three most common are auditory learners, visual learners, and tactile/kinesthetic learners. So when in the education field, it is best to have variety in one's teaching style in order to ensure that everyone in the classroom gets the most out of that particular subject. For example, in a lecture setting, students that are tactile learners may not fully understand the subject matter until it is put to use.

In high schools differentiated teaching is something that is used but it may not be fully used to its potential. One case of this being the representation of the catapult or trebuchet lab that is used to show students the mechanics of trebuchets or catapults. Students all over the country build catapults and trebuchets every year for one of their requirements, but the question is are they extracting all possible knowledge from this lab. I think not.

I believe that using the build of the catapult or trebuchets to not only show the mechanics behind the apparatuses, but to show key concepts such as projectile motion, and air resistance would be more beneficial to students. Doing this would integrate more key concepts of the high school curriculum and would use all types of learning styles in the classroom, hence being more beneficial. Before the effectiveness of a lab such as this can be tested, the actual lab needs to be designed and tested. This is the task at hand; first studying the projectile motion and air resistance coming from both a catapult and trebuchet, and then decided whether such a lab can be implemented in a high school setting based on error analysis and equipment.

Project Introduction

In this project, we will combine our knowledge of the mechanics of the torsion catapult and the trebuchet along with the mechanics of projectile motion to study the projectile motion and air resistance coming from both a catapult and trebuchet, and then decided whether such a

lab can be implemented in a high school setting based on the error analysis and analysis from equipment. This is a necessary project in order to make sure that such a lab can easily be done in a high school setting while straightforwardly showing basic principles of the catapult and trebuchet combination and the projectile motion of both. We will do this by choosing equipment that can easily be handled and found in a high school setting, and then use this equipment to analyze not only the catapult and trebuchet themselves to understand their functioning principles, but then investigate the projectile motion coming from both. If we can easily see then quantities we should be seeing (a simple projectile arc, acceleration due to gravity, air resistance, etc) only aided by uncomplicated graphs, then this lab can be implemented in a high school setting.

This total MQP was trying to encompass the spirit of physics: finding the truth. My motivation for choosing this project was to better prepare me for lab design in my future career as a high school teacher. In high schools, students are not trying to derive new principles or make huge discoveries; they are trying to learn the fundamentals of physics so that they can expand upon them in their (hopefully) future careers as scientists. This is "finding the truth" at its most basic form, where they are finding fundamental truths, in order to build up a trust with the subject of physics in their everyday lives. This is where my career will focus; helping others find their own truths in scientific settings.

Theoretical Projectile Motion

"Any object that is given an initial velocity and which subsequently follows a a path determined by the gravitational force acting on it and by the frictional resistance of the atmosphere is called a projectile." (Sears) The purpose of both the catapult and trebuchet is to launch a projectile a certain distance away. In physics we study the motion of the projectile with

equations that can yield the range, height, and velocity of the projectile. These are important quantities for reaching a certain distance, as was the objective of the catapult and trebuchet.

In a vacuum, meaning space containing no air or other obstacles, the motion of projectiles can be described with a few basic equations. The distance equation,

$$Y = V_{Oy}t + (1/2)\, at^2,$$

can be used to determine the height or range of the projectile at any given position. The height is in the y direction and range in the x direction generally in coordinate systems. In this equation, Y is either the height or range, V_O is the initial velocity in the x or y direction, t is the time, and a is the acceleration in the x or y direction. Keeping x and y quantities is very important, because in a vacuum the two directions do not affect one another.

Theoretically, the acceleration on the projectile is zero, meaning the velocity is the constant throughout its trajectory. The distance equation in the x direction becomes,

$$X = V_{Ox}t,$$

and this can be used to find the position in the x direction throughout the flight. The only obstacle in projectile's way in the y direction is acceleration due to gravity. Gravity is a constant 9.8 m/s^2, and the force due to gravity is what gives the projectile its parabolic path that will be seen later.

Taking the derivative with respect to time of the distance equation will yield a equation for velocity. The derivative of position with respect to time yields velocity, just as taking one more derivative will yield acceleration. For example, the distance equation in the y direction is

$$Y = V_{Oy}t + (1/2)\, at^2.$$

Taking the derivative of this with respect to t gives,

$$V_y = V_O + at.$$

This equation will give the velocity in the y direction at any point during the trajectory. Taking yet another derivative produces

$$A_y = a,$$

which is known as a constant of 9.8 m/s^2. (Young and Freeman)

This simple form of life is what if taught to high school classes across American, but another constant is that life is not so simple. In real systems, there are forces that affect the motion of a projectile, the main force being air resistance. "The most obvious fact about air resistance…is that it depends on the speed, v, of the object concerned. In addition…the direction of the force due to the motion through the air is opposite to the velocity, v." (Taylor 43) This means that air resistance is a dissipative force, causing the range and height of the projectile to be less than what it would have been in a vacuum. The figure below is representation of air resistance as a dissipative force. As shown, the projectile travels longer and higher without air resistance than with air resistance.

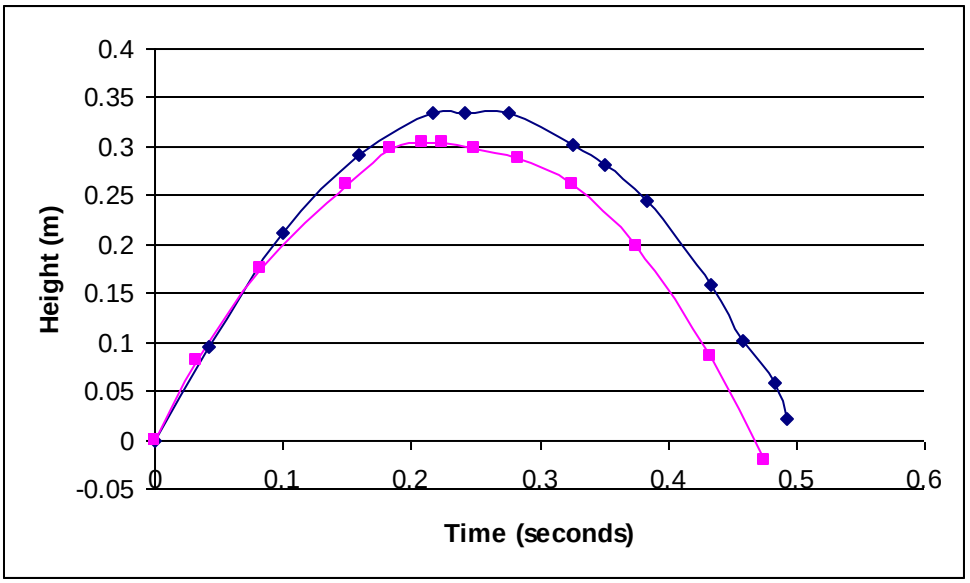

Figure 3: Projectile motion of marble and marble with added air resistance. The pink line is the graph with the added resistance as compared to the blue line, the regular ball.

Quantitatively, air resistance as a function of velocity can be described as

$$F(v) = F_{lin} + F_{quad}.$$

F_{lin} is the linear term of drag and it "arises from the viscous drag of the medium," (Taylor 44) or

$$F_{lin} = \beta D v.$$

Here, β is a constant of the air being $1.6*10^6$ N*s/m^2, D is the diameter of the projectile, and v is velocity. F_{quad} is the quadratic drag term arising "from the projectile having to accelerate the mass of air with which it is continually colliding." (Taylor 44) This term is

$$F_{quad} = \gamma D^2 v^2,$$

Where γ is another constant of air being 0.25 N*s^2/m^4, D is diameter of the projectile, and v is velocity. (Taylor 45)

Simply by the terms of linear and quadratic drag, one can see the high dependence on velocity. Logically, as velocity increases so does the force of air resistance. Also large objects traveling at the same velocity of a small object will have a high air resistance force.

Often though, one of the two air resistance forces, linear and quadratic, can be neglected depending on the size. For example, for very small objects, (i.e. liquid drop) the dominant force is linear and quadratic air resistance can be ignored. However, for larger objects (i.e balls, cars, planes) quadratic air resistance is the dominant force and linear air drag can be ignored. For the purpose of studying the projectile motion from catapults and trebuchets, we will look at the quadratic air resistance associated with the various balls, as quadratic air resistance is the dominant force.

Compared to the equation of motion for a projectile in a vacuum, the equation of motion for projectiles in real systems are quite complicated.

$$Ma_x = - \gamma D^2 * \text{sqrt}(v_x^2 + v_y^2 v_x)$$

$$Ma_y = -Mg - \gamma D^2 * \text{sqrt}(v_x^2 + v_y^2 v_y) \text{ (Taylor 62)}$$

Here, where M is the mass of the object, v_x is the velocity in the x direction, and v_y is the velocity in the y direction, the accelerations in the x and y directions depend on quantities in both directions. Before, in a vacuum, the individual accelerations depended only on quantities in their own directions. These two equations are even more difficult because "neither equation is the same as for an object that moves only in the x direction or only in the y direction…it turns out that the two equations cannot be solved analytically at all…This means that we cannot find the general solution." (Taylor 62) These equations can only be solved for specific initial conditions.

We will use these equations to compare the experimentally derived accelerations in the x and y direction of various projectiles, with the theoretical accelerations from these two equations.

With this form of comparison there will be considerable propagation of error. We are experimentally deriving the accelerations through analysis of position. It is known that velocity is the derivative of position and time, and acceleration is the derivative of velocity and time. So by knowing the change in position and the change in time, we are able to find acceleration by taking a double derivative. However, this process exemplifies the original error in position, which will be shown in later calculation.

Experimental Procedures – Catapult Projectile Motion

Materials and Equipment

In order to study projectile motion from catapults and trebuchets, several experiments need to be conducted. But before any experiment is conducted two main apparatuses need to be build, a catapult and trebuchet. Building a small scale catapult and trebuchet that can throw the projectile ten to twenty feet is best in order to take precise measurements of its projectile arc. To do this, we built a small table top trebuchet and catapult found as a kit though thinkgeek.com. We decided to follow the miniature designs of thinkgeek.com because young students across America have access to these kits and would probably use them if asked to build a small catapult or trebuchet in their class rooms. Also they are simple designs of a catapult and trebuchet that are easily understood and would be guaranteed to work under experimentation. This is pivotal because it is not the design of the catapult and trebuchet that is of interest but the projectile motion from the equipment.

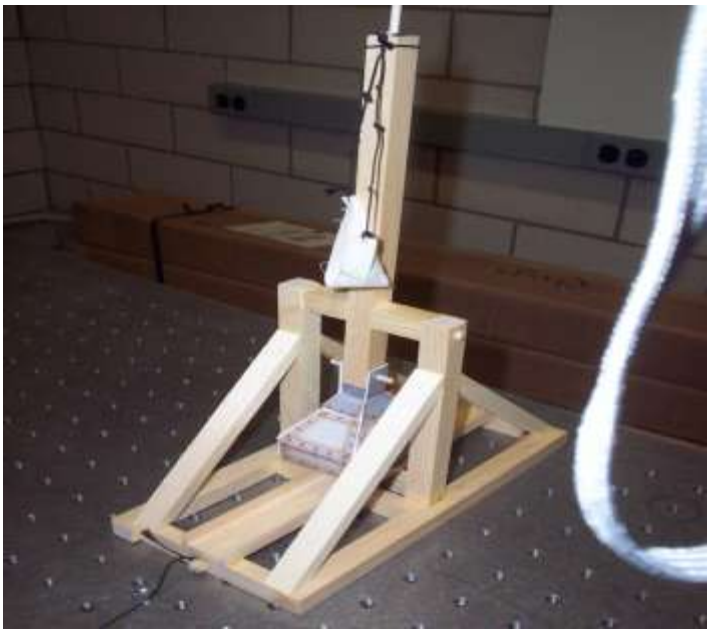

Figure 4: Actual build trebuchet used for experimentation

The trebuchet shown in the figure is the actual trebuchet used for the experimentation process. The actual instructions for the build of the trebuchet are not important as any simple design would do but a list of supplies are as follows: sling fabric, sling cord, slip rings, hurling stones, small pins, trigger pin, axel spacers, counterweight box, seventy-eight pennies, firing trough, hurling arm, side frames, uprights, brace, axle, cross frame, and drilled cross frame. All wood was pre-cut within the trebuchet kit, and was assembled using wood glue and braces. Instructions from thinkgeek.com were followed meticulously.

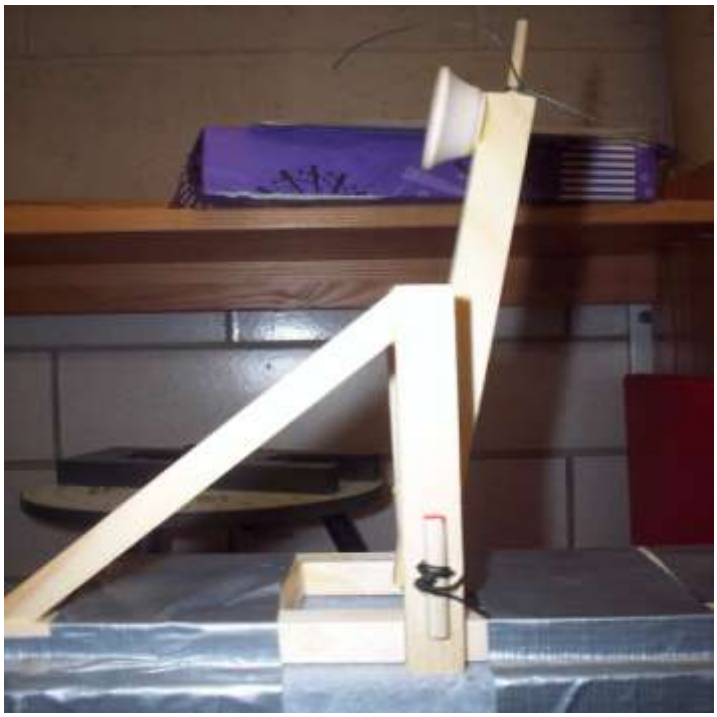

Figure 5: Actual catapult used in experimentation

The catapult shown in the figure is the actual catapult used in the experimentation process. The actual instructions for the build of the catapult is not necessary as any simple design would be sufficient for the project, but a list of supplies are as follows: hurling stones, trigger pin, torsioning pins, spoon, paper clip, skein cord, hurling arm, side frame, upright, brace, crash bar, and cross frame. All wood was pre-cut within the catapult kit, and was assembled using wood glue and braces. Instructions from thinkgeek.com were followed, again, meticulously.

These two apparatuses are used in two sets of experiments. The first set examines how the catapult throws the projectile. It is known that a torsion catapult uses the built up force within the twisted ropes to fire the projectile; what is interesting about a torsion catapult is how to increase the force contained within the ropes. In order to study this several more pieces of equipment are needed. These pieces include: the catapult built above, a protractor, and a computer program to measure the force exerted from the lever arm of the catapult. The best

program to use for this is Logger Pro 3.6.1. It is a common program that is used many high schools or equivalent programs are used. This program uses a force monitor that relays the force measurements so it can be easily watched, measured, and timed.

Figure 6: Photograph of actual force monitor used in experimentation

The force monitor needed to be connected in some way to the catapult's lever arm in order to measure the force from torsion to the lever arm. The figure above shows the force monitor used in the experiment. The force monitor is attached to a string which can sense the force exerted on the lever arm, these forces are measured by Logger Pro.

What is difficult is positioning the force monitor in such a way that it accurately measures the force exerted on the lever arm. After several trials is was determined that the most accurate measurements of force came from using a string made of material that is unable to stretch and to set up the force monitor-string system in such a way that the force from the level arm is redirected to the force monitor.

Figure 7: Shown is the force monitor-string system used for experiment. A system of pulleys was used to redirect the force from the lever arm to the force monitor.

After an attempt to tie the force monitor directly to the catapult's lever arm, it was determined that a system of pulleys was needed to redirect the force to the force monitor. In this ill-fated attempt, we attached a cotton string to both the force monitor and the lever arm of the catapult. There were no other apparatuses in this attempt. It was simply the force monitor and catapult stabilized to the counter, with a string attached between them. To change the angle of the catapult's lever arm, we untied the string and retired to change the tension and therefore the angle. We did this with the knowledge the tension in the string needed to hold the lever arm at a certain angle would be a measure the force exerted from the catapult at that particular angle. However there are two problems with this. The first problem being the cotton string itself. This particular string stretches under tension so it would not be able to give reproducible results. The second problem was the set up of the force monitor. The untying and retying system added too

much possible error into the system. A system needed to be designed where the results could be reproducible and the actual system mechanics stayed constant. A system of pulleys that redirect the force to the force monitor using nonmalleable string was determined to yield the best results. With this system the lever arm can easily be moved by shifting one pulley up and down a pole. It is able to be moved because the string length is constant between the catapult and the force monitor, so as one of the pulleys is moved up and down the first pole, the tension in the string causes the lever arm to change its angle to the crash bar. As the tension in the string is changed due to the changing position of the pulley, this is registered in the vertical force monitor, and we are able to see how the force is changed due to the changing angle of the lever arm. It is important that string attached to the force monitor is constantly vertical to the monitor because this would change the accuracy of the force measurement if the string was even somewhat at an angle to the force monitor.

The second set of experiments encompasses the actual study of projectile motion. These experiments record the projectile motion of the catapult, trebuchet, and a thrown ball in various ways with various balls. The equipment needed for this series of experiments is: a catapult, a trebuchet, a still shot 35mm camera, a strobe light, a digital video camera, and various balls used as projectiles. It is important that the 35mm camera has a shutter that is able to be held open, because this will be used with the strobe light to capture the motion of the projectile. As the shutter is held open, every time the strobe light pulses and image of the projectile is captured on film. So in one picture, one can see the entire arc of the projectile. Another way to do this is to use a digital video camera to capture the projectile arc. But, the projectile is traveling so fast that a camera functioning at regular film speed may not pick up the projectile in regular time. It is useful to have a “slow motion” option on the camera to fully appreciate the arc of the projectile.

Procedures and Preliminary Data

Force-Angle Measurements

Using the equipment stated in the above section, the data can now be collected following a specific procedure. First we set up the force monitor and catapult, just as it is shown in Figure 7. The catapult needs to be positioned higher than the actual pulley system to ensure that the lever arm can form a 90º angle the crash bar. Being able to draw the lever arm down to this angle will ensure a full picture of how or if the force changes as the angle of the lever arm to the crash bar increases. The lever arm is pulled down by shifting one pulley up and down a pole. It is able to be moved because the string length is constant between the catapult and the force monitor, so as one of the pulleys is moved up and down the first pole, the tension in the string causes the lever arm to change its angle with respect to the crash bar. Using the computer program Logger 3.6.1, we read the force measurements from the force monitor as we increase the angle.

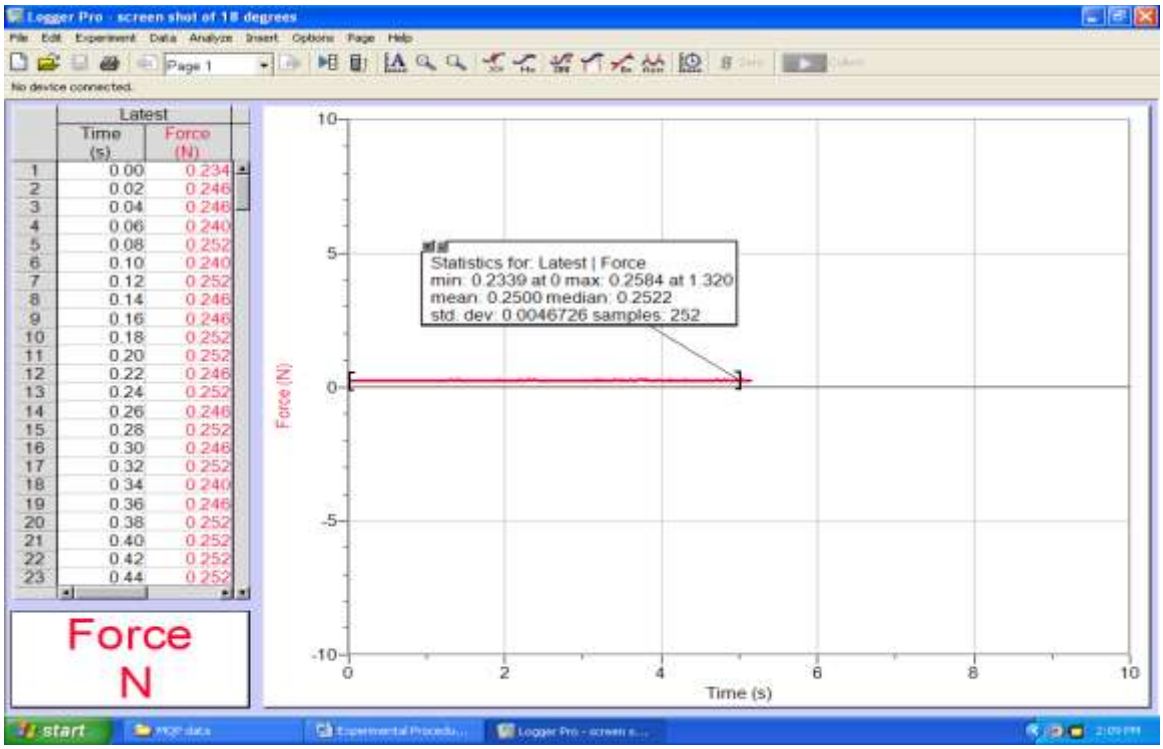

Figure 8: Screen shot of the Logger Pro 3.6.1 program measuring the force from the catapult, where the lever arm is positioned at a particular angle.

As we change the angle of the catapult's arm using the pulley, we carefully measure said angle using a protractor with respect to the crash bar and record it. Then using the Logger Pro program, we record the force for five seconds, and using the statistics application already in Logger Pro, we record the mean and standard deviation of the forces collected within those five seconds. The figure above is a screen shot of the Logger Pro program. The left hand corner shows the force at any particular second. The graph and data table next to it shows how the force changes over time. Since we are really measuring the tension in the string attached to the catapult, the force is not constant, but mean is a good approximation of the force needed to keep the lever arm at that specific angle and the standard deviation is the error in the measurements.

Angle (degrees)	Angle Error (degrees)	Average Force (N)	St. Dev. (N)
10	2	0.04467	0.005574
17	2	0.1105	0.0061983
21	2	0.1487	0.0069774
26	2	0.201	0.0068817
32	2	0.2596	0.0059898
39	2	0.3201	0.0058101
46	2	0.4105	0.0066403
52	2	0.5472	0.0060422
60	2	0.8765	0.0061027
67	2	1.562	0.006267
72	2	2.238	0.0075393

Table 1: Table of the force-angle measurement of the catapult. Included is the angle, error in the angle measurement, the average force, and the error in the force measurement.

The table above shows the data collected in the force-angle experiment for the catapult. Shown is the angle measured in degrees, the error in the angle, the average force measured in Newtons while the catapult's lever arm was positioned at the corresponding angle, and the standard deviation or error associated with that force.

Projectile Range Measurements

There are two different methods to capture the motion of a projectile, still shot photos and digital videos. The still shot photos are an older method of data taking but still very affective. What is needed here is the 35mm camera where the shutter is able to be held open. Specifically we used a Canon 35mm camera, setting the shutter to "B", which means that the shutter is held open as long as the shutter trigger is pressed down. The important thing about this process is not necessarily the make of the camera, but the speed of the film. The film needs to be able to capture the projectile as it passes through the air. Meaning the film speed needs to be faster than or as fast as the projectile.

Using this camera with the appropriate film, we theoretically set up the experiment in the following way. The camera needs to be completely horizontal or at a 90º angle to a blackened background or a background from which the projectile can be clearly established. We use a blackened background because we have covered the small projectile with a metallic covering, so that it can clearly be seen against the black background. After setting up the camera to a 90º angle to the back drop, we turn on the strobe light to an appropriate speed and turn off all other lights in the experimentation room. There is a setting on the strobe light, so that it can be set to whatever speed is needed or wanted. The faster the speed the more "dots" will appear along the projectile path in the actual photograph. After all the equipment is set up, one simply pitches the projectile, while another holds the camera shutter down for the entire motion of the arc and then

releases. When the picture is developed, what is seen is a projectile arc, where there are bright dots where the camera captured the projectile. Below is an example of strobe light photography.

Figure 9: This is an example of strobe light photography. Here a girl drops a ball, while the photographer holds the camera shutter open to capture the ball during the course of the drop. Every time the strobe shines the light, the image of the ball is captured.

Originally we wanted to use this kind of photography to capture the motion of a projectile coming from our catapult and trebuchet. However, after manually trying different film speeds like 400, 800, and 1600 film, we were not able to pick up the small projectile coming from the catapult and trebuchet. We could have tried a film speed of 3200, but to develop that kind of film would have logistically been too expensive and taken too long for the experimentation process. Adding on to the problem of film speed, we thought a compounding reason the ball was not being observed by the camera was because the projectile was too small in comparison. To distinguish whether film speed and size of the ball were the actual problems, we decided to conduct another experiment with projectile motion. A projectile is anything given an

initial velocity, so we opt to look at the projectile motion of a tossed ball. In comparison, we chose a ball that is some five times bigger than the initial projectile. This new ball has diameter of 95.25 mm, where the original ball had a diameter of 17.8mm. They were also made of different materials, the original ball being made of wood, and the new, bigger ball being made of foam. But they were both covered in the same metallic tape, so that the strobe was able to distinguish them from the blackened background. Tossing the foam ball at a reduced speed, we conducted the experiment again. The difference this time, when developed, we could see the projectile motion of the tossed ball in the still photograph.

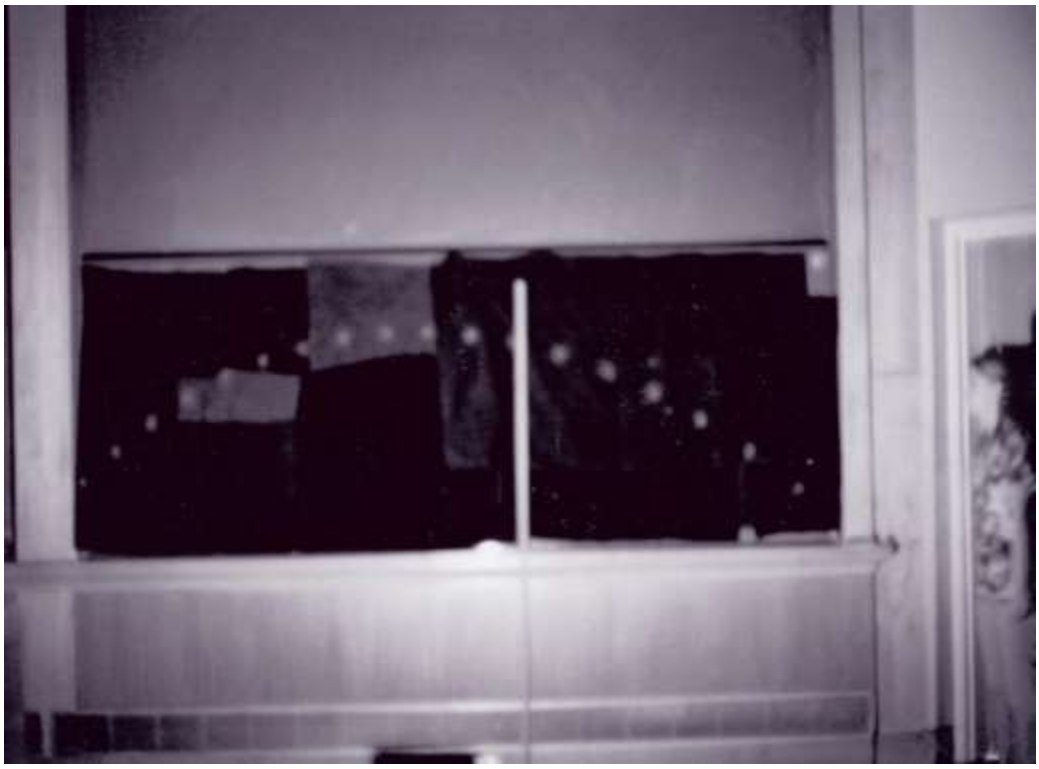

Figure 10: Actual developed photo of the tossed balls projectile motion. Every position of the ball corresponds to when the strobe light shining light on the ball.

When the picture is developed, we can inspect the projectile motion by quantitative analysis. We pick the first point to be our initial position, and then measure the horizontal and vertical position of every point every that in comparison to that initial position with a ruler in

inches. We also need the time of each position, and we find this from knowledge of our strobe light. The timing of each burst of light is derived from the setting on the strobe light. We set our strobe to be "1300 rpm." This means that there are 1300 revolutions per minute or the strobe pulses every .0462 seconds. This leaves no room for error in the time of our projectile motion because we know at every position that we see in the arc .0462 seconds have passed in time because of the setting of the strobe light. Quantitatively analyzing the figure above, we obtain the following data set.

X Position (inches)	Delta X (inches)	Y Position (inches)	Delta Y (inches)	Delta T (seconds)
0	0.0625	0	0.0625	0
0.1875	0.0625	0.1875	0.0625	0.0462
0.625	0.0625	0.4375	0.0625	0.0924
0.9375	0.0625	0.5625	0.0625	0.1386
1.125	0.0625	0.625	0.0625	0.1848
1.5	0.0625	0.6875	0.0625	0.231
1.75	0.0625	0.71875	0.0625	0.2772
2	0.0625	0.71875	0.0625	0.3234
2.25	0.0625	0.6875	0.0625	0.3696
2.75	0.0625	0.625	0.0625	0.4158
2.9375	0.0625	0.5625	0.0625	0.462
3.1875	0.0625	0.4375	0.0625	0.5082
3.4375	0.0625	0.3125	0.0625	0.5544
3.625	0.0625	0.125	0.0625	0.6006

Table 2: Data set containing the X position (horizontal), the error in the horizontal measurement, the Y position (vertical), the error in the vertical measurement, and the time associated with each horizontal and vertical measurement.

The figure above contains the X position or horizontal position measured from the initial point, including the possible error in our measurement, the Y position or vertical position measured from the initial point, including the possible error in the measurement, and the change in time associated with each X and Y position. Notice the first set of data (X, Y, T) is a set of zeros because that is our beginning position while every measurement following that is added onto that point.

While we have data for the projectile motion of a tossed ball, our main objective was to study the projectile motion from catapults and trebuchets, for which we still do not have data. To solve this problem we needed to introduce a new piece of equipment, the digital video camera. The digital video camera has a higher resolution and quicker turnaround time. With the still shot photography, it would take a couple of days to develop the film to determine whether projectile motion was detected, but with the digital video camera, one can simply replay the video in seconds to see if the projectile motion was captured by the high resolution camera. Because one of the main problems of the still shot photography was the speed of the ball, we thought it best to film the projectile in slow motion to ensure the capture of the high speed projectile motion. This was done by simply setting the camera to its slow motion option found in the menu of the camera. With the high resolution to pick up the small ball, the slow motion digital capture, and the small turnaround time, the problem of depicting the projectile motion of catapults and trebuchets is solved.

We set up the experiment again in a very similar way to the still shot photography. The digital camera needs to be completely horizontal or at a 90º angle to a blackened background or a background from which the projectile can be clearly established. This needs to be done because if the camera is slightly skewed or at anything but a 90º angle to background then the motion of

the projectile will be skewed to this angle. This will be a problem when analyzing the data because one cannot go easily from the projectile's digital position to converting it to its real position in meters. If the camera is horizontal to the background, then converting the digital position to the real position in meters is simply done by a conversion factor found later. If it is not horizontal to the background then one would need to account for this angle in calculations, which is only added work. We use a blackened background because we have covered the small projectile with a metallic covering, so that it can clearly be seen against the black background. After setting up the camera to a 90º angle to the blackened back drop, we simply fire the catapult and trebuchet while filming its motion. It is important to make sure to film the entire motion of the projectile from beginning to end to make sure we get a full picture of the motion. One might need to move the camera closer to the board or further from the board to ensure this happens. The only thing that will change by moving the camera in such a way is the conversion factor mentioned before and that will be discussed later.

Once the projectile motion is established on camera, the digital analysis can begin. Two computer programs are necessary for this step. The first being a program to watch the digital video and save still shots from the video and the second being a program to analyze each still shot, being able to determine its exact position in the shot. The first program we used was a program called "Virtualdubmod." This program downloaded from the internet at no cost, and it is perfect because you are able to save still shot versions of the video for a specific time that is clearly visible on the video.

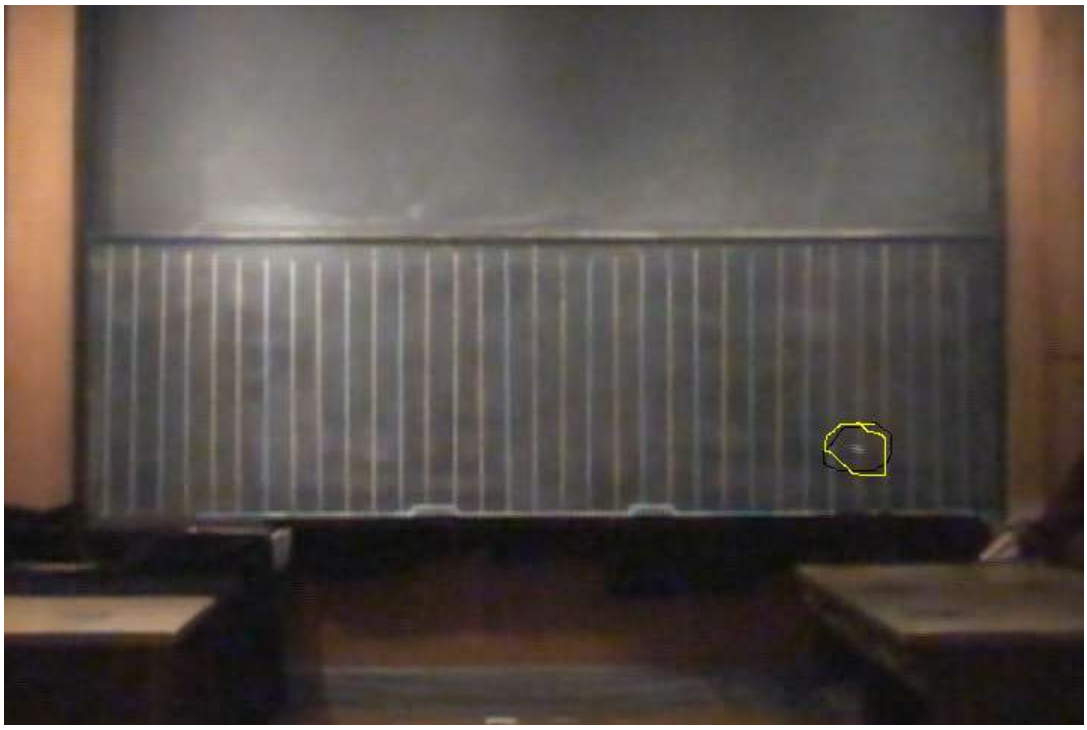

Figure 11: Still shot image taken from video of the projectile motion of the catapult. This particular image was taken at a time marked 1.568 seconds. The circled mark is the projectile as it travels through the air at the marked time

From the video, we know the time of each image, but a program to determine the position of each point is now needed. A perfect program for this is a program called "Paint," which is found in any program using any form of Windows. From Paint, we can determine the X and Y position of the projectile using the pixels of the pictures.

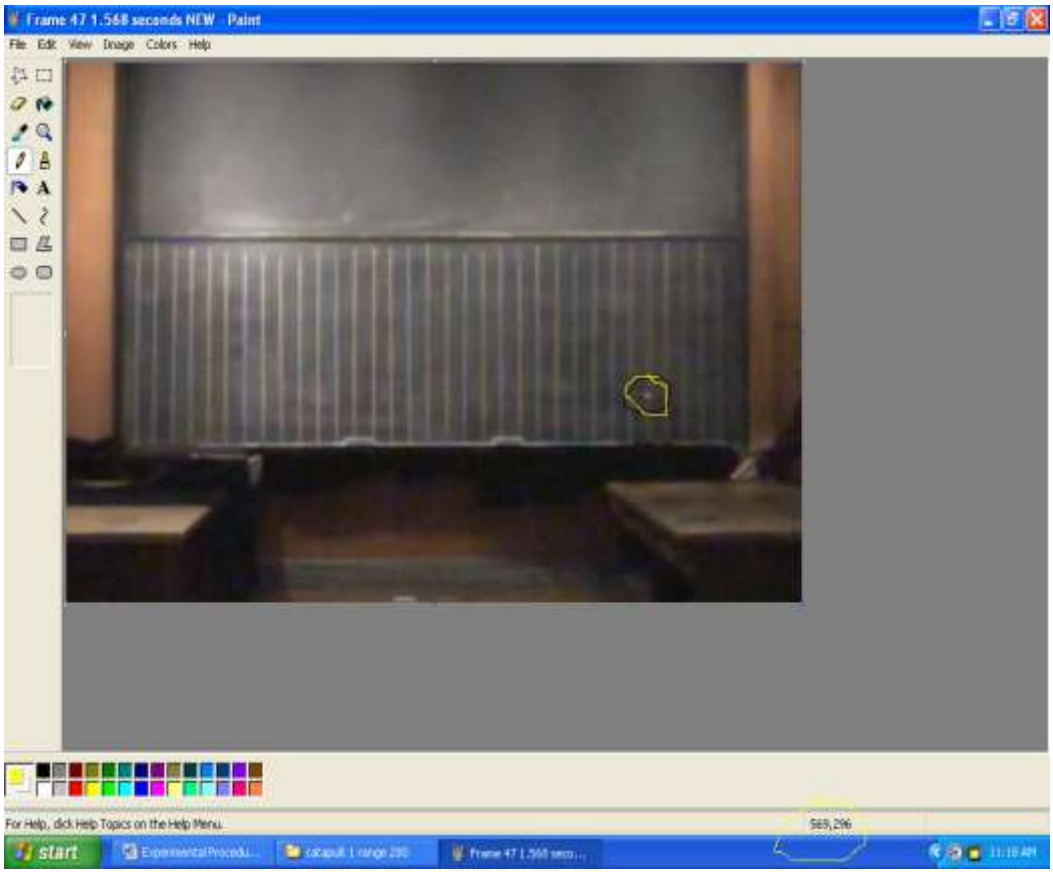

Figure 12: This is the paint image of the exact image before, only here we can see in the corner the pixel position, (569,296)

The figure above shows an example of using Paint to find the digital position of the projectile. Paint is probably the easiest program for this purpose because all that is done is putting the cursor over the position of the projectile and the bottom right hand corner shows the position in pixels, here it says the pixel position of the projectile is (569,296). This is the (X, Y) position. Doing a complete analysis of each video is done by taking several images of different positions of the projectile motion and then finding the digital pixel position of each location of the projectile. This is a tedious process but it is necessary in order for a complete picture of motion of the projectile.

position #	Position X (pixels)	Delta X (pixels)	Position Y (pixels)	Delta Y (Pixels)	time (seconds)

1	668	5	337	5	1.106
1.5	660	5	331	5	1.174
2	651	5	327	5	1.207
2.5	620	5	313	5	1.342
3	599	5	305	5	1.442
4	555	3	291	3	1.643
5	515	3	282	3	1.811
6	472	3	275	3	2.012
7	443	3	273	3	2.146
8	409	5	272	5	2.313
9	381	3	274	3	2.448
10	344	3	279	3	2.616
11	331	3	281	3	2.682
12	290	3	291	3	2.884
13	283	5	295	5	2.917
14	253	5	302	5	3.051
15	233	3	312	3	3.152
16	220	5	318	5	3.129
17	192	5	333	5	3.352
18	183	5	339	5	3.387
19	168	5	345	5	3.487

Table 3: Data of the projectile motion of the catapult containing X position in pixels, the error in the X position, the Y position in pixels, the error in the Y position, and the time associated for each position as shown from the camera.

Position #	Position X (Pixels)	Delta Position X (Pixels)	Position Y (Pixels)	Delta Position Y (Pixels)	time (seconds)
1	642	5	263	5	4.371

2	636	5	257	5	4.404
3	633	3	253	3	4.4438
4	621	5	242	5	4.505
5	602	3	224	3	4.638
6	598	5	219	5	4.671
7	590	5	212	5	4.738
8	578	5	204	5	4.805
9	562	5	192	5	4.905
10	561	3	190	3	4.938
11	555	3	186	3	4.972
12	531	3	169	3	5.138
13	504	3	154	3	5.339
14	498	3	151	3	5.372
15	467	3	138	3	5.606
16	436	3	128	3	5.839
17	421	3	125	3	5.939
18	399	3	123	3	6.106
19	380	3	123	3	6.24
20	359	3	124	3	6.406
21	315	3	133	3	6.74
22	307	5	136	5	6.807
23	271	5	151	5	7.074
24	216	5	189	5	7.508
25	186	3	215	3	7.741
26	166	3	236	3	7.908
27	158	3	245	3	7.975
28	133	5	276	5	8.175

29	113	5	300	5	8.342
30	97	5	314	5	8.442

Table 4: Data of the projectile motion of the trebuchet containing the X position in pixels, the error in the X position, the Y position in pixels, the error in the Y position, and the time associated for each position as shown from the camera.

The figure shows the data collected by digital analysis for the motion of the projectile coming from the catapult and the trebuchet. Each data set contains the X position, the error in the X position, the Y position, the error in the X position, and the time linked to each position as the camera displays it. The error in each positional point is relatively small because each positional point can be pin pointed with the cursor with superior accuracy with regards to physically measuring the position with a ruler as we did with the still shot photograph. The only reason there is error is because it is difficult to see exactly where the center of the projectile is located because what the naked eye is seeing is a splotch of light. The error is essentially the radius of the splotch of the light relative to where we guesstimate the center of the projectile to be.

One other thing that needs to be reconciled with regards to the data is the time. We filmed the projectile with the slow motion option of the camera, so the time associated with each position that was collected from the camera is wrong. This was discovered when some quick calculations were done to make sure our data was trustworthy. What we discovered was that our calculations were essentially a power of ten off. After making sure that digital analysis of each position was accurate, we turned our attention to the time. At first we thought the slow motion option recorded the correct time, but after a quick experiment we were proven wrong.

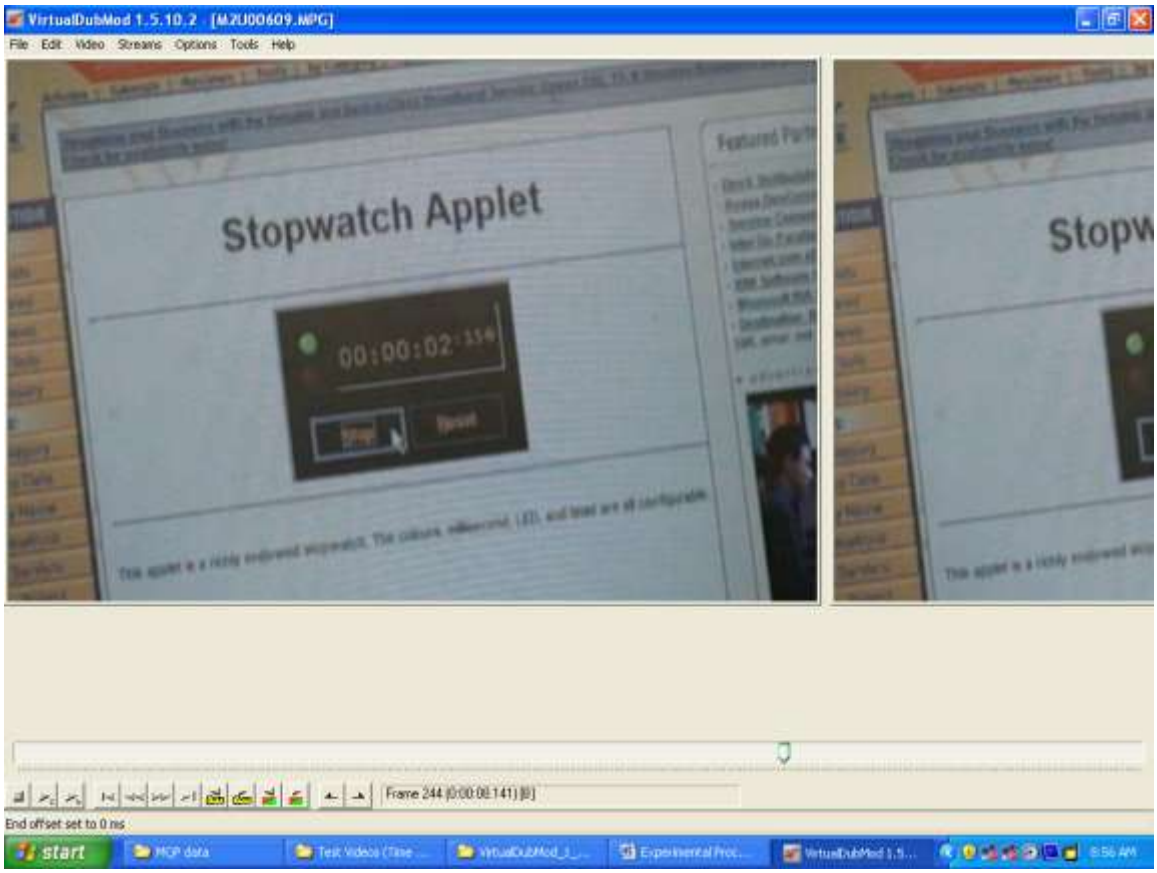

Figure 13: Screen shot of the "Time Verification Experiment." Shown is an online digital clock that is collecting accurate time, and the bottom of the screen showns the time that the virtual dub mode program is displaying. The two times are shown to be inconsistent with each other.

The experiment we conducted is a time verification experiment What we did was film a online stop watch which we knew to be accurate, and then watched it on the Virtualdubmode program to see if the time displayed was accurate. As shown in the figure, the time that the stopwatch displayed was inconsistent with the time that the virtuadubmode program displayed, in fact the virtualdubmode program displayed a time that was a factor of 4.022 larger than the actual time. This was verified by doing this experiment several times, and each time the program displayed a time that was a factor of 4.022 larger than the real time. So essentially, every time in the catapult and trebuchet data sets needs to be divided by 4.022 in order for the timing to be accurate and consistent with calculations done in following sections.

There will be error in each one of the times for two reasons. The first is that when the video camera works in the slow motion mode, the video is not continuous. The slow motion mode of the camera works by taking many shots of the area and then putting them back together. This particular camera takes about thirty frames per second. The second reason for error in the time is that computers have a refresh rate. When doing the time verification experiment, we were watching a computer screen to verify the correct real time, since the computer has a refresh rate there could be error in the actual time. For these two reasons, we will add in an error of .02 seconds for each time. This was determined because computers refresh themselves about sixty times per 1 second.

$$\text{Error} = 1 \text{ sec}/ 60 = .02 \text{ seconds}$$

This is considered is an over estimation of the error in the refresh rate to account for the possible error in the actual video.

Results – Catapult Projectile Motion

Webster's dictionary defines results as "an outcome, consequence of an operation or an answer to a calculation." (Results Definition) The following are the outcomes to our experiments, or the answers that will be discussed and analyze later.

Force-Angle Measurements

During the force-angle experiment we looked at the effect of changing the angle of the lever arm with respect to the break point. From the data we collected, as we increased the angle with respect to the break point, the force required to keep the lever arm in place increased.

Therefore, as the angle increases the force on the projectile increases. This is displayed graphically below. It is shown that as the angle increases, the force increases exponentially.

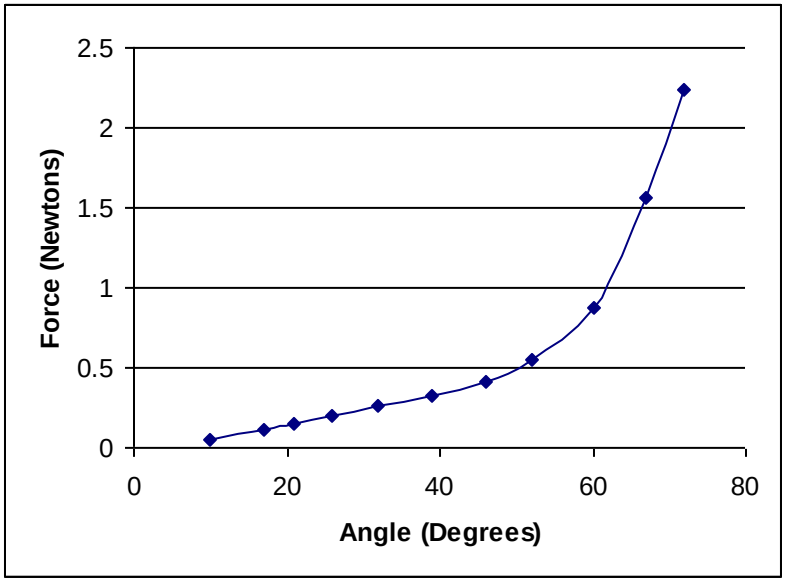

Figure 14: Graph of the data found in the Force-Angle experiment.

Projectile Motion

During the projectile motion experiments, using both the video camera and the 35mm camera, the goal was to analyze the projectile motion of the ball. So we have to show that projectile motion occurred. Before this can happen, we need to convert the data collected during the experiment to real life numbers. For example, to analyze the projectile motion of the catapult we used the digital video camera and found the positions of the ball in pixels. We need now to convert those pixels to measurements with regards to our real system in meters. What we need is something in the video that we are sure of its size in the real system. In our video, we know the background to be a blackboard of 3.4 meters by 1.2 meters because we physically measured it during the experiment. Using the paint program, we can look at the pixel dimensions of the blackboard, and then using those we can find a conversion factor. For the video of the catapult, the pixel dimension of the backboard is 619 pixels by 186 pixels.

186 pixels = 120 cm ---- 1 pixel = .6452 cm

619 pixels = 340 cm ---- 1 pixel = .5500 cm

Knowing the digital dimensions and the real dimension, conversions factors of .6452 in the Y direction and .55 in the X direction are found. We then simply multiply all our pixel positions by this conversion factor to find the position in the real system. The pixel positions do not start at a simple zero position. To make our calculations easier we will make our first position zero in both directions by subtracting the first positions measurement from each additional measurement after in its respective direction. After doing this the following this the data found.

position #	Converted X (m)	Delta X (m)	Converted Y(m)	Delta Y (m)	time (seconds)	Delta t (seconds)
1	0	0	0	0	0.275098696	0.004997252
1.5	0.044	0.0275	0.038712	0.03225	0.291839488	0.004997252
2	0.0935	0.0275	0.06452	0.03226	0.300084953	0.004997252
2.5	0.264	0.0275	0.154848	0.03226	0.333566538	0.004997252
3	0.3795	0.0275	0.2064	0.03226	0.358552796	0.004997252
4	0.6215	0.0165	0.2967	0.019356	0.408525311	0.004997252
5	0.8415	0.0165	0.35475	0.019356	0.450252361	0.004997252
6	1.078	0.0165	0.3999	0.019356	0.500224876	0.004997252
7	1.2375	0.0165	0.4128	0.019356	0.533506571	0.004997252
8	1.4245	0.0275	0.41925	0.03226	0.575183649	0.004997252
9	1.5785	0.0165	0.40635	0.019356	0.608665234	0.004997252
10	1.782	0.0165	0.3741	0.019356	0.650392284	0.004997252
11	1.8535	0.0165	0.3612	0.019356	0.666883214	0.004997252
12	2.079	0.0165	0.2967	0.019356	0.717105592	0.004997252
13	2.1175	0.0275	0.2709	0.03226	0.725351057	0.004997252

14	2.2825	0.0275	0.22575	0.03226	0.758582779	0.004997252
15	2.3925	0.0165	0.16125	0.019356	0.783569037	0.004997252
16	2.464	0.0275	0.12255	0.03226	0.80030983	0.004997252
17	2.618	0.0275	0.0258	0.03226	0.833791415	0.004997252
18	2.6675	0.0275	-0.0129	0.03226	0.84203688	0.004997252
19	2.75	0.0275	-0.0516	0.03226	0.867023137	0.004997252

Table 5: Converted data of Table 2: Data set containing the X position (horizontal), the error in the horizontal measurement, the Y position (vertical), the error in the vertical measurement, and the time associated with each horizontal and vertical measurement. Contains the position in meters and the converted real time of the catapult's projectile motion.

This table contains the converted positions in the X and Y directions in meters, with their respective errors, and the converted real time. This is the camera time divided by the 4.022 conversion factor found in the procedures section. Taking the X and Y positions and graphing them against each other, yields the below graph.

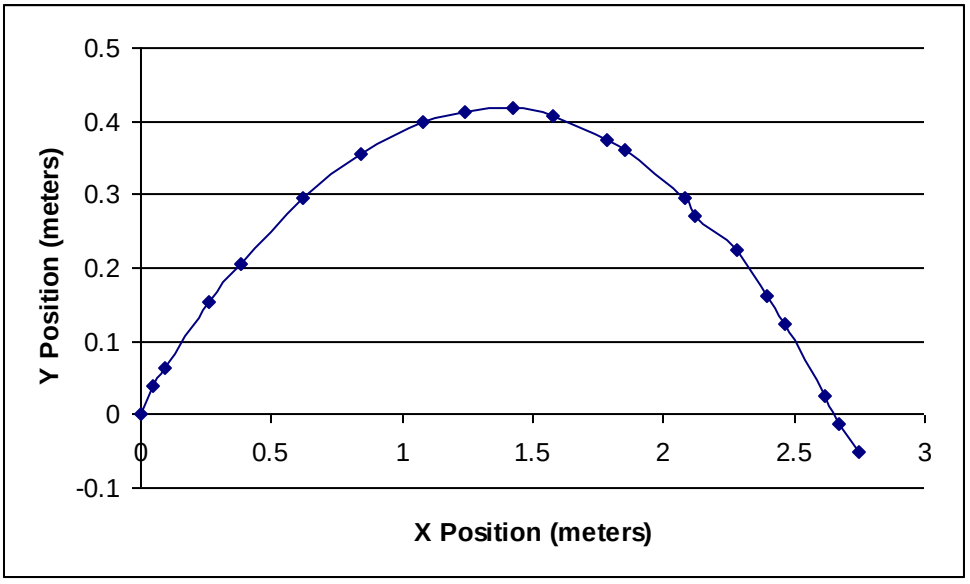

Figure 15: Graphical representation of the projectile motion of the catapult, containing the X and Y positions in meters

The figure above is a graphical representation of the data in Table 2: Data set containing the X position (horizontal), the error in the horizontal measurement, the Y position (vertical), the error in the vertical measurement, and the time associated with each horizontal and vertical measurement.. It shows the motion of the projectile as it came from the catapult. The motion is shown to be an arc, as expected. It is from this arc that we will further discuss the projectile motion coming from the catapult.

As with the catapult's data, we will do the same thing with the trebuchet's data. Using the paint program again, we can look at the pixel dimensions of the blackboard, and then using those we can find a new conversion factor. For the video of the trebuchet, the pixel dimension of the backboard is 508 pixels by 149 pixels.

149 pixels = 120 cm ---- 1 pixel = .6693 cm

508 pixels = 340 cm ---- 1 pixel = .8054 cm

Knowing the digital dimensions and the real dimension, conversions factors of .66693 in the Y direction and .8054 in the X direction are found. We then simply multiply all our pixel positions by this conversion factor to find the position in the real system. The pixel positions, again, do not start at a simple zero position. To make our calculations easier we will make our first position zero in both directions by subtracting the first positions measurement from each additional measurement after in its respective direction. After doing this the following this the data found for the trebuchet.

Position #	**X (m)**	**delta X (m)**	**Y (m)**	**delta Y (m)**	**Real Time (s)**	**Delta $T_{(real)}$ (m)**
1	0	0.033465	0	0.0405	1.092149318	0.004973

2	0.040158	0.033465	0.0486	0.0405	1.100394783	0.004973
3	0.060237	0.020079	0.081	0.0243	1.110339313	0.004973
4	0.140553	0.033465	0.1701	0.0405	1.125630903	0.004973
5	0.26772	0.020079	0.3159	0.0243	1.158862626	0.004973
6	0.294492	0.033465	0.3564	0.0405	1.167108091	0.004973
7	0.348036	0.033465	0.4131	0.0405	1.183848883	0.004973
8	0.428352	0.033465	0.4779	0.0405	1.200589676	0.004973
9	0.53544	0.033465	0.5751	0.0405	1.225575933	0.004973
10	0.542133	0.020079	0.5913	0.0243	1.233821398	0.004973
11	0.582291	0.020079	0.6237	0.0243	1.242316726	0.004973
12	0.742923	0.020079	0.7614	0.0243	1.283793913	0.004973
13	0.923634	0.020079	0.8829	0.0243	1.334016291	0.004973
14	0.963792	0.020079	0.9072	0.0243	1.342261756	0.004973
15	1.171275	0.020079	1.0125	0.0243	1.400729599	0.004973
16	1.378758	0.020079	1.0935	0.0243	1.458947579	0.004973
17	1.479153	0.020079	1.1178	0.0243	1.483933836	0.004973
18	1.626399	0.020079	1.134	0.0243	1.525660887	0.004973
19	1.753566	0.020079	1.134	0.0243	1.559142472	0.004973
20	1.894119	0.020079	1.1259	0.0243	1.600619659	0.004973
21	2.188611	0.020079	1.053	0.0243	1.684073759	0.004973
22	2.242155	0.033465	1.0287	0.0405	1.700814552	0.004973
23	2.483103	0.033465	0.9072	0.0405	1.76752786	0.004973
24	2.851218	0.033465	0.5994	0.0405	1.875968217	0.004973
25	3.052008	0.020079	0.3888	0.0243	1.934186198	0.004973
26	3.185868	0.020079	0.2187	0.0243	1.975913248	0.004973
27	3.239412	0.020079	0.1458	0.0243	1.99265404	0.004973
28	3.406737	0.033465	-	0.0405	2.042626555	0.004973

			0.1053			
29	3.540597	0.033465	-0.2997	0.0405	2.084353606	0.004973
30	3.647685	0.033465	-0.4131	0.0405	2.109339863	0.004973

Table 6: Converted data of Table 3: Data of the projectile motion of the catapult containing X position in pixels, the error in the X position, the Y position in pixels, the error in the Y position, and the time associated for each position as shown from the camera. contains the position in meters and the converted real time of the trebuchet's projectile motion.

This table contains the converted positions in the X and Y directions in meters, with their respective errors, and the converted real time. This is the camera time divided by the 4.022 conversion factor found in the procedures section. Taking the X and Y positions, and graphing them against each other, yields the following graph.

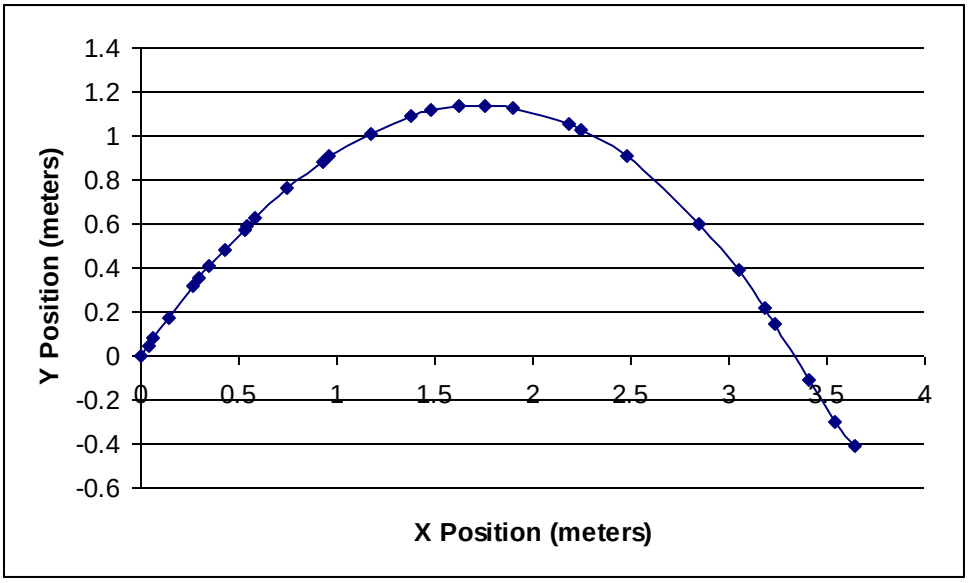

Figure 16: Graphical representation of the projectile motion of the trebuchet, containing the X and Y positions in meters.

The figure above is a graphical representation of the data in Table 3: Data of the projectile motion of the catapult containing X position in pixels, the error in the X position, the Y position in pixels, the error in the Y position, and the time associated for each position as shown from the camera.. It shows the motion of the projectile as it came from the trebuchet. The motion

is, again, shown to be an arc, as expected. It is from this arc that we will further discuss the projectile motion coming from the trebuchet.

To study the projectile motion of the tossed ball from the still photograph, we use a process very similar to the process used for the video camera. We, again, need to convert the data collected during the experiment to real life numbers. To analyze the projectile motion of the tossed we used the 35mm camera and found the positions of the ball, as measured by a ruler. We need now to convert those measurements to dimensions with regards to our real system in meters. What we need is something in the photo that we are sure of its size in the real system. In our photo, we know the background to be a blackboard of 3.4 meters by 1.2 meters because we physically measured it during the experiment. Using a ruler again, we can look at the dimensions of the blackboard measured in the picture, and then using those we can find a conversion factor. For the photo of the tossed ball, the dimensions of the backboard are 4.25 inches to 1.5 inches.

1.5 inches (camera) = 120 cm ---- 1 inch = 80 cm

4.25 inches (camera) = 340 cm ---- 1 inch = 80 cm

Knowing the digital dimensions and the real dimension, conversions factors of .8 in both the X and Y directions are found. We then simply multiply all our photograph positions by this conversion factor to find the position in the real system. Doing this yields the following data.

Con. X (m)	Con, Delta X (m)	Con, Y (m)	Con. Delta Y (m)	Delta T (seconds)	Delta T_ (seconds)
0	0.05	0	0.05	0	0.0231
0.15	0.05	0.15	0.05	0.0462	0.0693
0.5	0.05	0.35	0.05	0.0924	0.1155

0.75	0.05	0.45	0.05	0.1386	0.1617
0.9	0.05	0.5	0.05	0.1848	0.2079
1.2	0.05	0.55	0.05	0.231	0.2541
1.4	0.05	0.575	0.05	0.2772	0.3003
1.6	0.05	0.575	0.05	0.3234	0.3465
1.8	0.05	0.55	0.05	0.3696	0.3927
2.2	0.05	0.5	0.05	0.4158	0.4389
2.35	0.05	0.45	0.05	0.462	0.4851
2.55	0.05	0.35	0.05	0.5082	0.5313
2.75	0.05	0.25	0.05	0.5544	0.5775
2.9	0.05	0.1	0.05	0.6006	0.3003

Table 7: Converted data of Table 4: Data of the projectile motion of the trebuchet containing the X position in pixels, the error in the X position, the Y position in pixels, the error in the Y position, and the time associated for each position as shown from the camera. contains the position in meters and the time of the tossed ball's projectile motion

The figure contains the X and Y positions and their respective errors, along with their relevant time. This is the same time found in the original data found from the strobe timing. Below is a graphical representational data mentioned.

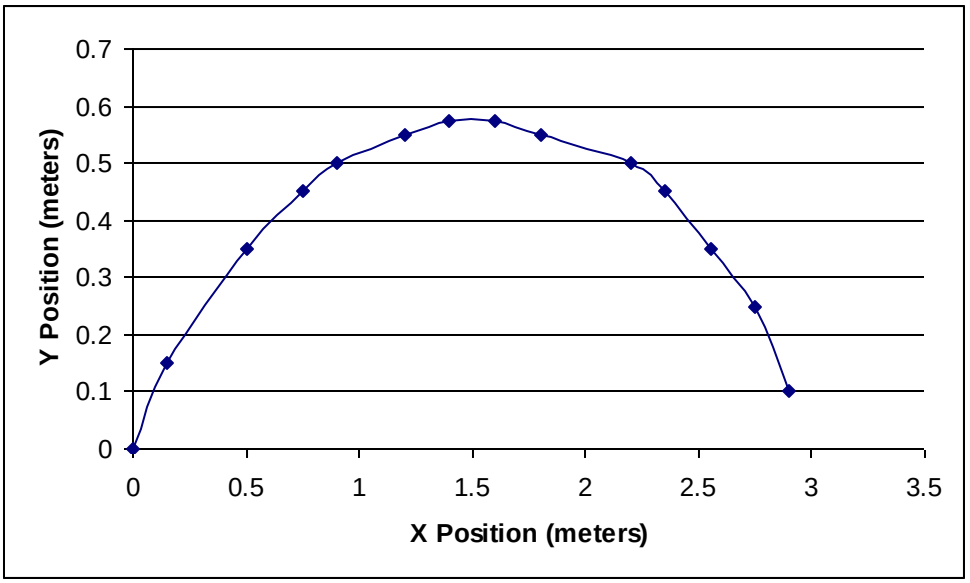

Figure 17: Graphical representation of the projectile motion of the tossed ball, containing the X and Y positions in meters.

The figure shows the arc that the projectile traveled in. It is the X and Y positions in meters graphed against each other. It is from this data and the time, which all other quantities will be derived from.

Discussion and Analysis – Catapult Projectile Motion

Force Angle Measurements

The purpose of conducting force-angle experiment was to examine how changing the angle of the lever arm with respect to the break affected the force on the projectile. We expect that as the angle increases, the force on the projectile also increases. We expect this simply by observing how the catapult works. The projectile travels the furthest when the lever arm is pulled down to the horizontal, and travels the least when the angle is very small. From these observations, we expect that as the angle increases the force increases. Our expectation is only reinforced by Hooke's law. The force is produced by the twisted strings of the catapult, or

torsion. We are measuring the force as the angle increases; from these two measurements we can calculate the torque from the equation

$$T = F \times r$$

Or

$$T = Fr\sin\theta.$$

Hooke's law states that

$$T = -k\theta \text{ (Torsion Spring)}$$

So the torque should increase linearly as the angle increases since the torsion coefficient remains constant.

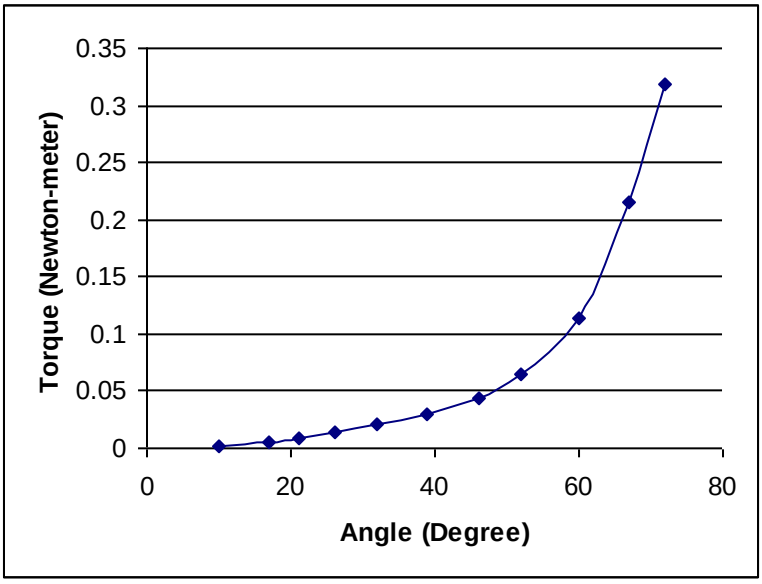

Figure 18: Graph of Torque vs. Angle for the catapult

.

The figure shows that the torque does increase as the angle increases with an upward slope, but it does not increase linearly as expected. Instead it appears to increase exponentially.

This suggests that the torsion coefficient may not be constant. The twisted string may be affected as the force is increased or over time.

Our observations of how the catapult worked only confirmed this suspicion. As we worked with the catapult over and over again, we noticed that the range of the catapult decreased with time and that we had to turn the strings more and more in order to get back to the range that we once were at.

It would be interesting to observe this phenomenon further. We could experiment to see what materials work best with the catapult, not only affecting the range but what materials follow with Hooke's law and do not stretch. Conducting the force-angle experiment with different materials would observe this trend. We could also look at the affect of time by conducting these experiments over several days or weeks. This is beyond the time allocated for this MQP, but it certainly is an interesting trend to look at with a class.

Projectile Motion

From the results of the original experiments, quantities like velocity and acceleration can be derived. We know that that velocity is the derivative of position with respect to time, and acceleration is the derivative of velocity with respect to time. So by knowing the change in position and the change in time, we are able to find acceleration by taking a double derivative. From the position and time quantities resultant of the data analysis, we will use the following equations to find velocity and acceleration,

$$V= (P_2 – P_1) / (T_2 – T_1)$$

$$A= (V_2 – V_1) / (T_2 – T_1)$$ (Resnick, Halliday and Krane),

where V is velocity, A is acceleration, P is position, and T is time. The definition of average velocity is the change in position over the change in time, just as acceleration is the change in velocity over the change in time. So using our converted positions and times, we can find the average velocity and average accelerations over the full course of motion.

With this, there is also definite need of error analysis. Using the digital camera, there is small error in the positions and an error in the time due to the time conversion from slow motion. There two errors will affect the calculations for velocity and acceleration, therefore the error needs to be propagated to these quantities. We will do this by using the equation

$$\delta q = \text{sqrt}(\delta q_x^2 + \delta q_y^2),$$

where

$$\delta q_x = q(x + \delta x, y) - q(x, y)$$

$$\delta q_y = q(x, y + \delta y) - q(x, y)$$

(Taylor, An Introduction to Error Analysis: The study of uncertainties in physical measurements).

Here the total error for q comes from two variables, we combine the two errors by following each equation, one adding in the error from x and holding y constant, and the other adding in the error from y and holding x constant. We do the same thing finding the error in velocity and in acceleration. For velocity, adding in each error in the X position, Y position, and time separately while holding the rest constant. For acceleration, adding in each error in the velocity calculated in the X and Y direction and the error in time separately while holding all other constant. Doing this and calculating the velocities in the X and Y direction, and the acceleration in the X and Y direction generates the data in the following table.

position #	V_x(m/s)	Delta V_x	A_x (m/s^2)	Delta A_x	V_y (m/s)	Delta V_y	A_y (m/s^2)	Delta A_y
1	3.742057	1.573369	27.54858	43.63296	2.582219	1.506295	-3.72867	41.27638
1.5	5.272359	1.304304	-10.9722	31.5715	2.783231	1.194595	-19.4293	28.69329
2	4.891578	0.89431	2.70405	19.11883	2.426633	0.834753	-14.9179	17.42105
2.5	4.769288	0.622856	3.580984	13.29734	1.8924	0.533064	-13.1462	10.69958
3	5.038192	0.52386	-3.07172	7.850676	1.617783	0.428956	-10.0384	5.98026
4	4.978213	0.461812	-4.0659	8.778078	1.125414	0.310967	-9.9143	6.803045
5	4.756516	0.493312	-2.77408	9.155697	0.697262	0.334136	-9.89907	6.311929
6	4.622541	0.612808	1.744002	11.61231	0.258142	0.502491	-11.4373	9.538386
7	4.537068	0.529933	2.481366	11.73145	-0.08582	0.3643	-9.17374	8.058926
8	4.753444	0.619684	-4.52021	12.83838	-0.60033	0.503439	-8.392	9.951372
9	4.723627	0.704845	-3.33502	16.81091	-0.77553	0.479729	-12.3092	13.27388
10	4.451885	0.590365	7.260295	20.70275	-1.16019	0.428627	-8.79351	16.74989
11	4.515303	0.77804	4.168772	22.33579	-1.54444	0.670563	-6.78373	19.22576
12	4.906311	1.152335	-11.1663	33.38609	-1.71058	0.954701	-15.2994	30.4383
13	4.723627	0.799755	-4.67449	24.17738	-1.88344	0.686321	-16.2803	21.86794
14	4.349696	1.198049	11.46795	37.81901	-2.47322	1.174148	-16.811	37.06795
15	4.49003	0.905001	-11.2654	37.41584	-2.697	0.842333	8.002335	36.7858
16	4.876932	1.257384	-45.5989	34.7061	-3.2461	1.229231	86.2014	36.81636
17	3.972108	1.460628	-36.2375	67.09934	-2.3291	1.465392	102.762	73.60212
18	3.167914	0.037629	3.7072	0.049026	-0.01532	0.038312	-0.01793	0.044834
19	3.171772	0.036557	3.688107	0.04383	-0.05951	0.037209	-0.0692	0.043267

Table 8: Derived quantities of velocity and acceleration from position and time.

The X and Y velocities in the table seem accurate with the system. The velocity in the X direction stays relatively constant, while the velocity in the Y direction starts high, then decreases on the way up the arc until it there is zero velocity and switches direction downward,

from there it increases in velocity until the end of the motion. In a perfect system, the acceleration in the X direction would be zero, and the acceleration in the X direction to be 9.8m/s^2. This is not a perfect system so we do expect there to be variation in those accelerations but it should be in the vicinity of the expected values. Looking at the values calculated for the acceleration in the X and Y direction, they do perform as expected.

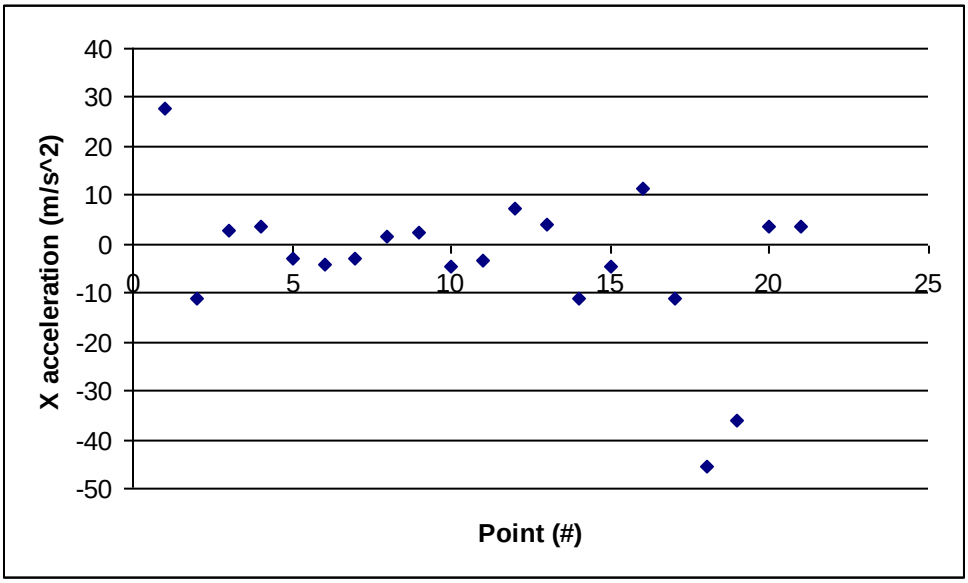

Figure 19: Graph of the X acceleration. The accelerations as each point are positioned around the zero line.

In the figure above, the X acceleration at each point is situated around the zero line, which is expected. The graph is similar for the acceleration in the Y direction, only the points are positioned around the 9.8 line.

What is really interesting about the table is how the error propagated though. Looking at the error values for the velocities, they seem to be a textbook case. This is because the error in time and the error in the positions are not related at all. However, looking at the error in the accelerations, they are extremely high in proportion to the calculated accelerations. All calculations were checked to ensure that the high error was not due to miscalculation. All

computations were proven correct, so there is in fact that large of an error. This is because the errors in the velocities are related to the error in time.

$$\delta q_x = q(x + \delta x, y) - q(x, y)$$

$$\delta q_y = q(x, y + \delta y) - q(x, y)$$

The two equations above give accurate error when the two variables' errors' are not related, but since the errors in velocities are related to the errors in time the error found for the accelerations are proportionally large. This high error, while seemingly shocking, actually reaffirms the fact that accelerations, velocities, and time are all related. While this is outwardly obvious to most, it is key to confirm the basic principles of physics while learning and experimenting. Even though the actual values for velocity and acceleration are consistent to what we predicted, because their calculated errors are so high they cannot completely be trusted as experimental data unless verified in some other way. Therefore the data that is best to work with are the positions and times.

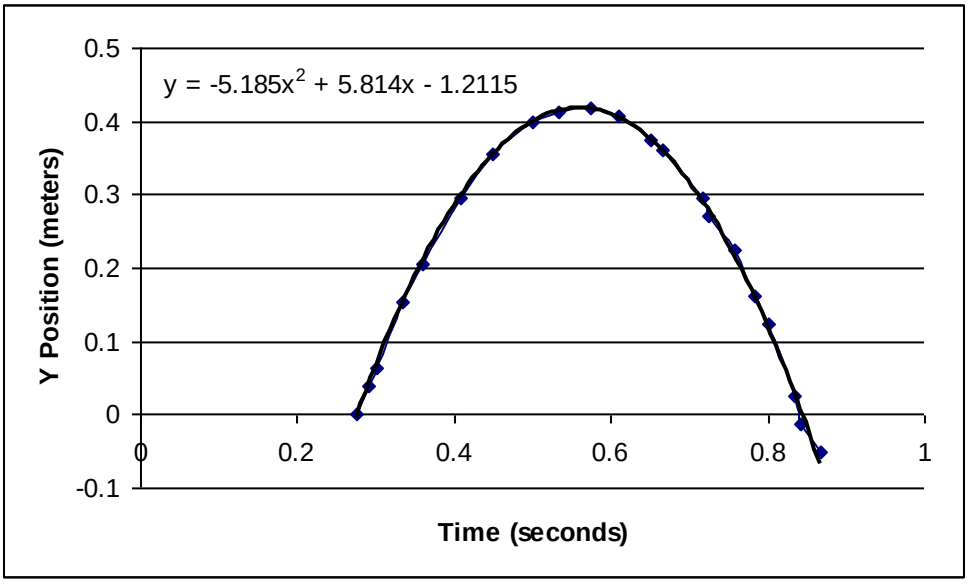

Figure 20: Graph of the Y Position versus time along with a fit of the polynomial shown that best fits the motion. This is the equation of motion is representative of $Y = V_O t + (1/2)\, at^2$, therefore the -5.185 illustrates the acceleration in the Y direction in the equation.

When graphing the Y positions versus the time, what is shown is a parabola like the equation $Y = V_O t + (1/2)\, at^2$. The figure above is the graphical representation of the Y position data and the time. Graphed along side is a parabolic equation that fits best with the data. The equation of the fit is on the graph. Looking at this equation, the number

-5.185 is the "(1/2)a" in $Y = V_O t + (1/2)\, at^2$. Therefore the average acceleration in the Y direction is -10.37 m/s^2. This is higher than -9.8 m/s^2, which is the value of the Y acceleration in a vacuum. This higher value of acceleration in the Y direction is evidence of air drag. A higher acceleration in the Y direction means the object is traveling slower than it would in a vacuum, due to the added negative acceleration. This is evidence of an added force, air friction.

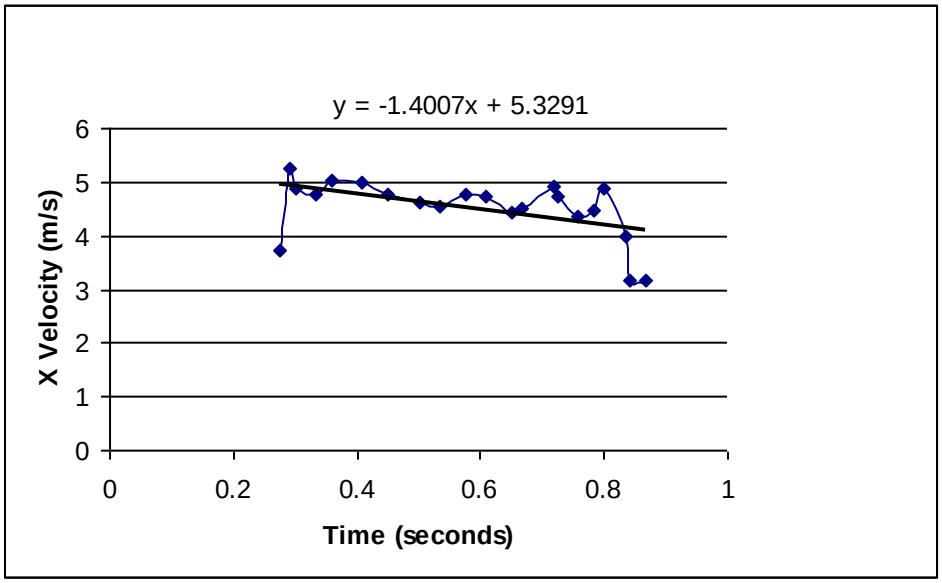

Figure 21: Graph of the X Velocity versus time. In a perfect system, this would be a straight line, meaning the X velocity is constant, since the X Velocity is downward sloping here; this is representative of air friction.

Graphing the X velocity against the time is only further evidence of air friction. In vacuum, The X velocity would be a straight line because it is constant. Here the X velocities calculated show a definite downward slope through the time of projectile motion. The downward slope means the X velocity over time is slowing, meaning there is a force causing it to slow; this force being air friction.

Seeing that there are two separate showings of air friction, we now can compare our calculated X and Y accelerations with theoretical values of X and Y accelerations with air friction. With this comparison, if they are shown to be consistent with that of the theoretical values, then there is more confidence in the actual calculated values considering the magnitude of the error associated with the accelerations.

Using the equations

$$Ma_x = - \gamma D^2 * \text{sqrt}(v_x^2 + v_y^2 v_x)$$

$$Ma_y = -Mg - \gamma D^2 * \text{sqrt}(v_x^2 + v_y^2 v_y)$$ (Taylor, Classical Mechanics 62),

we calculate theoretical values of acceleration using the experimentally calculated values of velocity, and other values like the mass of the ball. The actual calculated theoretical values of acceleration including errors are found in appendix. What is important is to see the theoretical values compared with the experimentally calculated values to see how they balance.

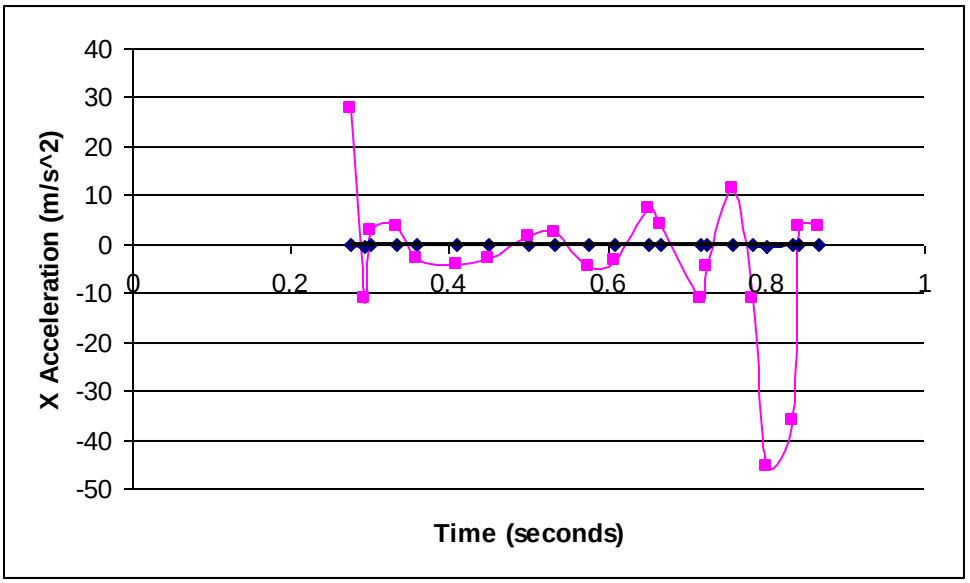

Figure 22: Graph of the X acceleration versus time for both the experimental values and the theoretical values of the X acceleration, where time is held constant. The experimentally values, when graphed pass directly though the theoretical values.

.

The above graph is a comparison of the theoretical values of the X acceleration compared with the experimentally calculated values of the X acceleration graphed against a constant time. The pink line is the experimentally calculated values and the blue line is the theoretical values of the X acceleration. When graphed together, the pink line passes though the blue line. Meaning, the experimental values follow right in line with theoretical values. Of course they will not be exact, because the way we calculated the acceleration is an average acceleration for the time, while the theoretical calculations are supposed to be instantaneous for each velocity. The average of the theoretical values is -0.233 +/- 0.072 m/s^2. Going back to figure, which is a graph of the X velocity vs. time, we see the slope of the line or the acceleration in the X direction is -1.4 m/s^2. However included in the graph are obvious outliers. Once those are taken out, the slope of the

line or the acceleration in the X direction is -0.23 m/s^2. This is exactly the theoretical value of the X acceleration.

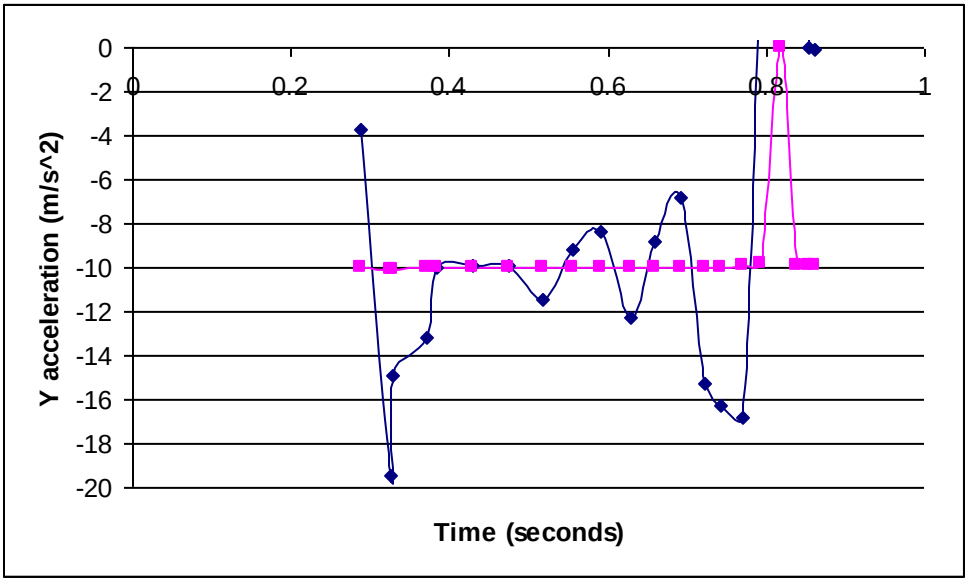

Figure 23: Graph of the Y acceleration versus time for both the experimental values and the theoretical values of the Y acceleration, where time is held constant. The experimentally values, when graphed pass directly though the theoretical values.

Having already compared the X accelerations, the theoretical values of the Y acceleration are graphed above with the experimental values. Again, the experimental values pass directly though the line of theoretical values, where the experimental values are the blue line and the theoretical values are the pink line. This again shows the experimental values follow right in line with theoretical values. Again, they will not be exact, because the way we calculated the acceleration is an average acceleration for the time, while the theoretical calculations are supposed to be instantaneous for each velocity. The average theoretical Y acceleration is -9.98 +/- 0.07.

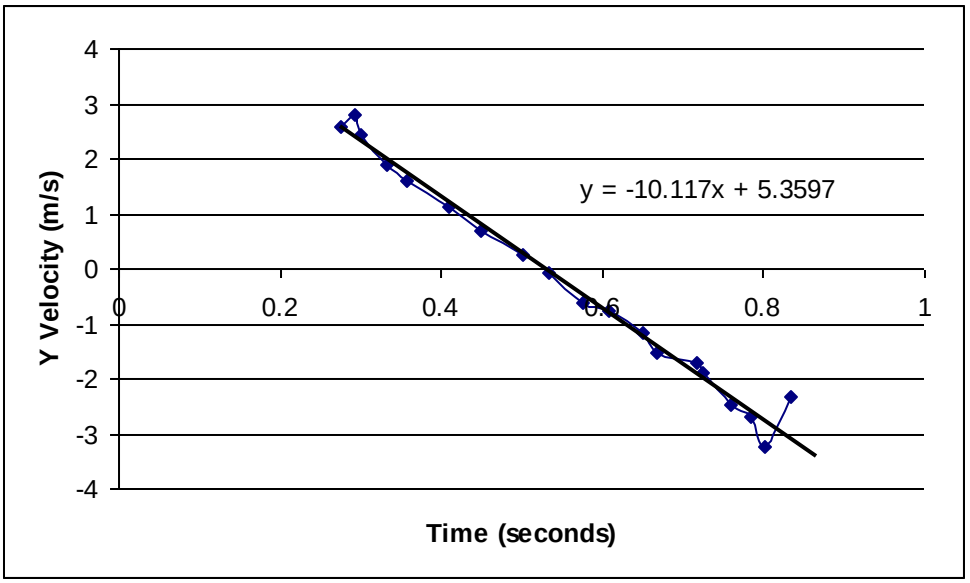

Figure 24: Graph of the Y velocity versus the associated time. The slope of this graph is the acceleration in the Y direction.

Shown in the figure above, when graphing the Y velocity versus the related time, the slope is the acceleration in the Y direction. The slope shown on the graph from the linear fit, the acceleration in the Y direction is -10.117 m/s^2. This is very similar to the theoretical Y acceleration value, so similar in fact that it verifies our experimental calculations for acceleration in the Y direction, also in the X direction from the above calculation.

In order to make sure that our experiment yields sound data, we need to compute and analyze the data for another apparatus to make sure that the analysis and experimentation process is reliable and not a fluke for the catapult. The other apparatus we will use, of course, is the trebuchet.

From the position and time quantities resultant of the trebuchet data analysis, we will use the following equations again to find velocity and acceleration,

$$V= (P_2 – P_1) / (T_2 – T_1)$$

$$A = (V_2 - V_1) / (T_2 - T_1)$$ (Resnick, Halliday and Krane 23),

where V is velocity, P is position, and T is time. To propagate the necessary data error, we will for second time use the equation

$$\delta q = \text{sqrt}(\delta q_x^2 + \delta q_y^2),$$

where

$$\delta q_x = q(x + \delta x, y) - q(x, y)$$

$$\delta q_y = q(x, y + \delta y) - q(x, y)$$

(Taylor, An Introduction to Error Analysis: The study of uncertainties in physical measurements 79)

When all is calculated, the following data set is established.

Position #	**V_x_ (m/s)**	**delta V_x**	**A_x_ (m/s^2)**	**Delta A_x**	**V_y_ (m/s)**	**Delta V_y**	**A_y_ (m/s^2)**	**delta A_y**
1	3.311546	2.364827	44.41563	120.839	4.452997	3.23458	17.86827	156.1172
2	3.978226	1.806073	-7.23468	76.9128	4.814528	2.678624	-8.75555	84.41263
3	4.275945	1.085117	-23.5896	39.96011	4.840972	1.004787	-21.1295	54.23635
4	3.711414	2.186601	8.624439	78.13253	4.491626	1.58507	-25.9621	74.29253
5	3.214407	1.42392	43.67462	79.02372	3.890138	2.219069	-0.26561	92.13758
6	3.998019	1.398764	-15.2682	71.76435	3.62886	1.883403	-5.75621	65.82286

7	4.491187	1.790648	-45.1601	83.29309	3.882374	1.52673	-26.1286	93.47241
8	3.423867	2.305215	23.77874	103.1785	3.412402	1.605552	-0.34143	72.56131
9	2.798613	2.536278	27.69441	83.69521	2.903088	3.147464	-2.29239	95.24963
10	4.018009	1.140516	-3.39366	18.05363	3.403871	0.842195	-12.8493	15.17168
11	3.722406	1.149278	-0.13835	19.73266	2.826622	0.433419	-11.7733	9.443786
12	3.777615	0.578012	-3.53644	16.33283	2.493678	0.661366	-14.3326	11.78183
13	3.712018	0.935041	-0.12813	13.29756	1.942641	0.554967	-7.38368	7.65589
14	3.556268	0.842811	1.558362	9.80546	1.596595	0.309914	-9.90064	6.089757
15	3.700268	0.782679	-0.68809	12.4906	1.265561	0.426795	-14.0098	8.449916
16	3.712018	0.499962	-1.97932	13.47657	0.607075	0.519147	-10.0779	9.813083
17	3.64869	0.51382	-2.2164	10.68321	0.215401	0.457384	-11.5039	7.207194
18	3.571563	0.815089	-0.98027	11.08913	-0.10806	0.458571	-8.62524	6.643466
19	3.482274	0.615763	0.413243	10.92183	-0.64836	0.277496	-9.76085	5.784419
20	3.47359	0.750944	0.040473	9.109017	-0.97011	0.476317	-16.1273	6.502288
21	3.52879	1.064068	-0.89084	11.47899	-1.74707	0.584981	-10.5448	5.160862
22	3.477307	0.368374	-0.7546	7.357381	-2.45099	0.341523	-7.94649	3.771428
23	3.413601	1.034797	-1.56301	8.725256	-3.11056	0.312392	-7.84368	6.283124
24	3.348341	1.202239	-0.47498	16.31422	-3.80909	0.543773	-13.225	13.07278
25	3.205249	0.530901	1.265792	18.06545	-4.15613	0.775144	-11.2178	16.07655
26	3.310719	0.473674	3.799873	50.29325	-4.8566	0.876191	3.065788	16.68145
27	3.284476	0.998302	-20.0214	12.73237	-4.85826	0.636656	59.52131	9.639929
28	3.611693	3.955196	-51.5584	108.6875	-4.61377	0.988733	121.0063	34.01805
29	1.698655	0.019405	0.8101	0.009451	-0.14379	0.019433	-0.06857	0.009269
30	1.729302	0.018094	0.823477	0.008671	-0.19584	0.019206	-0.09326	0.009146

Table 9: Derived quantities of velocity and acceleration from position and time

The X and Y velocities in the table, yet again, are accurate with the system. The velocity in the X direction stays relatively constant, while the velocity in the Y direction starts high, then

decreases on the way up the arc until it there is zero velocity and switches direction downward, from there it increases in velocity until the end of the motion. In a perfect system, the acceleration in the X direction would be zero, and the acceleration in the X direction to be 9.8m/s^2. This is not a vacuum, so we do expect there to be variation in those accelerations but it should be in the vicinity of the expected values. Looking at the values calculated for the acceleration in the X and Y direction, they do perform as expected.

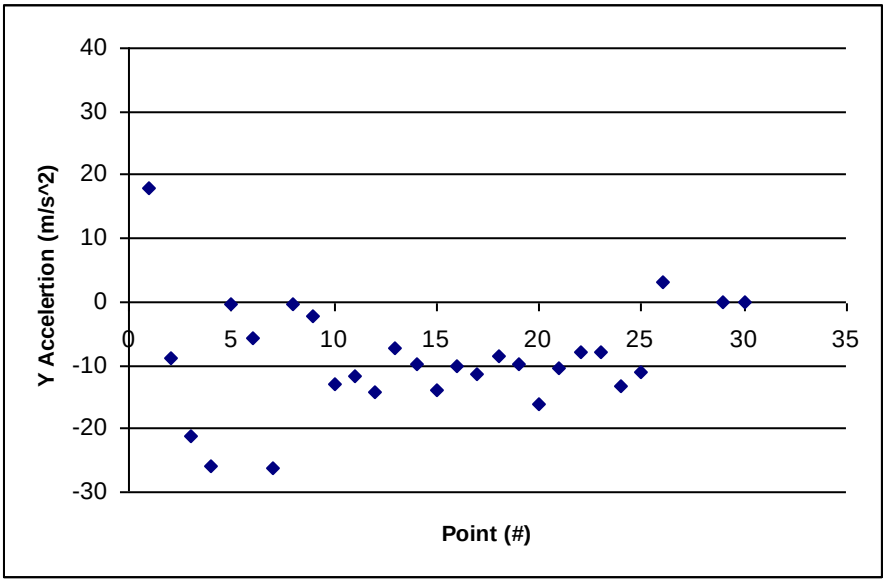

Figure 25: Graph of the Y acceleration. The accelerations as each point are positioned around the zero line.

In the figure above, the Y acceleration at each point is situated around the 9.8 line, which is expected. The graph is similar for the acceleration in the X direction, only the points are positioned around the zero line.

Looking at the error values again, we will see if there are similarities between the catapult data set and the trebuchet. They are expected to be because they were calculated the same way. This is another reaffirmation of the relation of errors. The errors in velocities again seem to be reasonable compared to the actual velocities. This is because the error in time and the error in the

positions are not related at all. However, looking at the error in the accelerations, they are again extremely high in proportion to the calculated accelerations. This is because the errors in the velocities are related to the error in time. This high reaffirms the fact that accelerations, velocities, and time are all related. Even though the actual values for velocity and acceleration are consistent to what we predicted, because their calculated errors are so high they cannot completely be trusted as experimental data unless verified in some other way. Therefore the data that is best to work with are the positions and times.

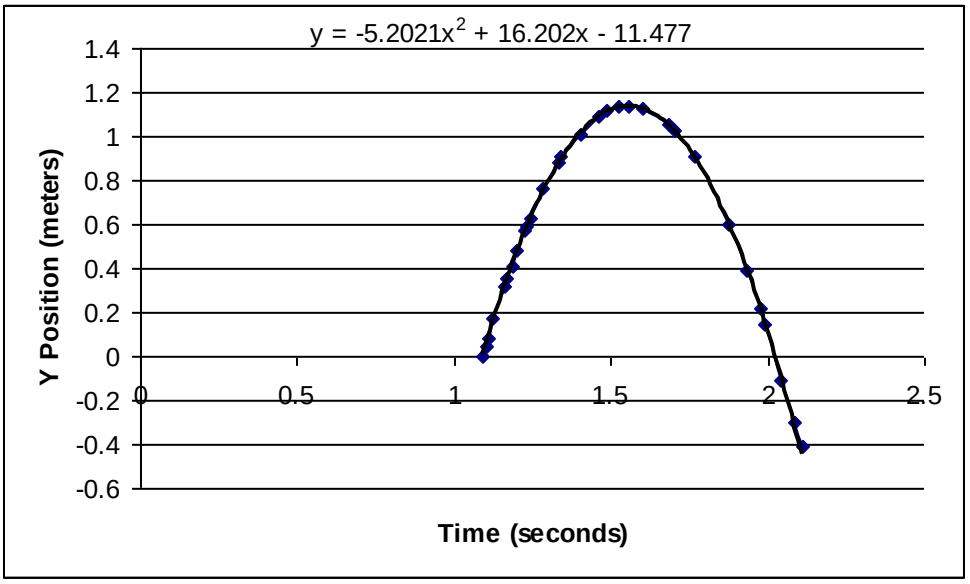

Figure 26: Graph of the Y Position versus time along with a fit of the polynomial shown that best fits the motion. This is the equation of motion is representative of $Y = V_O t + (1/2)\, at^2$, therefore the -5.2021 illustrates the acceleration in the Y direction in the equation.

When graphing the Y positions versus the time, what is shown is a parabola like the equation $Y = V_O t + (1/2)\, at^2$. The figure above is the graphical representation of the Y position data and the time. Graphed along side is a parabolic equation that fits best with the data. The equation of the fit is on the graph and this gives us valuable information about the data set. Looking at this equation, the number -5.2021 is the "(1/2)a" in $Y = V_O t + (1/2)\, at^2$. Therefore the average acceleration in the Y direction is -10.40 m/s^2. This is higher than -9.8 m/s^2, which is the

value of the Y acceleration in a vacuum. This higher value of acceleration in the Y direction is evidence of air drag. A higher acceleration in the Y direction means the object is traveling slower than it would in a vacuum, due to the added negative acceleration. This is evidence of an added force, air friction.

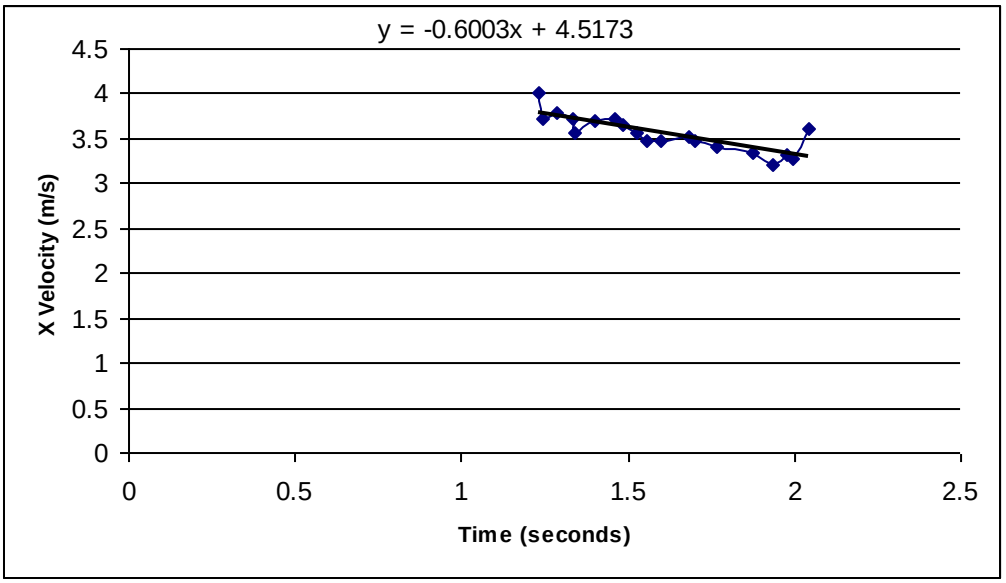

Figure 27: Graph of the X Velocity versus time. In a perfect system, this would be a straight line, meaning the X velocity is constant, since the X Velocity is downward sloping here; this is representative of air friction.

Graphing the X velocity against the time is only further evidence of air friction. In vacuum, The X velocity would be a straight line because it is constant. Here the X velocities calculated show a definite downward slope through the time of projectile motion. The downward slope means the X velocity over time is slowing, meaning there is a force causing it to slow; this force being air friction.

Because there is again evidence of air friction, we again use the equations

$$Ma_x = - \gamma D^2 * \mathrm{sqrt}(v_x^2 + v_y^2 v_x)$$

$$Ma_y = -Mg - \gamma D^2 * \mathrm{sqrt}(v_x^2 + v_y^2 v_y)$$ (Taylor, Classical Mechanics 62),

to calculate the theoretical values of acceleration using the experimentally calculated values of velocity, and other values like the mass of the ball. The actual calculated theoretical values of acceleration including errors are found in appendix. What is important is to see the theoretical values compared with the experimentally calculated values to see how they balance.

(A)

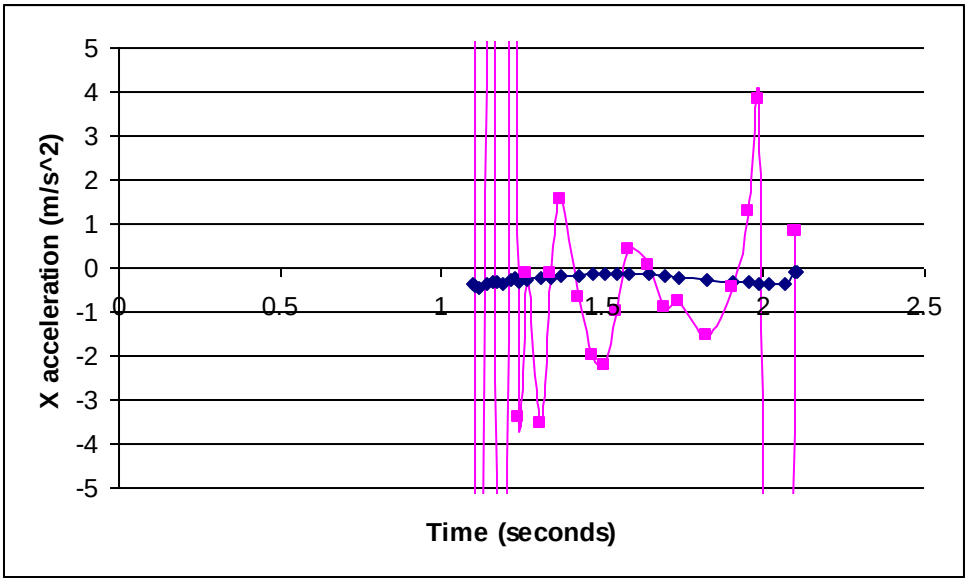

Figure 28: (A) Graph of the X acceleration versus time for both the experimental values and the theoretical values of the X acceleration, where time is held constant. The experimentally values, when graphed pass directly though the theoretical values. (B) Graph of the Y acceleration versus time for both the experimental values and the theoretical values of the Y acceleration, where time is held constant. The experimentally values, when graphed pass directly though the theoretical values.

(B)

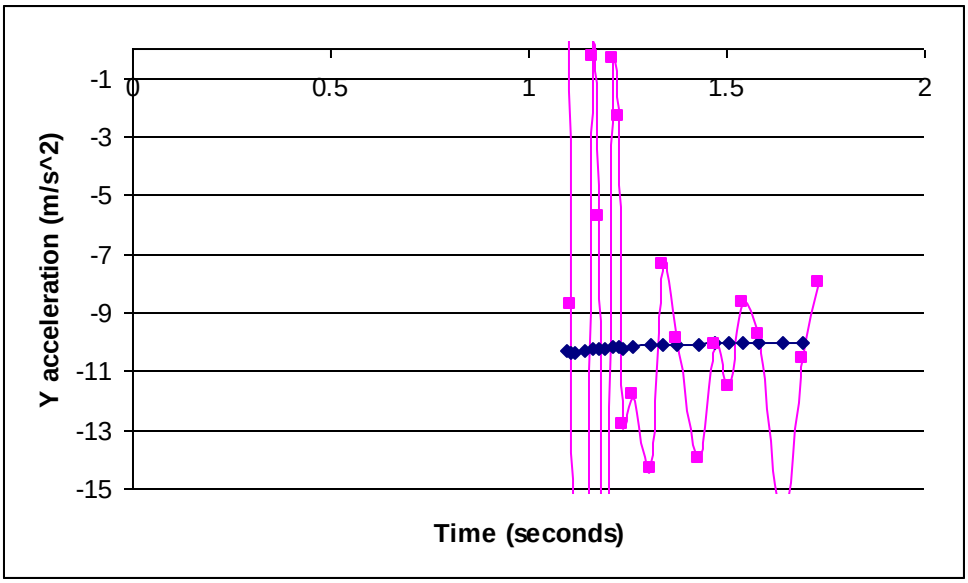

The above graphs are a comparison of the theoretical values of the acceleration compared with the experimentally calculated values of the acceleration graphed against a constant time. The graph labeled (A) is a graph of the theoretical and experimental X acceleration, where the pink are the experimental values and the blue line is the theoretical values. When graphed together, the pink line passes though the blue line. Meaning, the experimental values follow right in line with theoretical values. Again, they will not be exact, because the calculated accelerations are averages of acceleration for the time, while the theoretical calculations are supposed to be instantaneous for each velocity. The average of the theoretical values is -0.262 +/- 0.108 m/s^2. Going back to Figure 21: Graph of the X Velocity versus time. In a perfect system, this would be a straight line, meaning the X velocity is constant, since the X Velocity is downward sloping here; this is representative of air friction. We see the slope of the line or the acceleration in the X direction is -0.6003 m/s^2. However included in the graph are obvious outliers. Once those are taken out, the slope of the line or the acceleration in the X direction is lowered to -0.5195 m/s^2. This does not overlap with the theoretical X acceleration.

The theoretical values of the Y acceleration are graphed above with the experimental values in the Figure labeled (B). Again, the experimental values pass directly though the line of theoretical values, where the experimental values are the blue line and the theoretical values are the pink line. This again shows the experimental values follow right in line with theoretical values. Again, they will not be exact, because the way we calculated the acceleration is an

average acceleration for the time, while the theoretical calculations are supposed to be instantaneous for each velocity. The average theoretical Y acceleration is -10.1533 +/- 0.1939.

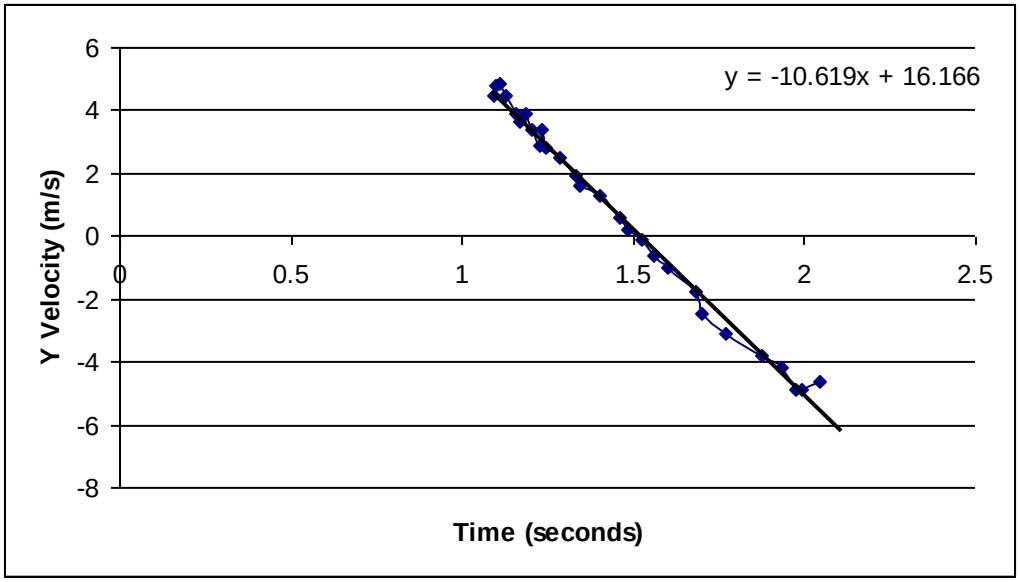

Figure 29: Graph of the Y velocity versus the time. The slope of this graph would then be the acceleration in the Y direction because the derivative of the velocity with respect to time is the acceleration.

Shown in the figure above, when graphing the Y velocity versus the related time, the slope is the acceleration in the Y direction. The slope shown on the graph from the linear fit, the acceleration in the Y direction is -10.619 m/s^2. This again does not overlap with the experimental value of Y acceleration but is very analogous.

We have now analyzed the data for the catapult and trebuchet taken from digital analysis. We have found with the pixel analysis of the each picture that there is a relatively small error for each position and a small error for each time due to the time conversion from slow motion and refresh rate of the computer screen. However, even with these small errors, the error propagates in such a way that the error in the velocities and especially the accelerations are extremely large. The reason for this large error is because of the derivative process. Velocity is the derivative of

position with respect to time and acceleration is the derivative of velocity with respect to time. When we propagate the error though, it becomes large because the error in velocity is related to the error in time. With a different kind of analysis, such as the still image analysis, there is a question whether there will be differences in the way the error propagates. There is this question because the errors in position and time are different for the still image analysis from the digital analysis. With the still image analysis there is a relatively large error in position because of the measurement process with a ruler and human error, however there is no error in time because of the strobe setting. We will use the same process of taking derivatives to find the velocities and acceleration and also the equation

$$\delta q = \text{sqrt}(\delta q_x^2 + \delta q_y^2),$$

where

$$\delta q_x = q(x + \delta x, y) - q(x, y)$$

$$\delta q_y = q(x, y + \delta y) - q(x, y)$$

(Taylor, An Introduction to Error Analysis: The study of uncertainties in physical measurements 79)

in order to propagate the necessary error. Doing the same process will let us see the difference, if any, in the propagation of error of this analysis compared to the digital analysis.

V_x (m/s)	**Delta V_x**	**V_y (m/s)**	**Delta V_y**	**A_x (m/s^2)**	**Delta V_x**	**A_y (m/s^2)**	**Delta A_y**
6.764069	5.204379	4.734848	2.602189	-4.88028	70.4413	-29.2817	64.17068
8.116883	1.711189	4.058442	1.577638	-9.76056	68.31439	-29.2817	52.26609
5.411255	1.530534	2.029221	1.542445	-1.9E-14	51.83756	-10.9806	47.97861
6.087662	4.29931	1.352814	1.577638	-4.88028	47.79579	-10.9806	47.82961

6.764069	1.577638	1.01461	1.533521	9.760562	58.3412	-14.6408	47.30601
5.411255	2.164502	0.338203	1.557206	14.64084	63.22077	-14.6408	48.38128
5.411255	2.164502	-0.3382	1.603527	-4.88028	51.71487	-10.9806	50.28318
8.116883	5.571228	-1.01461	1.670602	-19.5211	52.1753	-10.9806	49.85692
7.440476	2.303759	-1.35281	1.577638	-19.5211	56.98983	-14.6408	55.71221
4.734848	2.602189	-2.02922	2.033725	10.57394	70.2372	-14.6408	57.52938
5.411255	2.164502	-2.70563	1.711189	-3.37866	61.83162	35.38204	87.06175
4.734848	1.634611	-3.38203	2.303759	8.911817	199.531	-15.5418	227.9959
6.200397	4.448658	0.563672	5.601895	10.73662	14.46048	0.976056	20.51565
6.035631	1.649318	0.208125	0.058867	20.09867	27.30542	0.693058	0.196026

Table 10: Derived quantities of velocity and acceleration from position and time

The X and Y velocities in the table are accurate with the system. The velocity in the X direction stays relatively constant, while the velocity in the Y direction shows a definitive progression of starting high, then decreasing on the way up the arc until it there is zero velocity and switches direction downward; from there it increases in velocity until the end of the motion. In a vacuum, we expect the acceleration in the X direction to be zero while the acceleration in Y direction to be a constant 9.8 m/s^2. So in this non-perfect system containing air, we expect the acceleration values to bounce around their respective constant lines.

(A)

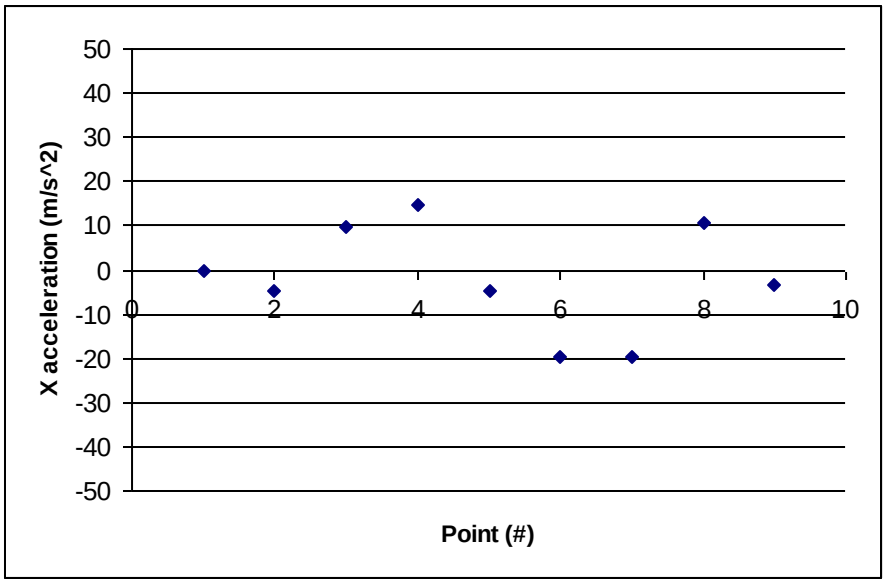

(B)

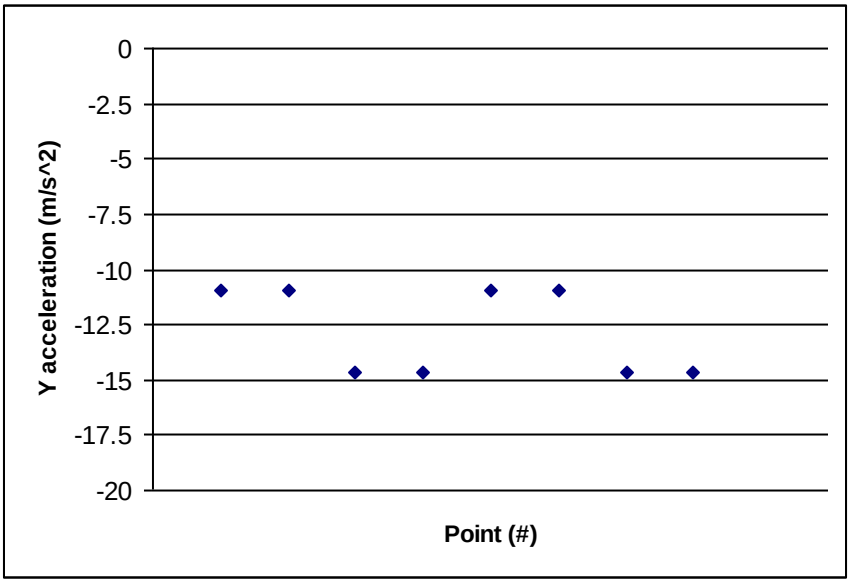

Figure 30: (A) Graph of the X acceleration. The accelerations as each point are positioned around the zero line. (B) Graph of the Y acceleration. The accelerations as each point are close to the 9.8 line.

In the figures above, the X acceleration at each point is situated around the zero line, which is expected. However the Y acceleration is only approximately at the -9.8 m/s^2 line. Looking at the error values again, we will see if there are similarities between here and both the

catapult and trebuchet data sets. Again, the error in the velocities seems reasonable for the calculated values, but the errors in the accelerations are at points four times larger than the calculated value. This is another reaffirmation of the relation of errors. Even though there were different forms of analysis, different reasons for error, and actual difference in the error; the total error propagated in the same way. The error became larger and larger because the relation in errors. If we were to take one more derivative, the error in that is expected to be that much larger than the error in acceleration. Because the errors are so high in acceleration it is again best to look at the data associated with positions and times, until we can again compare the accelerations with theoretical values.

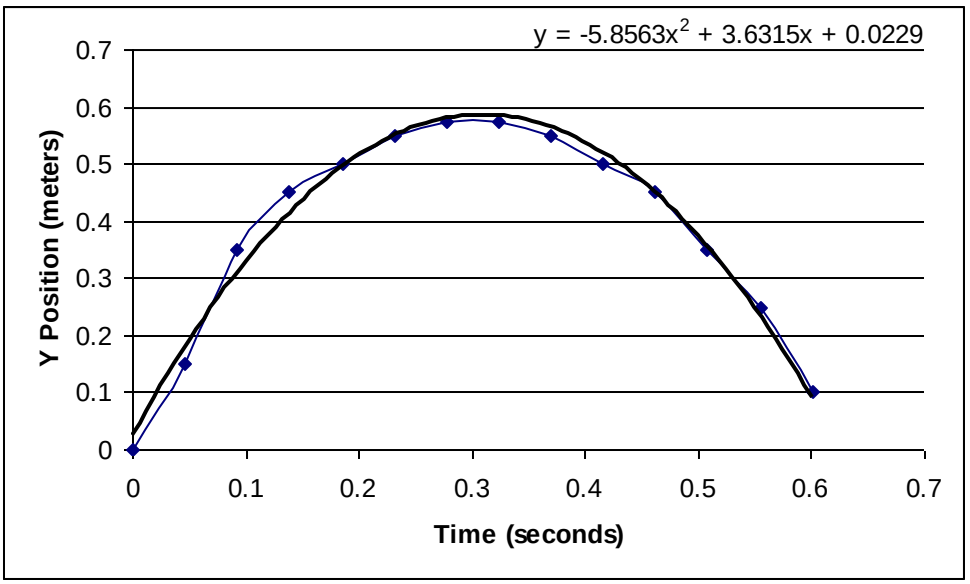

Figure 31: Graph of the Y Position versus time along with a fit of the polynomial shown that best fits the motion. This is the equation of motion is representative of $Y = V_O t + (1/2)\, at^2$, therefore the -5.8563 illustrates the acceleration in the Y direction in the equation.

When graphing the Y positions versus the time, what is shown is a parabola like the equation $Y = V_O t + (1/2)\, at^2$. The figure above is the graphical representation of the Y position data and the time. Graphed along side is a parabolic equation that fits best with the data. The equation of the fit is on the graph and this gives us valuable information about the data set.

However, looking at the figure the data set does not fit the tread line as well as the data did for the catapult and trebuchet. This is because there are simply not as many data points to work with for the tossed ball. With digital analysis there are infinitely many points to work but with the still shot image there are only as many as the strobe and the camera could capture on film. But, fitting the data set with a tread line that is most like the data is still the best way to retrieve information. Looking at this equation, the number -5.8563 is the "(1/2)a" in $Y = V_O t + (1/2)\, at^2$. Therefore the average acceleration in the Y direction is -11.72 m/s^2. This is higher than -9.8 m/s^2, which is the value of the Y acceleration in a vacuum. This higher value of acceleration in the Y direction is evidence of air drag. A higher acceleration in the Y direction means the object is traveling slower than it would in a vacuum, due to the added negative acceleration. This is evidence of an added force, air friction. It would seem that air friction affects the tossed foam ball more than the wooden ball projected from the catapult and trebuchet because the acceleration in the Y direction is significantly larger than it was measured for the catapult and trebuchet.

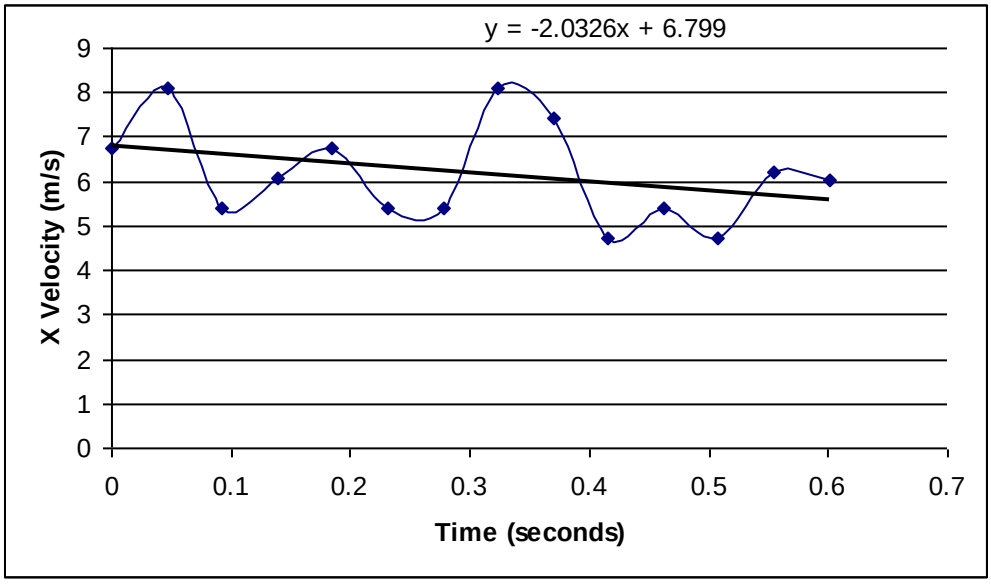

Figure 32: Graph of the X Velocity versus time. In a perfect system, this would be a straight line, meaning the X velocity is constant, since the X Velocity is downward sloping here; this is representative of air friction.

Graphing the X velocity against the time is further evidence that air friction affects the tossed foam ball more than the wooden ball projected from the catapult and trebuchet. Not only does the X velocity have a downward trend which suggests air friction, but the slope of that downward trend is larger than that of the trend of the catapult and trebuchet. The slope of the line is -2.0326, which actually means the average acceleration in the X direction is -2.0326 m/s^2.

Knowing there is air friction against the ball, we can use the equations

$$Ma_x = - \gamma D^2 * sqrt(v_x^2 + v_y^2 v_x)$$

$$Ma_y = -Mg - \gamma D^2 * sqrt(v_x^2 + v_y^2 v_y)$$ (Taylor, Classical Mechanics 62),

to calculate the theoretical values of acceleration using the experimentally calculated values of velocity, and other values like the mass of the ball in order to compare these values to the experimentally calculated values. The actual calculated theoretical values of acceleration including errors are found in appendix. What is important is to see the theoretical values compared with the experimentally calculated values to see how they balance.

(A)

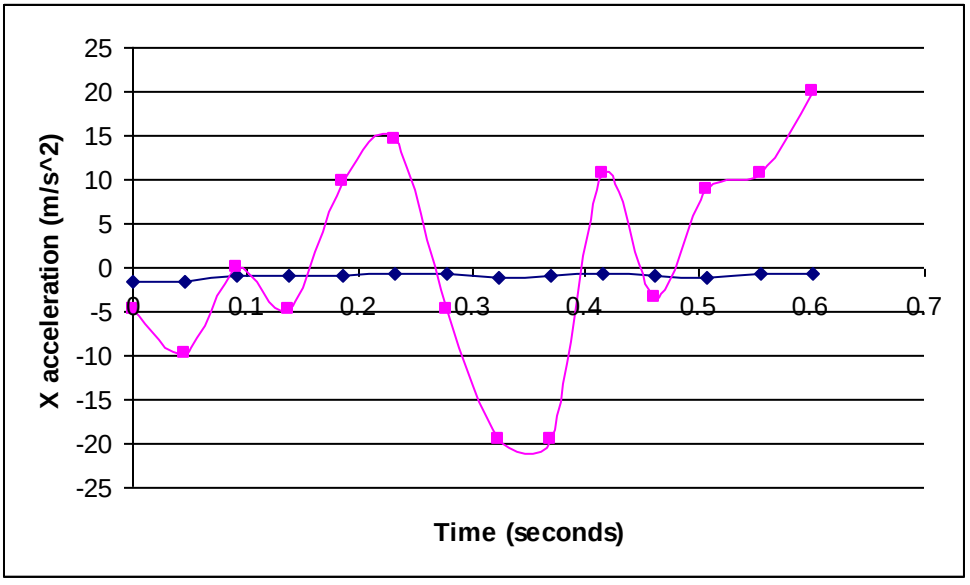

(B)

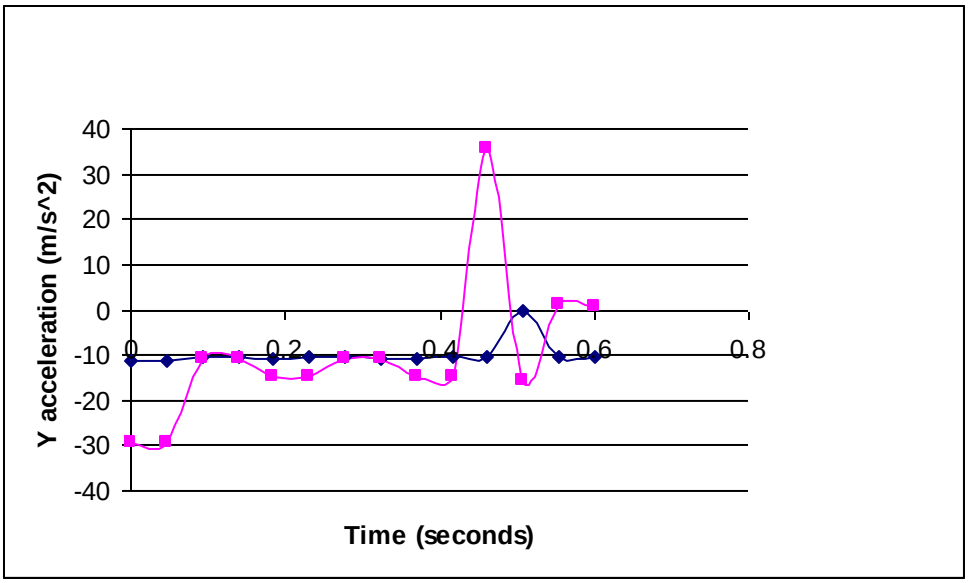

Figure 33: (A) Graph of the X acceleration versus time for both the experimental values and the theoretical values of the X acceleration, where time is held constant. The experimentally values, when graphed pass directly though the theoretical values. (B) Graph of the Y acceleration versus time for both the experimental values and the theoretical values of the Y acceleration, where time is held constant. The experimentally values, when graphed pass directly though the theoretical values.

The above graphs are a comparison of the theoretical values of the acceleration compared with the experimentally calculated values of the acceleration graphed against a constant time. The graph labeled (A) is a graph of the theoretical and experimental X acceleration, where the pink are the experimental values and the blue line is the theoretical values. When graphed together, the pink line passes though the blue line. Meaning, the experimental values follow right in line with theoretical values. Again, they will not be exact, because the calculated accelerations are averages of acceleration for the time, while the theoretical calculations are supposed to be instantaneous for each velocity. The average of the theoretical values is -0.964 +/- 0.518 m/s^2. Going back to figure, which is a graph of the X velocity vs. time, we see the slope of the line or

the acceleration in the X direction is -2.0326 m/s^2. There are no obvious outliers in the graph, so that slope stands. This does not overlap at all with the theoretical X acceleration.

The theoretical values of the Y acceleration are graphed above with the experimental values in the Figure labeled (B). Again, the experimental values pass directly though the line of theoretical values, where the experimental values are the pink line and the theoretical values are the blue line. This again shows the experimental values follow right in line with theoretical values. Again, they will not be exact, because the way we calculated the acceleration is an average acceleration for the time, while the theoretical calculations are supposed to be instantaneous for each velocity. The average theoretical Y acceleration is -10.6321 +/- 0.4612.

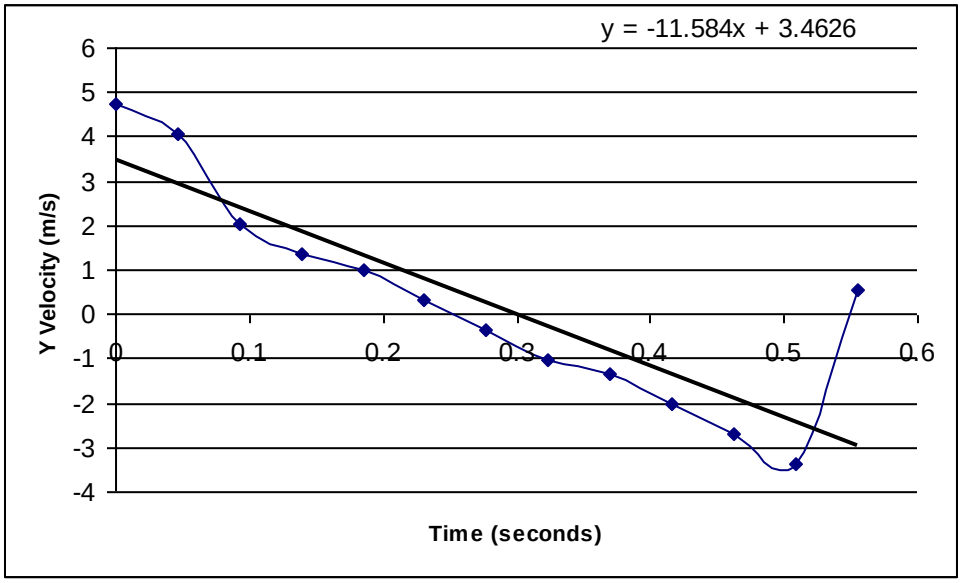

Figure 34: Graph of the Y velocity versus the time. The slope of this graph would then be the acceleration in the Y direction because the derivative of the velocity with respect to time is the acceleration.

Shown in the figure above, when graphing the Y velocity versus the related time, the slope is the acceleration in the Y direction. The slope shown on the graph from the linear fit, the acceleration in the Y direction is -11.584 m/s^2. This again does not over lap with the experimental value of Y acceleration being -10.6321 +/- 0.4612.

The experimental data for the tossed ball does not coincide with the theoretical data as well as the catapult and trebuchet did for their respective data. The reason for this could be the fact that the catapult and trebuchet experimental data fit much better with the tread lines associated with each graph. Each tread line fit illustrated information about data set, and if the data set did not accurately fit the tread line then the information that we perceived, is not as reliable.

It is interesting to see how well each experimental data set fit with its respective tread line. We study this trend though residuals. Residuals being the difference between the datum point and the tread line fit point. Looking at this we can see not only how well each data set fit the tread line, but then if there is a trend of the data to fit the tread line a certain way. We then can normalize all the data to better compare them on an even basis.

time (seconds)	Normalized Time= T/T_h	Converted Y(m)	Normalized height= Y/Y_h	F(T) = Fit	Residual = Y- F(t)	Normalized residual = res/Y_h
0.275098696	0.478279757	0	0	-0.00447	0.004473	0.010666
0.291839488	0.507384883	0.038712	0.092307692	0.043647	-0.00493	-0.01177
0.300084953	0.521720243	0.06452	0.153846154	0.06628	-0.00176	-0.0042
0.333566538	0.579930495	0.154848	0.369230769	0.150938	0.00391	0.009322
0.358552796	0.623370982	0.206464	0.492307692	0.206542	-7.8E-05	-0.00019
0.408525311	0.710251955	0.296792	0.707692308	0.298326	-0.00153	-0.00366

0.450252361	0.782797567	0.35486	0.846153846	0.355127	-0.00027	-0.00064
0.500224876	0.86967854	0.400024	0.953846154	0.399391	0.000633	0.001509
0.533506571	0.927541268	0.412928	0.984615385	0.414504	-0.00158	-0.00376
0.575183649	1	0.41938	1	0.417232	0.002148	0.005122
0.608665234	1.058210252	0.406476	0.969230769	0.406375	0.000101	0.00024
0.650392284	1.130755864	0.374216	0.892307692	0.376573	-0.00236	-0.00562
0.666883214	1.159426586	0.361312	0.861538462	0.359817	0.001495	0.003564
0.717105592	1.246741963	0.296792	0.707692308	0.291415	0.005377	0.012821
0.725351057	1.261077324	0.270984	0.646153846	0.277685	-0.0067	-0.01598
0.758582779	1.318853171	0.22582	0.538461538	0.215203	0.010617	0.025315
0.783569037	1.362293658	0.1613	0.384615385	0.160682	0.000618	0.001474
0.80030983	1.391398784	0.122588	0.292307692	0.120531	0.002057	0.004906
0.833791415	1.449609036	0.025808	0.061538462	0.031509	-0.0057	-0.01359
0.84203688	1.463944396	-0.012904	-0.030769231	0.007802	-0.02071	-0.04937
0.867023137	1.507384883	-0.051616	-0.123076923	-0.06834	0.016727	0.039885

Table 11: Residual data set of the catapult. It includes, the time in seconds, the normalized time, the Y position in meters, the normalized Y position, the fit value, F(t), at each time, the residual value, Y-F(t), and the normalized residual

The figure above is an example of a residual data set. . It includes, the time in seconds, the normalized time, the Y position in meters, the normalized Y position, the fit value, F(t), at each time, the residual value, Y-F(t), and the normalized residual. The fit values, F(t), are points along the fit curve, calculated from the equation of the tread line at each time, t. The residual is then that fit value subtracted from the experimental Y position, Y. Everything is then normalized so it can easily be compared with other residual values.

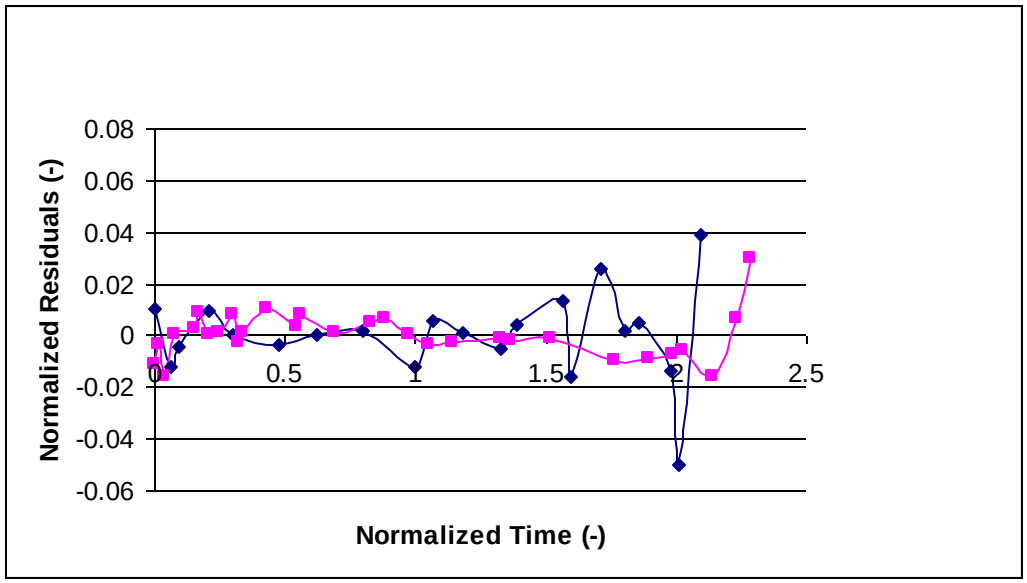

Figure 35: Normalized residuals versus the normalized time for both the catapult and trebuchet. The catapult data is blue and the trebuchet data is in pink.

Shown in the figure is normalized residual data for the catapult and trebuchet graphed against the normalized time. The catapult data is in blue and the trebuchet data is in pink. As shown, the normalized residuals are extremely small, because the lines of data are extremely close to the zero line. But it is also seen that both catapult and trebuchet graphed lines shown the same general trend.

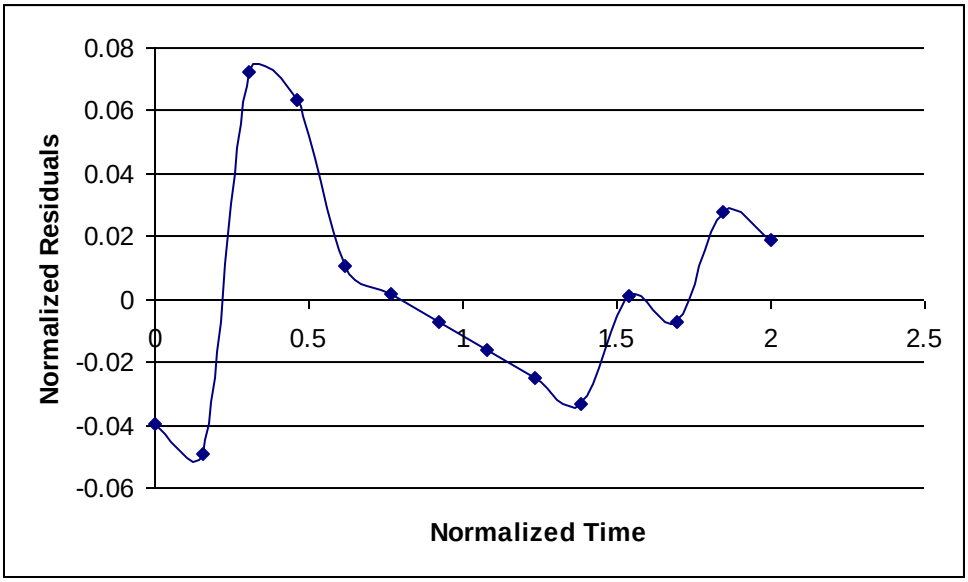

Figure 36: Graph of the normalized residuals of the tossed ball versus the normalized time.

When graphing the normalized residuals versus the normalized times of the tossed ball, it is shown from the figure that the residuals are much higher for the data set of the tossed ball than for the data sets of the catapult and trebuchet. It also shows a different trend for the residuals. But is this just accidental?

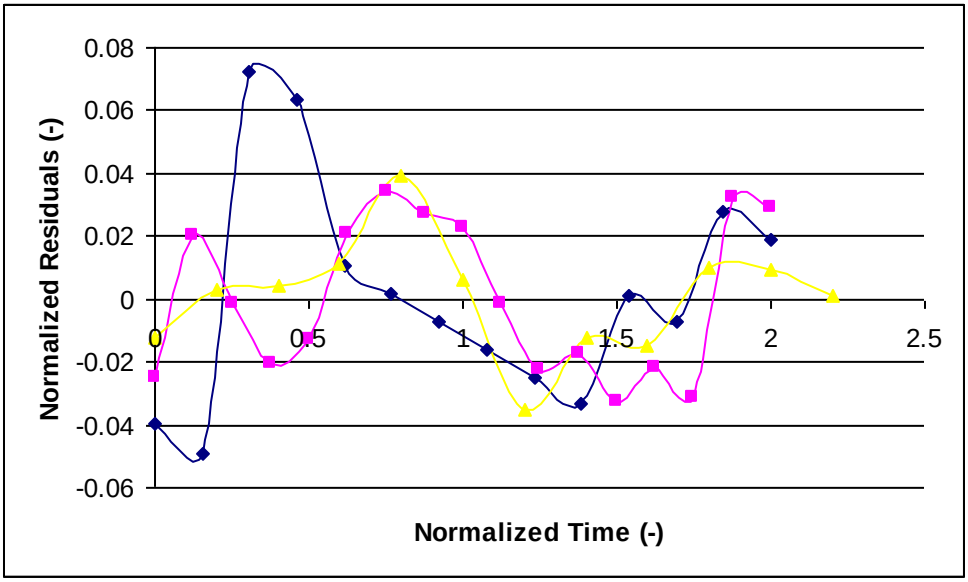

Figure 37: Graph of the normalized residuals of three tossed ball experimental data sets versus the normalized time.

In order to see whether the residuals of the tossed ball data set in Figure were simply a fluke, we must analyze the residual data sets of other tossed ball experiments. The data set in figure was of a tossed ball when the strobe was set to 1300 rpm. What we then did was redo the experiment for the same tossed ball only setting the speed to 800 rpm and 1600 rpm. We then analyzed their respective still shot photos for the position and time, and then found all the residuals data points needed. There data charts are found in the appendix, what is important to see is their general trend. In Figure, we see the general trend of all three data sets compared against each other. As shown, the residuals for each experiment are still much higher than that of the residual catapult and trebuchet, but all three experiments which were tested at different strobe

speeds, show the same general trend of residual data. This trend being different that the trend of the residual data of the catapult and trebuchet. Now, several questions arise. Is the difference because of the difference in analysis? Is the difference because the balls are of different weights and sizes? Is the difference because the difference in firing the projectiles? We can eliminate some of these questions by conducting another experiment.

This experiment has the same procedures but involves different types of balls to see whether the difference in the size, weight, material of the ball was the reason for the different residual pattern. We fire either the catapult or trebuchet (because the catapult and trebuchet where shown to have the same residual trend) off with projectile balls of different size, mass, and material and then use digital analysis to examine the projectile motion of each ball.

Figure 38: Picture of all projectile balls used during experiment. Included is the large foam ball in a metallic covering, a small wooden ball in metallic covering, a small wooden ball, a ball bearing, a marble in metallic covering, and a marble.

The figure above shows the scale of all experimental balls. The large foam ball has a diameter of 95.25 +/- 3.175 mm with a mass of 19.0 +/- 0.10 g, the small wooden ball in metallic

covering has a diameter of 17.8 +/- 1.90 mm with a mass of 2.0 +/- 0.1 g, the small marble ball in metallic covering has a diameter of 16.4 +/- 2.07 mm with a mass of 5.8 +/- 0.1 g, the small marble ball with a diameter of 15.5 +/- 0.50 mm with a mass of 5.6 +/- 0.1 g, and the last projectile is a ball bearing with a diameter of 18.0 +/- 0.1 mm with a mass of 28.4 +/- 0.1 g. We use digital analysis to examine the projectile motion of these various balls, and doing the same calculations as before, continuing until we get to the residual data found before. This is the data we want to compare against all the rest. These balls were all of different diameters, weights, and materials so if they all show the same residual trend, then the trends have to do with either digital analysis or the how the projectile was launched.

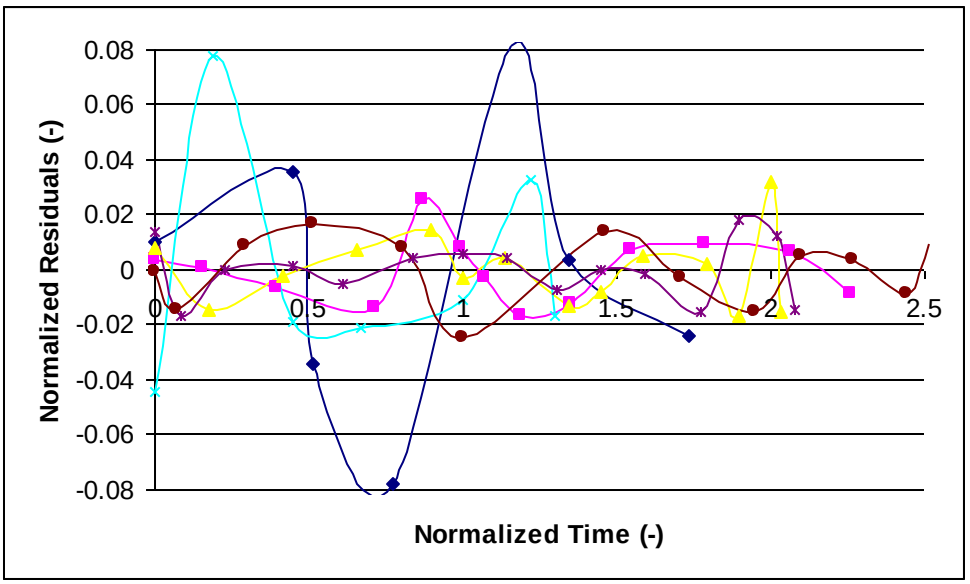

Figure 39: Normalized Residuals versus normalized time for the various balls

Above is the comparison of the residual data of the various balls. The blue line are the residuals of the ball bearing; the pink line is the marble in metallic covering; the yellow is the marble; the teal line is the wooden ball; the purple line is the marble; and the red line is the marble in metallic covering. The purple and red lines were shot from the trebuchet while all others projected from the catapult. While there are some similarities, there are there is not an

overwhelming convincing trend. Meaning the reason for the difference in trends for the original data sets is not in fact the difference in the weights of the balls. If this were the case, then the ball bearing would have shown the residual trend as in Figure, but there were not enough similarities in either graph to warrant the similarity. The reason for the difference in trends was also not the difference in firing the projectile. If the reason for the trend shown in Figure was the fact that it was being thrown from an apparatus then all other balls (including the heavier) would have shown that same trend, but they did not. While we eliminated these two possibilities, there are still two more, the difference in the size of the projectile and the difference in data analysis.

We believe that the difference in residuals trends has more to do with the data analysis than the size of the projectile ball. We have this suspicion because residual trends are the difference in the data figure from the data fit. When using digital analysis, the residuals are much smaller because there are more datum points, so the fit tends to be much tighter when it has more points to work with. When using the physical analysis used in the still shot photos, there is only a set amount of points to work with, being much less than with the digital analysis. Because there are fewer points, the fit is not as exact, leaving a different residual pattern.

In order to test this theory another larger apparatus would have to be built, specifically a larger catapult or trebuchet that could handle larger diameters of balls. Using this larger apparatus, perform the projectile launch and do all the sets laid out before. However, only use one digital analysis. If we launch the large foam ball from this apparatus, and the trend becomes the trend shown in Figure instead of in Figure, then we know the difference in trends is not because of the different size of the balls, but because of the different data analysis. This is beyond the scope and time limit of this MQP because of time constraints, but it can and should be done.

Conclusion – Catapult Projectile Motion

Through this portion of the total MQP project we initially wanted to answer only a few questions. The first being, is this experiment feasible in a high school setting? In the smallest amount of words, yes it is. The equipment used was nothing too extravagant that it would probably already be found in a high school audio visual room, this being the camera. The video camera was the most important piece of equipment, as it allowed us to track the motion of the projectile and from this derive the velocities and acceleration. The other equipment used, the catapult/trebuchet, computer programs, and large room, are already found in high schools everywhere (computer programs found on internet and large spaces) or could be made by high school students (catapult/trebuchet). The build of the catapult and trebuchet by the high school students themselves would be a very enriching activity as it builds the students design skills and creativity. Projectile motion can be shown from basically anything that throws a ball, so no matter the design of the catapult or trebuchet, projectile motion can be shown. This leads in to our other question, is this experiment reproducible? If the lab works once that's fine, but if it cannot be done over and over again, then it cannot be used in a high school setting or really anywhere. The results need to be reproducible in order for the experiment to be valid. As said before no matter the design of the catapult or trebuchet, projectile motion can be shown from the use of the digital video camera. We tested this when we simply tossed the ball in the air with our arm. Projectile motion was easily shown no matter what apparatus initialized the motion. So, yes this experiment is reproducible. The biggest question of the experiment is whether projectile motion, acceleration due to gravity, and air resistance can easily be seen? Foremost projectile motion is easily seen from graphs such as Figure 15: Graphical representation of the projectile motion of the catapult, containing the X and Y positions in meters. This arc is what is explained

to high school students as the projectile arc. Secondly, acceleration due to gravity and air resistance is seen through analysis by derivatives, but with very large error. The reason for this error (propagation of error through derivatives) is accounted for and can be explained to students, but further research is needed to find a data taking method where such error is not present. I believe that only higher tech equipment can produce this, thereby this experiment could not be done in a high school where such equipment is not found. However, I consider this experiment to be valid and even though there is high accountable error. Acceleration due to gravity and air resistance can easily be shown in graphical form where the average acceleration is fitted to the arc of motion. This analysis is the most accurate because the only data being used is the initial data, where positions and times were the most accurate. This form of analysis also uses the fitted equation as an equation like,

$$Y= Y_o + V_o t + .5at^2.$$

This equation is one of the most valuable equations in high school mechanics, so fitting the arc with this equation and matching up values would really be the most beneficial to high school students.

With the broad questions answered, we now look into questions that arose during the experimentation process. What is the best way of recording the motion of the projectile? Plainly, the digital video camera is the best data taking method for this experiment for several reasons. First, the still action shot is not reliable, and the results cannot be viewed right away. This causes a time lapse between data taking and data analysis. In a high school setting where time is extremely valuable, so you want to make sure you are using equipment that promotes efficiency. Secondly, the digital method gives very precise positions of the projectile. In the still shot photo,

there is more room for human error. It is true that the digital camera causes an error in the time scale, but this error is minuscule. The digital analysis of projectile motion is all in all a much more efficient data taking process. Another question that arose during experimentation was whether the wear and tear on the projectile machines affected the projectile motion. The twisted string is affected as the force is increased or over time or even used over time. This is evident in experimentation when the torque and angle did not increase linearly together. Our observations of how the catapult worked also confirmed this fact. As we worked with the catapult over and over again, we noticed that the range of the catapult decreased with time and that we had to turn the strings more and more in order to get back to the range that we once were at. The decaying string affected the force from the catapult and therefore the range of the projectile arc.

Overall, the projectile motion experiment with catapults was a success. We pioneered uncomplicated view of projectile motion using low-tech equipment. Through our analysis of the projectile arc we were able to verify acceleration due to gravity and the effect of air resistance on the projectile. This experiment was such a success that it will be implemented in a public high school beginning in the 2009-2010 school year. This research will continue to help students "find the truth" about projectile motion in the coming years, which is the biggest accomplishment of this project.

Introduction – Corked Bats

Sports science is an area of study that has been gaining popularity within the fields of engineering and physics over the last few decades. Sports science can include, but is not limited to, the study of the equipment used by players and the way that they use it, to optimize performance from both the equipment and the players. This paper will specifically be concerned

with the study of how baseball bat performance is affected by the material that the bats are composed of and whether or not filling a bat with a lighter material (corking the bat) makes a positive or negative difference in performance.

The sport of baseball began in the United States in 1860, but the idea of corking bats has been around for perhaps just as long. In the past twenty-two years four different Major League Baseball players have been suspended for 7 to 10 games each for getting caught using a corked bat, the most recent being Sammy Sosa. (Associated Press, 2003) However, while the use of corked bats is illegal in professional baseball, there is a great deal of information that says this modification should make little to no difference in the performance achieved by batters, except perhaps psychologically.

Many hypotheses have been proposed to explain the effectiveness of this technique and just how it provides an advantage, some holding more scientific weight than others. By examining the mechanics of the ball and bat collision, the standard swing form and speed, and the effect of the size and weight of the bat, we will be able to determine the physical reasons and situations for which the use of cork in a bat does make a difference in a batter's ability to hit the ball farther, if this is in fact the case at all.

To investigate this interaction, as well as the effects on the interaction after modifying a bat in several different ways, a machine was constructed borrowing from the design of a catapult, to swing the bats. While this device was not able to produce bat speeds as fast as those of a professional baseball player, it did swing the bats in a consistent and quick manner and at the same angle each time, following through to the same point each time. Unfortunately, while very consistent and useful at eliminating outside influences on the bat-ball interaction, due to some

other issues with the design which could not be overcome in the scope of this project, the distance traveled by the ball was significantly less than that of a ball hit by a person and the data produced was not conclusive.

Following this setback a second approach was taken to investigate the matter. This time the mechanical response of each bat was tested using Vernier data capture equipment and recording oscillations produced from a ball colliding with a suspended bat. The bats were each suspended from a rotational sensor which recorded how long it would take each bat (wood unmodified, aluminum, and several modified versions of the wood bat) to ring down to rest after the collision as well as the amplitude and period of its movements.

These two different sets of experiments, while not conclusively providing physical evidence for or against the effectiveness of corked baseball bats, did help provide some further information on possible testing methods and mechanical responses of the various bats. In the following section is a background on the physics of baseball bats and the bat-ball interaction, and information about previous research that has been conducted on baseball bat performance in general as well as that involving modifications to bats. After this is an explanation of the methodology of my work and the results obtained, followed by the conclusions and suggestions for further research on the topic.

Background – Corked Bats

What is a Corked Bat?

To cork a baseball bat in the traditional way, you simply drill a hole that is approximately 1-inch in diameter and between 5 to 8-inches deep down the bats axis of symmetry from the top (here defined at the end furthest from the batter when held in the normal way). Then the hole is

filled with some light-weight material (foam, Styrofoam, superballs, cork, etc.) and plugged with another piece of wood in some fashion that would presumably hide the fact that you have tampered with the bat. More recently however, Sammy Sosa was caught using a bat that was corked all the way down in the tapered region of the bat, which has a completely different affect. (Adair, 2002) For this paper we will concern ourselves with the original method and pay notice to the second method only to acknowledge that tests and equations based on that particular method of corking can be expected to have completely different results and are not what we are looking at here.

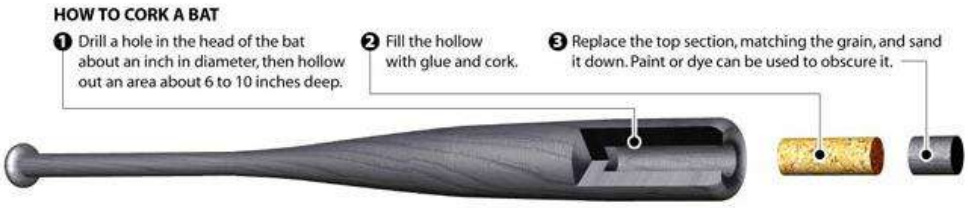

Figure 40: Diagram of the most common way to cork a wooden baseball bat. (Associated Press, 2003)

Figure 40 shows the most common way of corking a wooden baseball bat. Typically the hole that is drilled out can be anywhere from 5/8" to 1" in diameter and between 5 – 10 inches deep. In the modification phase of the project we found that most standard drill bits and setup only allow for 6 inches of depth because the drill bits themselves are only this long.

Why Would I Want to Cork My Bat?

While bat manufacturers do but millions of dollars into research and development in order to produce bats that hit farther with less effort, wood bats haven't changed much lately and a lot of new bat "technology" is in the field of aluminum and composite bats. For those of us

playing softball, little league, or perhaps even college baseball this is great news and we have many new design options to choose from. For professional baseball players, however, this has set a limit on bat performance ability because they are only allowed to use the traditional wooden bats.

In an attempt to overcome this limit some players have made attempts to modify bats on their own. Players believe that corking bats can be advantageous for multiple reasons, but much of this boils down to perpetuated superstition and the argument of being able to swing the bat faster because it is lighter and less of the mass is at the barrel end of the bat. The reason for corking it and not just leaving an empty hole (even lighter) would be the difference in sound from a solid wood bat and higher likelihood of the bat breaking upon impact. (Russel, 2008) Whether this is the case or not, corking bats is at the very least enough of an issue that Major League Baseball has a specific rule against it:

"(A batter is out for illegal action when) he uses or attempts to use a bat that, in the umpire's judgment, has been altered or tampered with in such a way to improve the distance factor or cause an unusual reaction on the baseball."

- *Major League Baseball Rule 6.06(d)* (Associated Press, 2003)

And there are even proposed designs for devices to detect these bats using radar and ultrasound scanners. (P. Gamache, 2007) To understand whether or not this argument holds any truth we must examine how bats work and the bat-ball collision.

Comparing Bats

The two most important factors in a baseball (or softball) bat's performance are its barrel construction and weight distribution. This is because the bat's moment-of-inertia (MOI) directly affects how quickly the bat can be swung in comparison to its weight. These factors affect bat performance so greatly that the National Collegiate Athletic Association (NCAA) has actually set standards for minimum weight and MOI on non-wood bats to limit the performance. (Shaw, 2006)

Barrel construction can differ in many ways for aluminum or composite bats, but for wooden bats it is pretty standard. Therefore we will concern ourselves with the second factor of importance – the moment-of-inertia. The current industry standard for baseball bat testing specifies the following conditions for testing regulation:

"the moment-of-inertia of a softball or baseball bat to be measured with reference to a pivot point on the handle, 6-inches from the knob end of the bat.[6] The bat is gripped at the 6-inch point in a pivot support that allows the bat to swing back and forth like a pendulum. The period (time for one complete pendulum swing) is measured carefully with an infrared triggered timing mechanism." (Russel, 2008)

And from this we get the equation used for the moment of inertia of any bat:

$$I = (T^2 mgd) / 4\pi^2$$

The moment-of-inertia of the bat is important because of something called the swing weight of the bat. The swing weight is the weight that the bat feels like when actually being swung and can differ from the true weight by as much several ounces. A bat's swing weight is dependent not only on the mass of the bat but also on its balance point (Russel, 2008). By adjusting the weight distribution of a bat and its balance point a bat can be made to feel

significantly lighter and therefore enable a player to swing it faster without losing the actual mass that is participating in transferring energy to the ball during collision.

This factor has been the focus of numerous scientific studies and has led to the standardization and regulations in the manufacture of all bats approved for NCAA play. A minimum moment-of-inertia requirement for each specific bat length was established in 2000 by the NCAA to keep the performance of aluminum and composite bats more closely tied to their wooden counterparts. They also introduced the "-3 rule",

> "the weight of the bat (in ounces, without the grip) minus the length of the bat (in inches) must be no less than -3" (Shaw, 2006)

in order to keep the game more fair and safe for the players at this level.

The Physics of It All: Bat-Ball Interactions

When we take a look at the basic mechanics of a bat-ball interaction we have to consider several key factors: the ball's velocity, the bat's velocity, the recoil factor of the interaction, *r*, and the coefficient of restitution or bounciness, *e*, of the bat. If we want to know the speed of a ball after it leaves the bat, the batted ball speed (BBS), we look at the following equations given by Dr. Allan M. Nathan.

$$BBS = v_f = [(e-r)/(1+r)]v_{ball} + [(1+e)/(1+r)]\, v_{bat}$$

Where the recoil factor, *r*, is the ratio of the mass of the ball and the effective mass of the bat.

$$r = m_{ball} / M_{bat}$$

So from knowing how fast a pitch is going once it hits the bat and how fast the bat was going, plus some information about the bat which can typically be looked up through the manufacturer or previous research, we can know how fast a ball will be traveling once it has made contact with the bat in a clean hit. The interactions are typically assumed to take place at the bat's "sweet spot", the place at where the bat has little to no vibration when the ball hits. This eliminates the need to take other factors into consideration for this interaction and simplifies the equations.

Knowing the ball's velocity when it leaves the bat is not the whole story however. We must also consider how fast it will be going before it lands if we are to evaluate how far it will travel and make further comparisons. Here we examine the collision efficiency of the bat-ball interaction, q. The collision efficiency is simply given by:

$$q = (v_f - v_{bat})/(v_{ball} + v_{bat})$$

Therefore the final velocity of the batted ball is

$$v_f = q\, v_{ball} + (1 + q)\, v_{bat}$$

From these simple equations we have all that is needed to make basic comparisons between any two bats. If the bats are modified this would change the recoil factor and/or coefficient of restitution and these changes will be reflected in the resulting equations and all comparisons.

Now if we want to start making predictions and comparisons about how far a batted ball will travel we turn to the range formula from basic mechanics. We must use the adjusted formula for a projectile landing at a different height than its release. So we have:

$R = (v_o^2 sin\theta)/g$ as the general range formula and

$$x = v_{ox}\, t,$$

$y = v_{oy}\, t - \frac{1}{2} g t^2$ are the equations for the x and y coordinates of the balls position upon landing, where time t is given by

$$t = (v_{oy} / g) +/- \sqrt{[(v^2_{oy}/g^2) - (2y/g)]}.$$

And now we have the necessary components to start making our comparisons and predictions once we determine the type of bat(s) being used and look up the corresponding coefficient of restitution for each bat.

What Has Current Research Covered?

Based on these basic physics concepts and some other more detailed concepts (these would only come into play when more advanced equipment is used) a great deal of research has already been done on baseball and softball bat performance. Bat manufacturers want to be able to very precisely test and compare bat performance as they seek to constantly improve the equipment and regulatory commissions want to make sure that the equipment being used remains fair and safe for play.

From within this research we can find some data on bat performance, the effects of bat modifications, and whether there is any scientific validity behind the notion of corking a wooden bat. Theoretical research and current methods of testing tell us the following:

- The traditional method of corking a wooden bat on the top end should provide no more advantage than either sanding down the barrel to slightly narrow it or

choking up on your grip by about 1.5 inches. Both of which are legal methods of improving bat performance in professional baseball. (Russel, 2008)

- Hollowing out the barrel of the bat should be more effective than refilling it with cork or a similar substance.

The current methods of physical testing, however, rely on a human swinging the bat or the bat remaining stationary, while an air cannon fires the ball at a designated speed. Additionally, under these testing conditions bats typically broke after 3 impacts, severely limiting the data that could be collected. (Shaw, 2006)

According to Russel (2008), the "one experiment that has not been carried out to date is a carefully conducted field test. This would involve real players swinging at pitched balls, with careful measurements (requiring multiple high-speed video cameras) of pitched ball speeds, bat swing speeds, hit ball speeds, impact locations, bat moment-of-inertia, and vibrational frequency data." While Russel continues to say that this is a direction that he may move in with his research, currently I can find no evidence that this experiment has been carried out.

The initial focus of this project stems from where the current research leaves off. The intention of this project was to find a way to move a step closer to this field testing while keeping the behavior of the bat more standardize than it is when being swung by human participants yet more realistic in its motion than when pinned in place while the ball is fired at it.

Experimental Procedure – Corked Bats

Construction and Design

This initial design process involved trying to determine the best type of mechanical device that could be used to swing the bat in a manner most similar to that of a human and hit the ball at a designated location and time. Multiple design options were taken into consideration, but given the limited equipment and time available the design selected was that based on the idea of a torsion catapult.

Figure 41: Basic torsion catapult. Taken from www.blog.spectrum-scientifics.com/?p=57

This design was selected and modified for its simplicity, the ability to aim the arm, adjustability, and the ability to obtain a great deal of power compared to the size of the machine. Figure 41 shows a basic torsion-powered catapult. This particular design is only a few inches tall and can fire the ball an average of 15 feet. In picking this design it was hypothesized that if a model this small could fire the ball this distance then when the design was scaled up to appropriate proportions for a bat, the range would also increase proportionally, hopefully transferring energy in a bat-ball collision just as efficiently. By measuring the landing point of each ball, it was hoped that this data would allow us to work backward with the range formula,

finding the velocity of the batted ball, and using this data as a comparison in addition to the physical distance traveled by each ball.

Measurements were taken of a standard wooden bat to be used in experimentation and this was compared the lever-arm of a small catapult to establish scale. From here the design was modified to create a swinging motion instead of a throwing motion. It was built so that the bat would swing roughly around the height of an average batter. In place of the lever-arm a small wooden cradle was constructed to hold the bat so that its position was fixed in relation to the machine and to allow the bat to be changed out with other bats or taken out for maintenance. A representation of this machine can be seen in Figure 42 and Figure 43. Figure 44 is a picture of the completed batting machine without the bat in place.

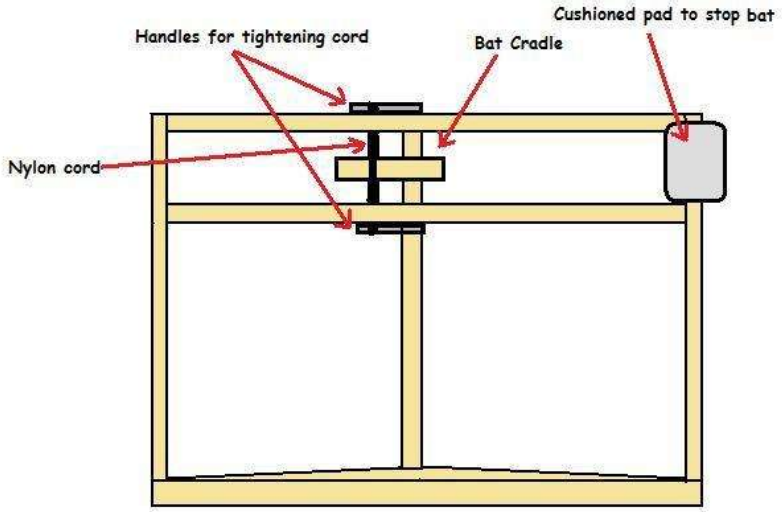

Figure 42: Batting machine design front-view

As can be seen in Figure 42, there was also a cushioned pad made of foam added to place where the bat stops to lessen damage to the bat and lengthen the amount of testing that could be done without breaking the bats.

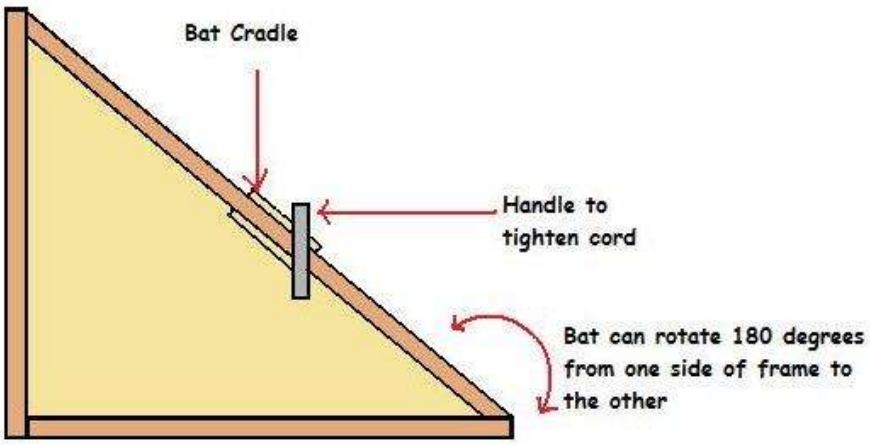

Figure 43: Batting machine design top-view

We see in Figure 43 that, from the top-view, the batting machine resembles the catapult as seen from the side.

In the design of this machine there were several factors to be considered that also arise in the design of a functional catapult. Stability is the first concern, followed by the material used to create the torsion. The issue of stability was addressed by using steel reinforcements screwed in at all the joints, the same type that can be purchased at any home improvement store to reinforce the joints and connections between boards in an outdoor deck. These reinforcements held up to multiple rounds of testing and, while the machine was slightly less rigid than when initially assembled, there were no major issues at any joints. Finding the right material to power the lever-arm, however, was a bit more of a challenge.

Figure 44: Batting machine frame work

Wanting a material that would not have too much elastic deformation a twine was tried, the highest strength available at the store. This material however, broke under less than the amount of tension needed to adequately rotate the bat. Next clothing line and bungee cord were both tested. Clothing line exhibited high amounts of plastic deformation, changing the force being exerted and loosing tension drastically, and then finally just breaking. The bungee cord had far too much elastic deformation and would hardly move the bat. Based on this trial and error to figure out the properties of the materials and corresponding effects the next material tried was a

nylon cord with a test rating of 210 lbs. While perhaps not perfect, this material held up well, exhibited low plastic and elastic deformation, and was able to move the bat at powerful speeds.

To increase the amount of force with which the bat was being swung the cord was run through three times so that three lengths of cord were on either side of the bat cradle to increase the tension. The length of cord and the number of turns used to tighten for each set of testing was exactly the same to keep measurements standardized.

With the tension cord in place the next step was to fit the bat into the cradle. All three bats were within a few ounces of each other in weight so it was necessary to construct a counterbalance to keep any one of these bats level when swinging. This was accomplished by attaching a threaded steel rod to the end of the bat cradle opposite of where the bat comes out. On this rod were two pieces of threaded steel that could be adjusted to different positions on the rod and fastened in place with a bolt, allowing for balance regardless of bat weight. While this cradle and counterweight method might seem to have negative effects on the results of the experiment, Keith Keonig of the University of Mississippi has done conclusive studies showing that how the bat is gripped at the handle does not affect batted ball speed and each bat was adjusted to be level by creating a balance point at the same place on the cradle.

With a functional batting machine completed, the next piece of equipment to design and create was one to be used in placing the ball within range of the bat. Due to the unavailability of an air cannon such as the one used by researchers at UMass Lowell and with no means, within the scope of this project, to create one that would be reliable and accurate, it was decided that a tee, similar to those used in tee ball, would be an effective means of ball placement. While it was understood that this would significantly lessen the batted ball speed, providing a consistent and

measureable speed and constantly ensuring that the ball was within range of the bat was deemed more valuable to reproducibility of valid results.

A standing tee, however, was not as effective as would have been hoped once testing began. To replace the ineffective, traditional-style tee, an air-powered tee was created. This tee, powered by the motor and hose from a standard workshop vacuum, levitated the ball one inch above the tee, rotating towards that bat at a constant speed. An illustration of the air-tee setup is shown in Figure 45 below.

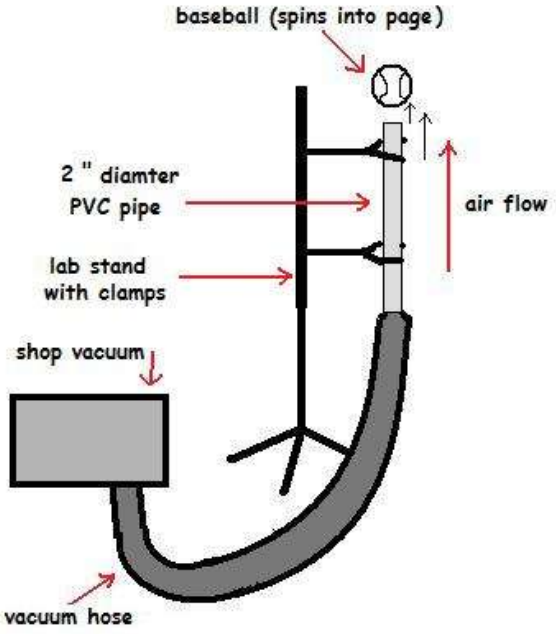

Figure 45: Diagram of basic air-tee construction. The vacuum is on the reverse setting as indicated by the arrows for air flow.

The second set of testing was done using Vernier rotational data sensor to test the mechanical response of the bat with ball impact at low speeds. A hole was drilled through each bat handle, perpendicular to the axis of symmetry, approx 5/8 inches in diameter to allow the bat to pivot from the same point, 3 inches below the knob end of the bat. A high friction string was

used to connect the knob on the bat handle to rotational sensor and measure the angle of rotation and velocity of the oscillations. The rotational motion sensor was connected to a data sensor which linked directly to a computer in the lab and recorded all testing data. A close up view of this setup can be seen in Figure 46 and Figure 47 shows the Vernier Lab Pro© interface.

Figure 46: Close-up view of rotational sensor setup with wooden bat in place.

The Vernier equipment recorded the data automatically into the LoggerPro software installed on the computer, time-stamping each data point in the oscillations.

To send the ball into motion at a consistent speed while allowing room for adjustments, a v-shaped ramp (chosen to keep the ball running along the top edges of the ramp in a straight path) was set up for launching. Marks were made on the ramp at three different launch points and the ramp was affixed to adjustable clamps to allow for data to be taken under varied impact points on the bat and impact speeds (dependent on where ball released on ramp). Figure 48 is a

photo of the entire setup for the data taken with the Vernier equipment. It shows the ramp, rotational sensor, bat and ramp positions.

Figure 47: Vernier LabPro interface that was used with the rotational sensor for data capture during the second phase of testing.

Figure 48: Entire setup for Vernier rotational sensor data collection

In order to modify the wooden bat for testing a hole was drilled down the center of the barrel measuring 1 inch in diameter by 6 inches deep. These dimensions are based on the typical dimensions used for corking bats and the drill bits available for use. The process used mirrored that described in the introduction section.

Testing

Once the batting machine and air-tee were both functional the first step in testing was determining the proper alignment of the two for successful data collection. This was essentially a trial and error process that involved adjusting the angle of the batting machine relative to the ground (settled on 10 degrees so that batted balls followed a typical projectile path) and alignment of the tee and the batting machine relative to one another. (It should be noted that testing was conducted inside so some positions are given relative to a hallway wall) The alignment settled upon placed the center of the tee (ball's midpoint) lined up with a point on the bat 3 inches (7.62 cm) down the shaft. This point was selected because, while the "sweet spot" on a bat is typically considered to be approximately 6 inches (15.24 cm) from the top of the bat, the most powerful hits supposedly come from a point that is a few inches closer to the top. (Sweet Spot, 2007) The back corner of the batting machine (see diagram in figure 10 below) was placed directly against the wall and the front corner of the machine was 9.75 inches (24.77 cm) out from the wall. The floor was then marked off with tape so that all equipment could be replaced in exactly the same positions if the system moved itself out of place or for setting up at the beginning of each testing session.

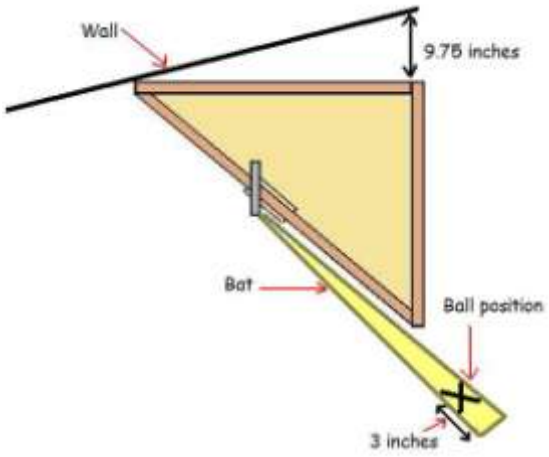

Figure 49: Batting machine alignment

With everything aligned the first phase of testing was for the deterioration of the 210 lb test nylon cord. This was done so that a timeframe for taking data could be established based on how long the cord took to experience noticeable deformation. The first wooden bat, a Louisville Slugger R161, was used for this process. Through this testing it was found that using the cord or leaving it in a position of tension for more than 30 minutes rendered it useless for data taking because after this amount of time a noticeable amount of deterioration in the distance of the batted ball could be seen, all other factors being completely equal. A section of cord that had been in place for 30 minutes was measured and found to be 5.0 cm longer than original length of 339.0 cm.

With this in mind the actual testing for batted ball distance began. There were three bats to be used for this testing, two wooden bats and one aluminum bat (manufactured by Easton). A grid was taped off on the floor with 12inches (30.48 cm) between each strip of tape (from back edge to back edge of each piece), starting 866 cm away from the initial position of the ball. As each ball landed a person watching near the projected landing area taped off the balls landing position. Figure 11 shows a picture of this “live action” scatter plot. With this method of testing

the landing position can be inserted into the range formula and this, combined with the ball and bat collision data, to make comparisons of the batted ball's velocity. This works out because the mass of each bat, the ball, the bat velocity, the ball's initial velocity, the height and x-position from which the ball leaves the tee, and the quality factor all remain the same, therefore canceling each other out for the purpose of calculations.

Figure 50: "Live action" scatter plot created by true landing points of each batted ball during testing

During this testing the bat cradle actually broke while testing the second wooden bat, a Louisville Slugger C271. A design flaw was discovered at this point when it was realized that the point where the knob of the bat was resting in the cradle was dug out directly above a knot in the wood, significantly weakening the structure. Prolonged pressure from the tension of the rope and repeated vibrations being transferred from collisions eventually caused this to break in mid-swing on the 15th hit with the C271 bat. A second cradle was constructed out of the same type of wood and of the same dimensions as a replacement. This cradle lasted the remainder of the testing.

Once the initial data from the wooden and aluminum bats was compared we determined that this was not effective method to find any true difference in performance. Therefore it was decided that proceeding on to the second round of testing was the most efficient use of time.

The second phase of testing was completed with the Vernier equipment. This started with getting the bat properly aligned so that when pushed the system produced smooth oscillations. Once the system was aligned in this manner testing and data collection began. There were several types of tests done with this equipment: the ball being dropped from the same place on the ramp but impacting in two different spots on each bat, the ball hitting the same point on each bat from one of three different starting positions on the ramp, and the ball leaving the same point on the ramp, hitting the same point on the wooden bat, with a different material being used for corking each time.

Measurements were taken of the positioning of all the equipment for these tests to ensure accuracy and some of the measurements are potentially useful for calculations. The end of the ramp was positioned 11.5 cm from the barrel of the bat. During all phases of this testing, the angle of the ramp with reference to the table top of 43 degrees though the height of the ramp was adjusted to change the impact point of the bat-ball interactions. Ball release points on the ramp were marked off at 81.75 cm, 54.75 cm, and 31 cm, the center of the ball lining up with this location upon release for each test. Additionally, a lightweight lubricant was applied to the area of the bat pivoting on the rod to reduce the affects of friction on the bats' oscillations.

Analysis

A graph of the data points representing the landing position of each ball batted by the C161 and the Easton aluminum bat is presented in figure 12. Using the batting machine we did

not find any conclusive evidence of a difference between the two wooden bats or even between the wooden bats and the aluminum bat. While it is given from both field testing and previous research that the aluminum bat should have a further range, we see in the graph that this was not reflected from the testing. This was a serious issue and the motivator for moving on to the Vernier data taking because all the background research shows that the use of an aluminum bat under identical conditions should add noticeable amount of distance to a batted ball.

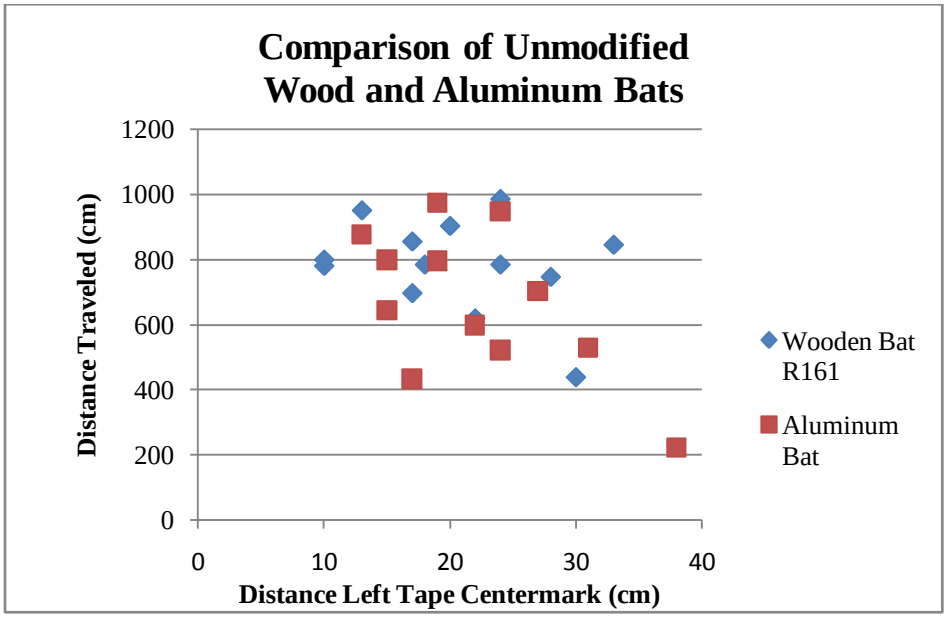

Figure 51: Scatter plot representing the landing position of batted balls from the R161 and Easton aluminum bats

The inconclusiveness of the data however does not discredit the consistency and validity of the experimental procedure. Balls batted with the machine traveled within a range of 6.06 to 9.86 meters and this is only about 10 - 12 % of the distance a typical batted ball in real-world circumstances. Table 1 presents the typical factors that affect the distance traveled by a batted ball. Considering these factors we can assume that the lack of distance produced by the batting machine and air-tee combo can be attributed to several key elements of the design that accumulated in a more drastic fashion than anticipated. These factors include, but are not

necessarily limited to, energy absorbed by the batting machine itself that did not transfer into the bat-ball collision, and using a ball with zero initial velocity. It should be noted, however, that testing was intentionally conducted indoors to remove the majority of these factors so that the bat would be the only major influence indicated here that would have significant affect on the ball distances.

1000 feet of altitude	+ 7 feet
10 degrees of air temp	+ 4 feet
10 degrees of ball temp	+ 4 feet
1 inch drop in Barometer	+ 6 feet
1 mph following wind	+3 feet
Ball at 100 % humidity	-30 feet
Pitch, +5 mph	+ 3.5 feet
Hit along foul line	+ 11 feet
Aluminum Bat	+30 feet

Table 12: Factors that affect the distance traveled by a batted ball (Adair, 2002).

So while it seems that we should be seeing a difference in the wood and aluminum bats from this testing this was not the case. This was the reasoning for moving on to the second method of testing.

With the second phase of testing, while not necessarily saying anything definitive about whether a certain type of bat would outperform a different model, there was a lot more data that showed noticeable difference between the various bats. We see in a comparison of Figure 52 and Figure 53 that there is a noticeable difference in the ring-down oscillations of the two different bats in their unmodified states. We also see that the amplitudes of the oscillations for the

aluminum bat are nearly half that of the wooden bat but that the periods are almost identical. Based on the general concepts of mechanics we could assume from that this indicates that less energy was absorbed by the aluminum bat than the wooden bat, as this energy represents itself in the movement of the bat. Since the energy from the collision was not transferred to the bat we can assume that it was transferred to the ball, which would have, in real world circumstances, provided a higher batted ball speed and therefore a greater distance traveled than the ball that collided with the wooden bat under the same circumstances. These comparisons are based on collisions occurring in the "sweet spot" range, meaning that the bat should experience little to no vibration in a real world collision, but it should also be taken into account that the two bats could have a different sweet spot based on their individual different center of masses.

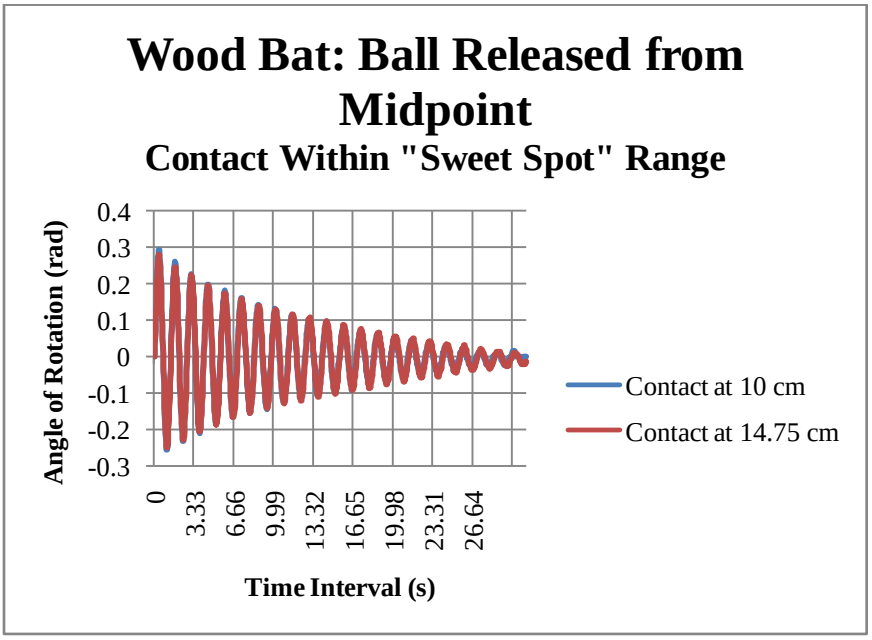

Figure 52: Ringdown of wooden bat R161 after collision in the "sweet spot" range.

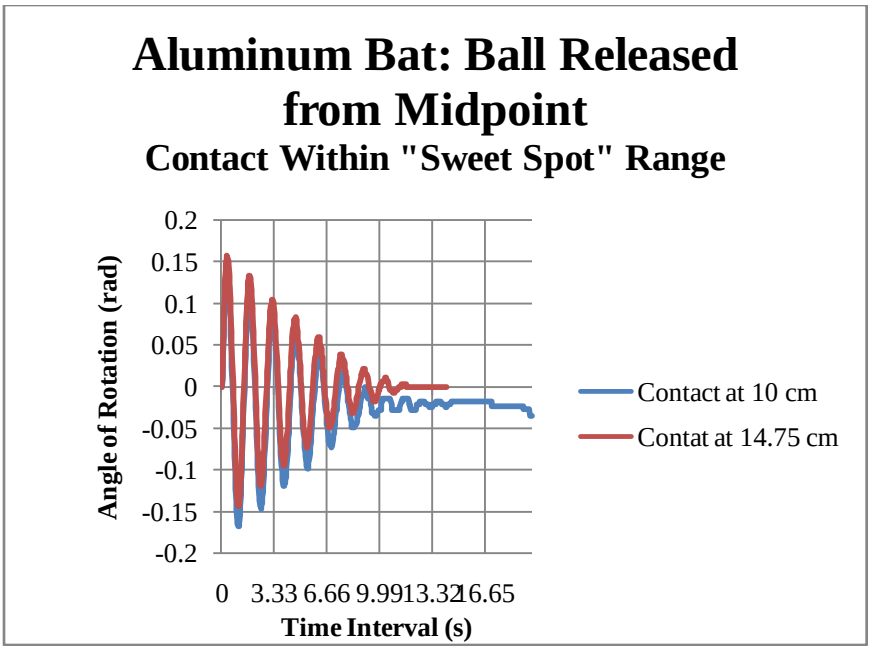

Figure 53:Ringdown of aluminum bat after collision in the "sweet spot" range.

When looking at the two bats individually we see that there is a significant difference in their mechanical responses to the bat-ball collision at this low speed. For the wooden bat we see that, with the ball was released the three different points on the ramp and making contact at the same point on the bat, we have almost identical periods and ringdown times, but a noticeable difference in the amplitude of the oscillations. This can be seen clearly in Figure 54 below.

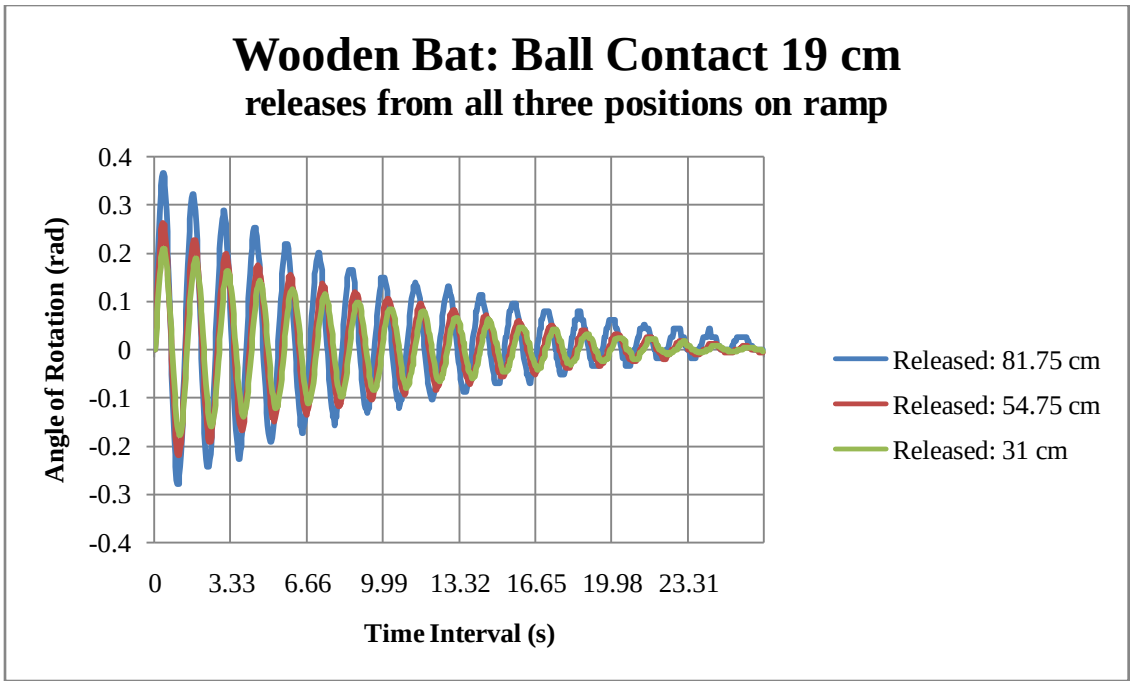

Figure 54: Ringdown of wooden bat with contact 19 cm from end. Ball was released from three differnet positions on the ramp

Figure 55 represents the behavior of the aluminum bat under these same conditions and shows completely different behavior, both in the bat itself and from the wooden bat. We see that when the ball was released at lower points on the ramp (therefore making contact with the bat at a lower velocity) that we have a very quick ringdown of low amplitude. From the uppermost release point on the ramp, however, we see that the amplitude, period, and duration of ringdown are very similar to those of the wooden bat. This indicates that the place where the bat-ball collision takes place does truly matter, but seemingly much more so for the aluminum bat.

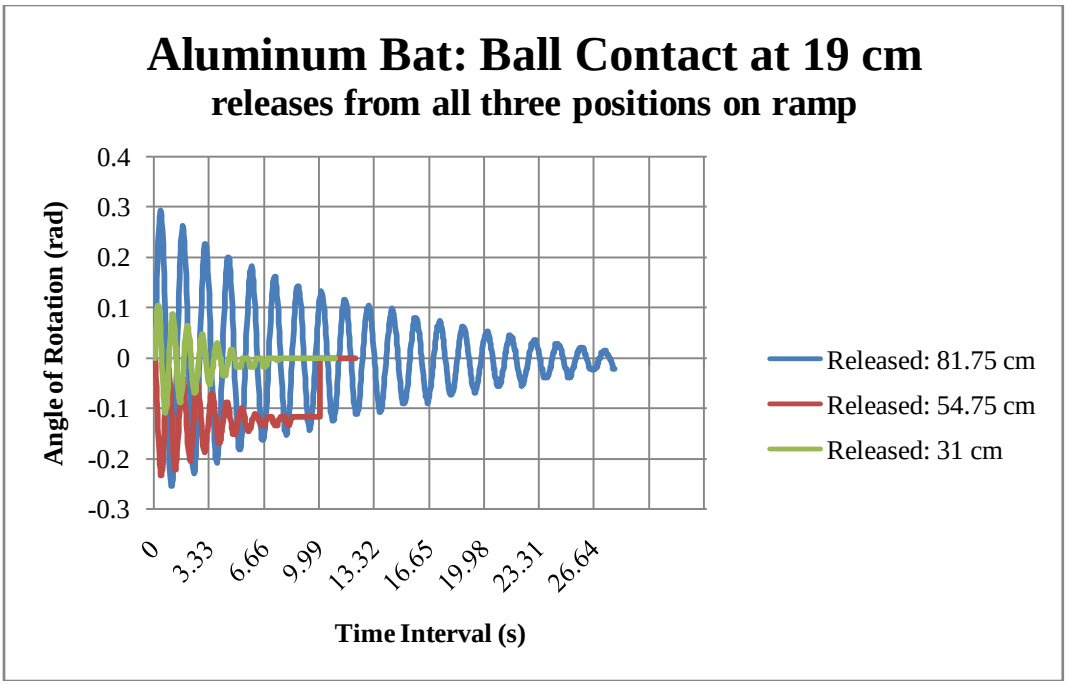

Figure 55: Ringdown of aluminum bat with contact 19 cm from end. Ball was released from three different positions on the ramp.

From here were proceeded to modify the wooden bat and evaluate its response under four different conditions. For each of these four tests the collision point was at 14.75 cm (approximately 5.8 inches) since this is the collision point closest to the indicated sweet spot for this type of bat, in hopes that the best results would be seen here. As we see in Figure 56, collisions were tested on the bat once it was hollowed out and then again when filled with cork, packing foam, and finally steel ball bearings. Each collision was done with the ball being released from the midpoint of the ramp.

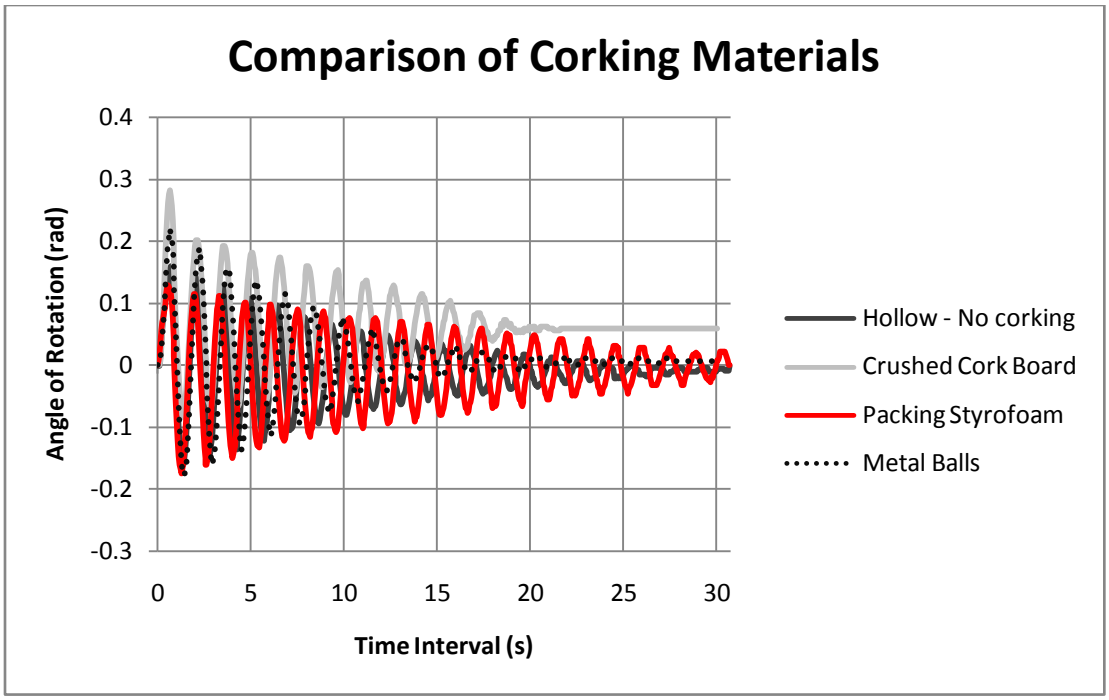

Figure 56: Ringdown of modified wooden bat. Collision at 14.75 cm and ball released from ramp midpoint.

It appears that the packing foam had the best ringdown, followed by the steel balls, hollow bat, and crushed cork board in that order.

Conclusions – Corked Bats

While the experiments done in both phases of testing did not necessarily provide the results hoped for, they still provided a great deal of useful information and laid the ground for some very interesting future experiments. Following are some conclusive observations and recommendations for future work.

With the batting machine testing the entire setup would have to be reevaluated. While energy loss appeared to be minimal in the machine itself, perhaps the lack of initial velocity of the ball is not a trivial issue. The real idea behind creating the batting machine was to try to regulate the swing and eliminate inconsistencies that would occur from a human batter, while not

remaining completely motionless or fixed at a point allowing rotation after impact like many lab tests. Also, there is the potential issue that arises from counter-balancing the bat. If the arm just became an extension of each bat then they would all have the same balance point and this would change the moment-of-inertia. Perhaps in future work an alternative design could be proposed for either the machine itself or the method its interaction with the ball. Perhaps with more sophisticated equipment and more durable sensors there is a halfway point to be found that could provide more substantial results.

In terms of the data collected from the Vernier equipment, we see the definite differences between bats that we expected based on research. We also saw a genuine difference in the mechanical response of each bat based on the location of the collision and the velocity of the ball. This was to be expected since much research has already been done under similar circumstances, but since this approach was significantly different than most of the research and something that can be done with much less sophisticated equipment, the results are certainly not trivial.

For future project work it might be plausible, using the Vernier equipment, to do a more in-depth study of the specific locations on each bat from where the barrel begins to where it ends, and comparing this to all the same points on bats of other materials (aluminum, wood, composite) and with several bats corked in different ways (Sammy Sosa style vs traditional method that was the focus of this paper). While this is certainly not moving in the direction of a more complete field testing, it seems like it could turn up some very interesting results and I feel that Dr. Allan will probably have the field testing aspect covered in the near future.

Introduction – Solid State Tesla Coils

Background

A Tesla coil is a high frequency, resonant, air-core transformer. In addition to the coil, a driver circuit has to be built to run the coil as the standard output voltage for an outlet is 110-120v at 60 Hz. The high frequency aspect of a Tesla coil comes directly from the phenomenon known as resonance. Smaller Tesla coils will have a resonant frequency around a few hundred kilohertz. The larger Tesla coils can have lower resonant frequencies from the tens of kilohertz up to the boundary range of the smaller Tesla coils. (Johnson)

Figure 57: Standard Tesla Coil in Atwater Kent at Worcester Polytechnic Institute

Standard Tesla Coil Driver

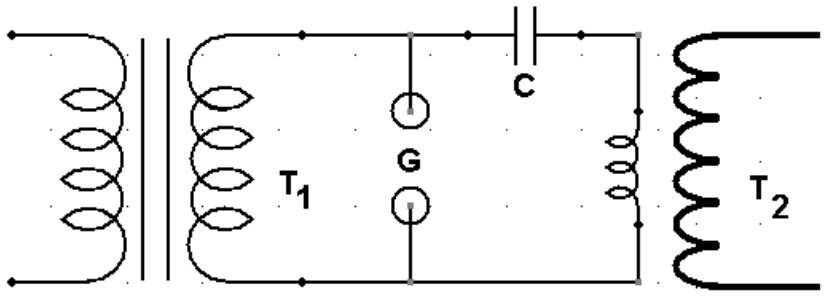

Figure 58: Basic Tesla Coil Circuit

The standard driving force for a Tesla coil consists usually of a high voltage transformer, a capacitor bank, a spark gap, and the primary coil of the Tesla coil. This is shown in Figure 58. T_1 is a high voltage transformer, commonly a neon transformer is used. Neon transformers range from around 1 kV upward to 9 kV or more. (Information Unlimited) While G is a spark gap of a predetermined size that acts like a switch at a certain voltage. While C is the high voltage capacitor bank, this is used to store energy before the spark gap becomes active. T_2 in Figure 58 includes the primary and secondary, however for the driver circuit the primary is the more important component.

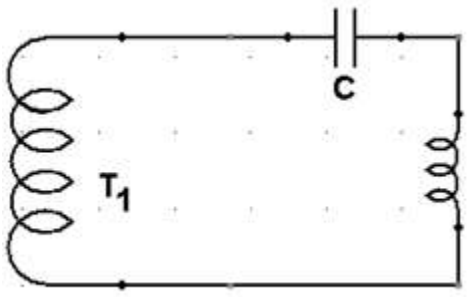

Figure 59: Reduced Circuit while the Capacitor Bank is Charging (Spark Gap off)

By feeding in an AC power source, T_1 will amplify the input voltage source. As seen in Figure 59, the capacitor bank, also known as a tank capacitor, is charging up to oppose the change of voltage across its plates. The inductor is opposing the change of current and storing

energy in a magnetic field. This stores some of the Tesla coil driver's energy into a capacitor and also into the inductor's magnetic field.

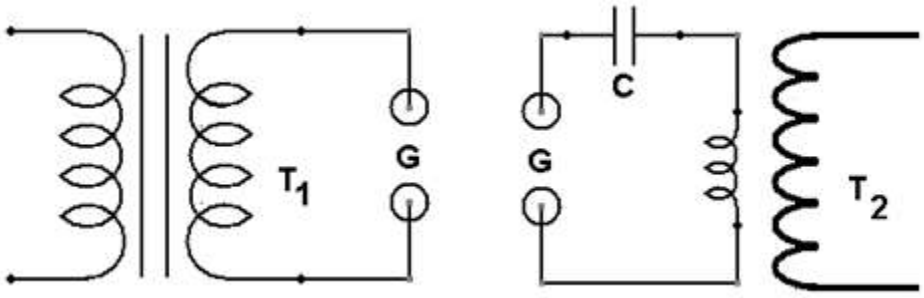

Figure 60: Tesla Coil Driver Circuit (Spark Gap On)

When the spark gap starts to conduct, this effectively creates two circuits as shown in Figure 60. The left side is the creator and maintainer of the spark gap. Usually, an inductor will be placed in line with this to protect the secondary from destroying itself during the arcing process. The right side of the circuit forms the oscillator portion where the circuit is in resonance. The gap provides the majority of the resistance for the oscillator portion.

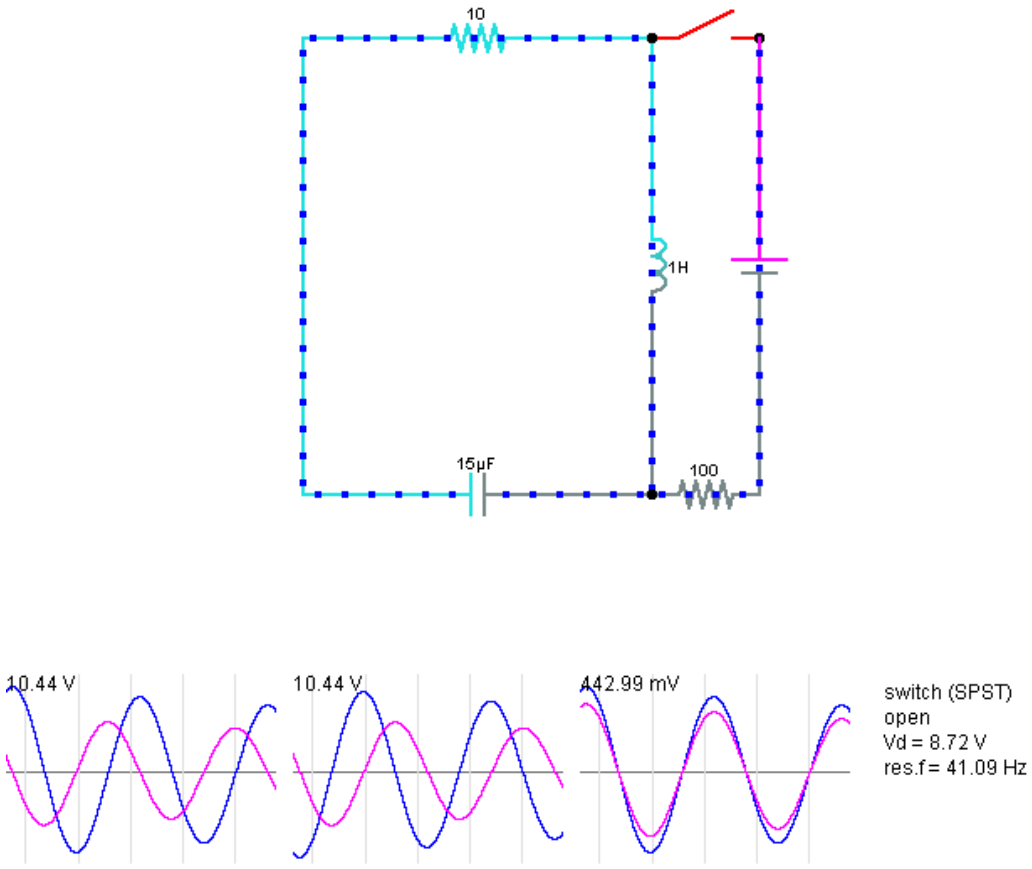

Figure 61: An RCL Oscillator (Falstad)

Figure 61 demonstrates the oscillation principle of the RCL circuit. When the switch is closed, the capacitor and inductor will charge up accordingly. This is similar to the circuit shown in Figure 59, where the circuit is undergoing a charging stage. When the switch is open, the circuit starts to oscillate. It is damped by the 10 Ω resistor, which ultimately creates an envelope effect to the oscillations. When compared to the Tesla coil driver, consider that the gap is the switch. When the spark gap is off, the capacitor and inductor will charge up to the point where the spark gap turns on. As soon as the spark gap is activated, this allows for the oscillation. The primary coil for the Tesla coil is looking for the oscillations, so the relatively slow change in voltage across the primary is insignificant compared to the RCL circuit oscillations. When the RCL circuit is tuned properly, very large voltages on the secondary can be achieved.

Solid State Tesla Coil Driver

A solid state Tesla coil relies upon solid state devices such as bi-polar junction transistors (BJTs) or metal-oxide semiconductor field effect transistors (MOSFETS) to provide the oscillations to control the primary coil. Instead of using an RCL circuit to provide the oscillation, a variable circuit can be built to drive the solid state devices. This is usually done with some sort of timer circuit like the 555 timer or the TL494 pulse width modulation (PWM) controller.

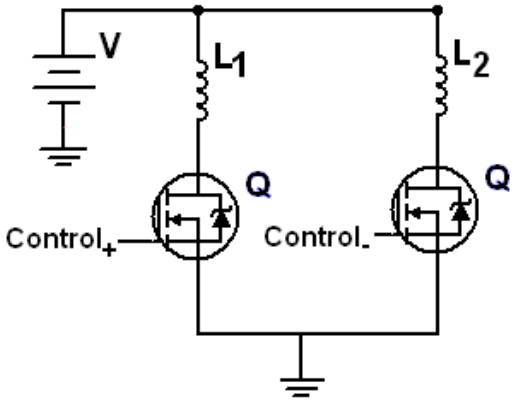

Figure 62 - Simplified Solid-State Driver (Hunt)

Shown in Figure 62, is one of the simplest driver solutions for the solid state Tesla coil. L_1 is wound clockwise around the base of the Tesla coil. L_2 is the primary coil that is wound counter-clockwise around the base of the Tesla coil. This provides a way to capture the negative and positive waves of the Tesla coil despite only technically using a positive voltage source. (Hunt)

The Resonating Secondary of a Tesla Coil with Capacitive Loads

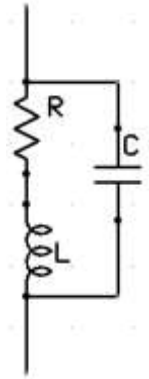

Figure 63: Standard View of a Secondary Coil of a Tesla Coil

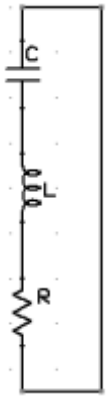

Figure 64: Visually Simpler Model for a Secondary Tesla Coil (Johnson)

As shown in Figure 63, the secondary winding of a coil can be modeled as a resistor in series with an inductor while the capacitor is in parallel with both pieces. The resistance comes from the large amount of wire used to create the secondary windings. The inductance is based on the standard physics of a single layer, tightly wound coil. Figure 64 is the same as Figure 63 but this slightly different look makes dealing with a capacitive load easier.

$$L = \frac{\mu N^2 A}{\ell}$$

Equation 1: Inductance of a Single Layer, Tightly Wound Coil (Nave, Increasing Current in a Coil)

In Equation 1, μ is the permeability of free space, which is equal to $4\pi*10^{-7}$ H/m. N is the number of turns present in the coil. A is the cross sectional area of a winding. This takes into

account how tightly wound the coil is. The ℓ stands for the length of the coil. This not the unwound length of the coil but instead it is the overall length of the windings. A way of viewing this would be to ask how tall the coil is.

The capacitor in this simplified version of the Tesla coil comes directly from the voltage difference between the top and the bottom. When charge is separated in any fashion, this creates a parasitic capacitance. Thus, just like two plates being separated by a small distance, this coil creates a capacitance because of the amount of charge at the top versus the amount of charge at the bottom. If the coil was operated below its resonant frequency, then the empirical formulas created by Medhurst could be used. However, his test set up placed the coil sideways over a ground plane while operating the coil at much lower frequencies than the self-resonant frequency. The Medhurst formulas can be used to give an estimate when the inductance is known with some certainty. (Nicholson)

$$C_{MED}[pF] = K * d[cm]$$

Equation 2: Medhurst's Empirical Formula (Lux)

$$K = \frac{0.28\frac{\ell}{d}}{\ln\left(1+\frac{\ell}{2d}\right)} + \left(\frac{\frac{\ell}{d}+2}{12\pi}\right)^2 + \frac{1.672}{4\pi\frac{\ell}{d}+1} - 0.36$$

Equation 3: Derived Equation for Medhurst's K Constant (Jermanis)

$\frac{\ell}{d}$	K
5.0	0.81
4.5	0.77
4.0	0.72
3.5	0.67
3.0	0.61
2.5	0.56
2.0	0.50
1.5	0.47
1.0	0.46

Table 13: Table of Empirical K values for Medhurst's Equation (Lux)

Using Equation 3, a Medhurst constant can be calculated for a value of $\frac{\ell}{d}$ between 0.1 and 50. Table 13 is a collection of results from Medhurst's original testing. A Tesla coil will often be altered by a toroid or sphere load on the top. This changes the representation of the secondary coil.

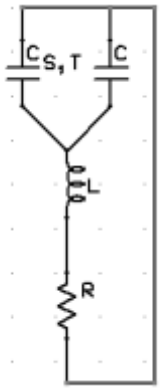

Figure 65: Equivalent Circuit Representation of the Secondary Coil with a Capacitive Load

Figure 65 is the equivalent circuit representation because the load sits on top, while the secondary is usually tied to ground. That allows for the circuit to be modeled as shown in Figure 65.

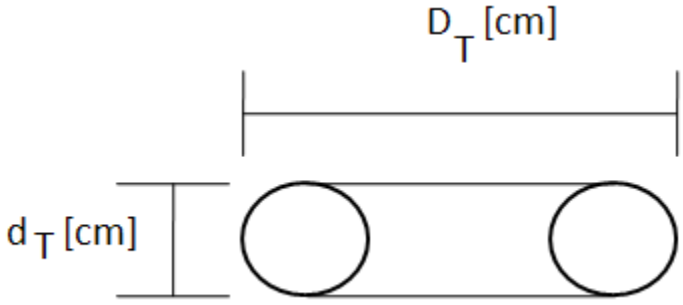

Figure 66: Toroidal Dimensions for Analysis

$$C_T[pF] = \frac{1.8(D_T - d_T)}{\ln\left(\frac{8(D_T - d_T)}{d_T}\right)}$$

Equation 4: Toroidal Capacitance for $d_T/D_T < 0.25$ (Johnson)

$$C_T[pF] = 0.37D_T + 0.23d_t$$

Equation 5: Toroidal Capacitance for $d_T/D_T > 0.25$ (Johnson)

In order to choose the proper formula for calculating the impedance of a toroidal load, a quick check of the ratio between d_T and D_T. These dimensions are shown in Figure 66. For a toroid where d_T is less than 25% the size of D_T, Equation 4 is used. However, another option is where d_T is greater than 25% of the size of D_T. These are a bit more uncommon but yield a simpler equation as seen in Equation 5. These equations are empirical in their nature. Capacitors used commonly in everyday life have tolerance of 20%. Thus, using the empirical formulas for toroids is more than acceptable.

$$C_{S_C}[F] = \frac{4\pi\varepsilon_0}{\frac{1}{r_a} - \frac{1}{r_b}}$$

Equation 6: Capacitance of a Spherical Capacitor (Nave, Spherical Capacitor)

$$\lim_{r_b \to \infty} \frac{4\pi\varepsilon_0}{\frac{1}{r_a} - \frac{1}{r_b}} = 4\pi\varepsilon_0 r_a = C_S[F]$$

Equation 7: Spherical Load Derivation (Johnson)

Equation 7 is the derivation of the spherical load using the spherical capacitor idea. In order to use Equation 6, two concentric spheres need to be used. One sits inside the other with the inner sphere having a radius of r_a while the outer sphere having a radius of r_b. If the outer sphere, which has the radius of r_b is extended out to infinity, this reduces Equation 6 to Equation 7. This can be done if we assume that we originally had an r_b and by its nonexistence, the sphere is theoretically extended the outer sphere to infinity. Thus, instead of a toroid being used, a sphere can take its place on top of the Tesla coil.

Since, capacitance will add when placed in parallel, C_{MED}, the calculated Medhurst empirical capacitance for a coil, can be added to the capacitance of the toroidal or spherical load. If a toroid or spherical load is not present, this reduces the circuit back to Figure 63. With either condition, the resonant frequency of the secondary coil can be found by solving a differential equation.

$$v(t) = L\frac{d^2q}{dt} + R\frac{dq}{dt} + \frac{1}{C}q(t)$$

Equation 8: Differential Equation for Voltage across the Capacitor (Blinder)

$$\frac{d^2q}{dt} + \frac{R}{L}\frac{dq}{dt} + \frac{1}{LC}q(t) = \frac{v(t)}{L}$$

Equation 9: Manipulation of the Series RLC Differential Equation

$$f_0 = \frac{1}{2\pi\sqrt{LC}} = \frac{\omega_0}{2\pi}$$

Equation 10: Solving the Differential Equation Yields the Resonant Frequency

With the result from Equation 10, an approximate resonant frequency of the Tesla coil can be determined using the calculated inductance, the calculated Medhurst capacitance with a capacitive load if desired, and the resistance of the wire itself. When an arc occurs, there will be a resistive load introduced to the system.

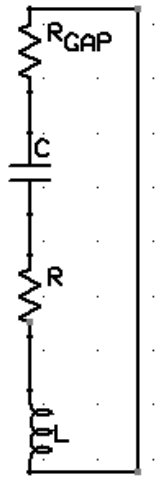

Figure 67: Circuit with Arcing

$$Z_C = \frac{1}{j\omega C} = \frac{1}{j2\pi fC}$$

Equation 11: Capacitive Impedance

$$Z_L = jwL = j2\pi fL$$

Equation 12: Inductive Impedance

As can be seen in Figure 67, the air gap creates a resistance in completing the original circuit. When the circuit is at resonance, Z_L and Z_C, the inductive and capacitive impedances will cancel each other and leave only the resistive loads.

$$20\Omega + \frac{1}{j * 2\pi f * 20pF} + 20000\Omega + j * 2\pi f * 200mH = 20020$$

Equation 13: Sample Resonance Calculation using Impedances [Step 1]

$$\frac{1}{j * 2\pi f * 20pF} + j * 2\pi f * 200mH = 0$$

Equation 14: Sample Resonance Calculation using Impedances [Step 2]

$$-\frac{1}{j * 2\pi f * 20pF} = \mathrm{j} * 2\pi\mathrm{f} * 200\mathrm{mH}$$

Equation 15: Sample Resonance Calculation using Impedances [Step 3]

$$-\frac{1}{20pF} = -4\pi^2 f^2 * 200mH$$

Equation 16: Sample Resonance Calculation using Impedances [Step 4]

$$\sqrt{\frac{1}{20pF * 200mH * 4\pi^2}} = f \cong 79577.5\ kHz$$

Equation 17: Sample Resonance Calculation using Impedances [Step 5]

By following Equation 13 to Equation 17, a resonant frequency can be found through a more rigorous step than the result from Equation 10. The answer is the same, however, whether it is calculated using impedances or whether it is calculated using the derivation from the

differential equation. Using the complex impedance method works for demonstrating that there is a voltage divider set up when the coil is at resonance. Since the complex impedances cancel one another, the remainder is the resistance of the wire and the gap. If the gap has a significantly higher resistance, then almost all of the voltage will be across the gap.

When the gap is not arcing, the resistance is considered to be very high or infinite. This allows a large voltage to accumulate at either end of the coil. At a sufficiently high enough voltage, the break down voltage, the air will start to conduct electricity and act as a resistor of a smaller value. The model presented here is a simplification of all the elements that can be considered with a Tesla Coil's secondary stage and the science behind arcing.

Methodology – Solid State Tesla Coil

Design – Secondary Coil

The design process focused around creating the secondary coil. Two near-identical coils were made with the specification of using a 0.0889 meters (3.5 inches) outer diameter PVC tube as the base. The inner diameter of the PVC is 0.0762 meters (3 inches) and is what a retailer specifies their product by. The outer diameter was the major specification to be worked with while 1 meter was chosen for a coil length to make calculations easier.

$$K = \frac{0.28\frac{1}{0.0889}}{\ln\left(1+\frac{1}{2*0.0889}\right)} + \left(\frac{\frac{1}{0.0889}+2}{12\pi}\right)^2 + \frac{1.672}{4\pi\frac{1}{0.0889}+1} - 0.36 = 1.44$$

Equation 18: Design Calculation of Medhurst's Constant for the Coils

$$C_{MED}[pF] = 1.44 * 8.89[cm] = 12.8\,pF$$

Equation 19: Medhurst Capacitance Calculation for the Coils

Following Equation 2 and Equation 3, and substituting values in for ℓ and d yields the results demonstrated in Equation 18 and Equation 19. While the Medhurst capacitance has been

calculated, the inductance still needs to be calculated to find the natural resonant frequency. Knowing that we are using the standard American Wire Gauge (AWG), there are specific values associated with each gauge. I selected 22 gauge wire for my Tesla coils based on availability in the Physics department.

AWG	Conductor Diameter (Inches)	Conductor Diameter (Millimeters)	Ohms Per 1000 Feet	Ohms Per 1000 Meters	Maximum Frequency for 100% skin depth of a solid conductor copper
22	0.0254	0.64516	16.14	52.9392	42 kHz
23	0.0226	0.57404	20.36	66.7808	53 kHz
24	0.0201	0.51054	25.67	84.1976	68 kHz
25	0.0179	0.45466	32.37	106.1736	85 kHz
26	0.0159	0.40386	40.81	133.8568	107 kHz
27	0.0142	0.36068	51.47	168.8216	130 kHz
28	0.0126	0.32004	64.9	212.872	170 kHz
29	0.0113	0.28702	81.83	268.4024	210 kHz
30	0.01	0.254	103.2	338.496	270 kHz

Table 14: American Wire Gauge Basic Information (PowerStream Technology)

Shown in Table 14 are a few selected wire gauges. A common gauge to use is 30. As can be seen from the above, there is a maximum frequency before 100% skin depth of a solid conductive piece of copper. The skin depth acts as additional impedance to the flow of current and is clearly frequency dependant but it also shares a component with how the wire is constructed. As easily deducible from the chart, thinner allows for a higher frequency to pass through before the wire is overcome by the maximum skin depth. Once that frequency is exceeded then R_{AC} is no longer equal to R_{DC}.

With 22 AWG wire, a problem arises. Tesla coils normally operate at high frequencies in the 100 kHz range. Also, to be able to reproduce sound with the Tesla coil it is necessary to have a resonant frequency of at least 44,000 Hz. This is dictated by the Nyquist frequency, where the

Nyquist frequency is determined by 2 * the highest frequency to be reproduced. Humans are normally quoted as being able to hear from 20 to 20,000 Hz. (Choudhary) However, the upper threshold of human hearing is normally regarded as 22,000 Hz. This creates our base point for the Nyquist frequency and yields the 44,000 Hz. (Bressoud). Thus, the design will have to take into account that R_{DC} is not equal to R_{AC}.

$$R_{DC} = 52.9392\frac{[\Omega]}{1000\ [m]} * \frac{1\ [m]}{0.00064516\ [m]} * 0.0889\pi[m] = 22.9\Omega$$

Equation 20: DC Resistance without Insulation Adjustment

$$L = \frac{\mu N^2 A}{\ell} = \frac{4\pi * 10^{-7} * 1550^2 * \pi * 0.04445^2}{1} = 18.73\ mH$$

Equation 21: Calculated Inductance without Insulation Adjustment

$$R_{DC} = 52.9392\frac{[\Omega]}{1000\ [m]} * \frac{1\ [m]}{0.0006858\ [m]} * 0.0889\pi\ [m] = 21.6\ \Omega$$

Equation 22: DC Resistance with Insulation Adjustment

$$L = \frac{4\pi * 10^{-7} * 1458^2 * \pi * 0.04445^2}{1} = 16.58\ mH$$

Equation 23: Calculated Inductance without Insulation Adjustment

Equation 20 and Equation 21 describe the DC resistance and inductance that would be present if the insulation around the wire is not taken into account. As can be seen in Equation 22 and Equation 23, there is a difference between the DC resistances of 1.3Ω while there is a difference of 2.15 mH between the two inductances.

$$f_{RES} = \frac{1}{2\pi\sqrt{LC}} = \frac{1}{2\pi\sqrt{0.01873 * 12.8 * 10^{-12}}} = 325{,}047\ Hz$$

Equation 24: Resonant Frequency Calculation without the Insulation Adjustment

$$f_{RES} = \frac{1}{2\pi\sqrt{LC}} = \frac{1}{2\pi\sqrt{0.01658 *\ \ 12.8 * 10^{-12}}} = 345{,}480\ Hz$$

Equation 25: Resonant Frequency Calculation with the Insulation Adjustment

As shown in Equation 24 and Equation 25, a small difference in the inductance makes for a significant swing of the resonant frequency. This would prove to be a challenge for a standard Tesla coil design process since that system has to be tuned to oscillate at the proper frequency. However, with a solid state driver, the frequency can be shifted over an entire spectrum.

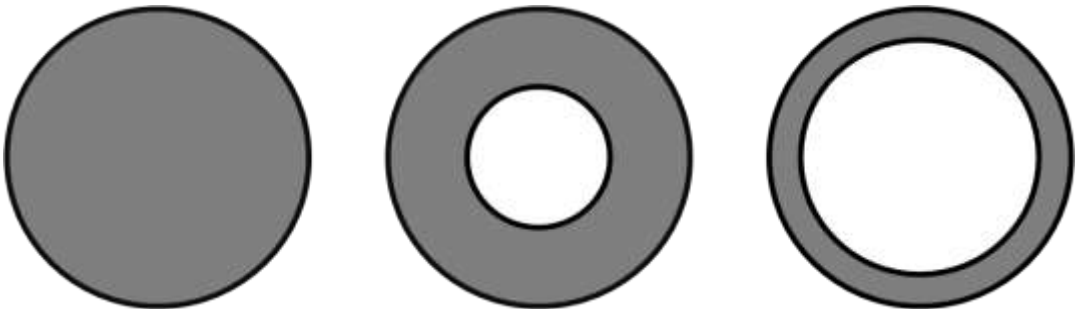

Figure 68: Visualization of the Skin Effect

$$\delta = \frac{1}{\sqrt{\pi f \mu \sigma}}$$

Equation 26: Skin Depth Equation (Ludwig and Bogdanov)

$$R_{AC} \approx R_{DC} \frac{r}{2\delta}$$

Equation 27: Approximate Value of R_{AC} (Ludwig and Bogdanov)

$$R_{AC} \approx \frac{1}{2\pi r} \sqrt{\frac{\mu \omega}{2\sigma}} \pi N d$$

Equation 28: Alternative Calculation for R_{AC} without including R_{DC} Explicitly (Jones)

As shown in Figure 68, the conducting electrons as the frequency increases tend towards the outside. This is the skin effect. When examining a piece of wire, the skin depth can be calculated to find how much of the conductor is conducting. The numerical definition of the skin depth is when there is a reduction in the current density to e^{-1} (≈37%) from the surface current density. Equation 26 can be employed to find the skin depth (δ). An approximate value of the AC resistance can be then found from Equation 27. That is because when Equation 27 was derived with a basic assumption of high-frequency conditions. Equation 28 is an alternative method that

first calculates the resistivity per unit of measure. Then the πNd come into play as the length of the wire in meters that gives the total resistance.

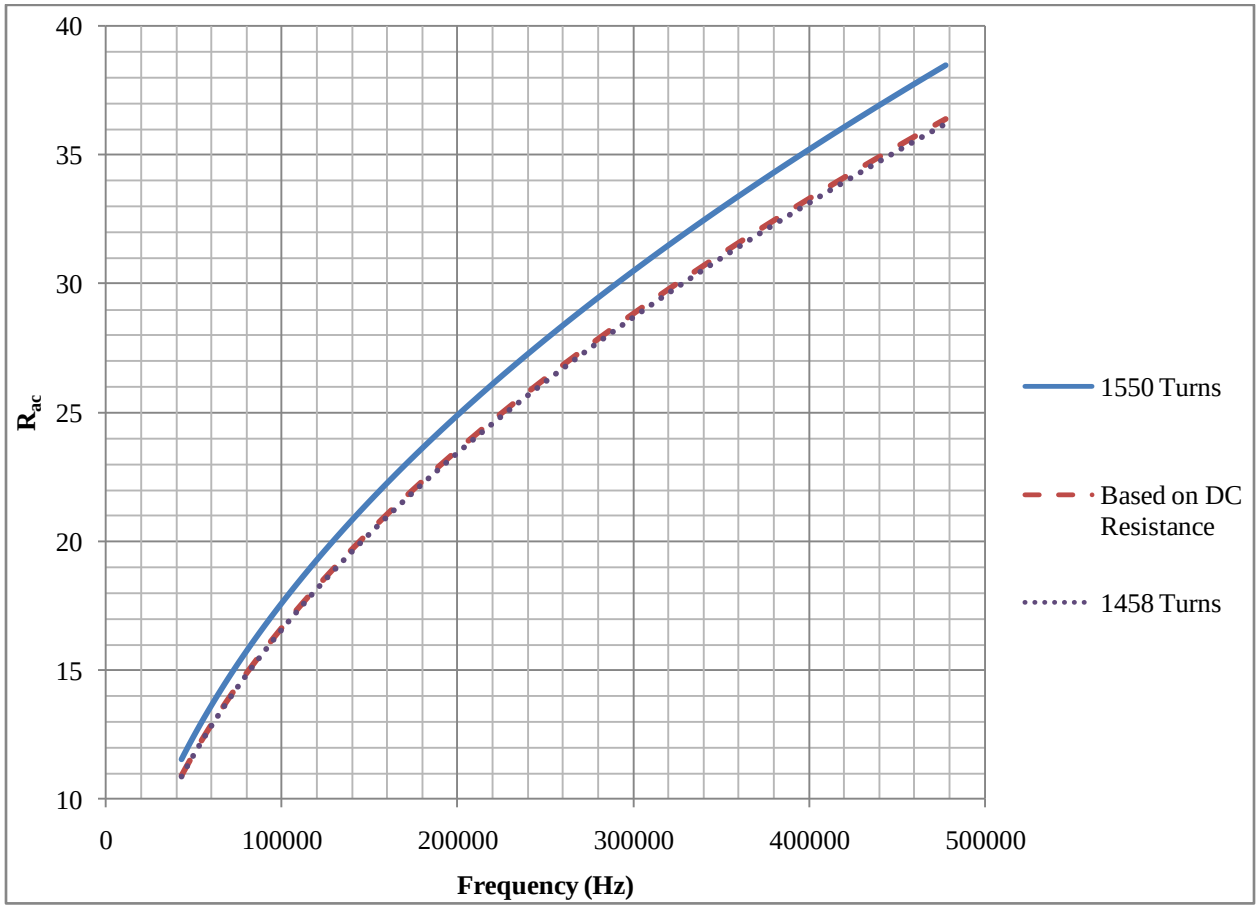

Figure 69: Plot of R_{AC} from 42 kHz to 475 kHz

As can be seen from Figure 69: Plot of RAC from 42 kHz to 475 kHzFigure 69, the calculated value for R_{AC} varies widely but the most interesting point is that the expected value for R_{AC} drops below the calculated 21.6 to 22.9 Ω to almost 10 Ω at 42 kHz. Thus, the effective resistance at either resonant frequency calculated before in Equation 24 and Equation 25. The takeaway from this analysis is that a resistance of at least 21.6 Ω will be present at the output.

Another aspect of coils that is interesting to calculate is the quality of the coil. The quality of a coil can range anywhere from 0 to infinity but typically will not be above 1000. This is because the resistance of the coil.

$$Q = \frac{\omega L}{R} = \frac{\mathrm{X_L}}{\mathrm{R}}$$

Equation 29: Calculating Quality of a Coil

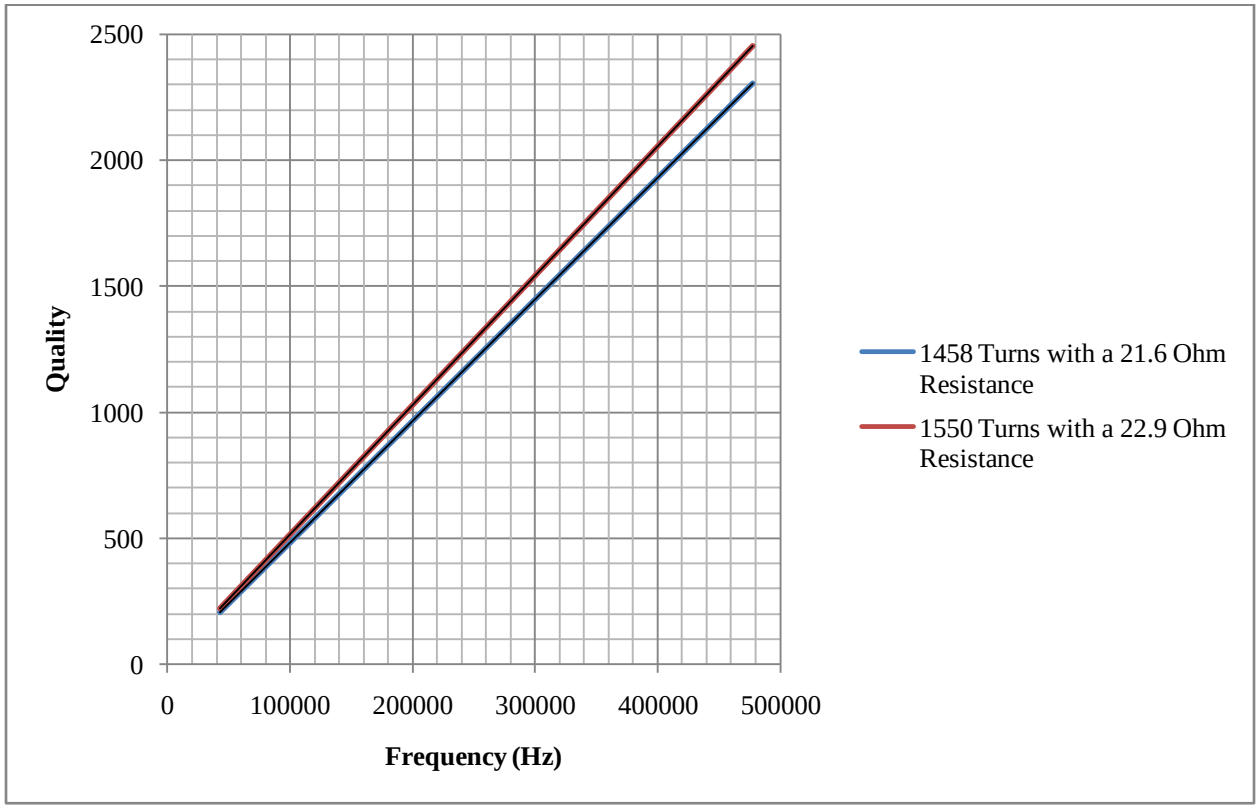

Figure 70: Graph of Quality from 42kHz to 475kHz

Figure 70 shows the quality of a coil while being swept over a large frequency range. Since the DC resistance is considered to be constant, the equation yields a clearly linear result. However, as the frequency increases, there will be additional losses in the coil that are not graphed here. Thus, the quality of the coil will more than likely not reach the projected levels in the graph. This is still a valuable tool in understanding what is happening with the coil and some things to expect.

Design – Solid State Driver

While a solid state driver for a Tesla coil can be as easy as making a 555 timer with a power MOSFET, the task of making a PWM version is a bit bigger of an undertaking. The decision came early on in the design process that because of the lack of multiple electrical engineers and electrical-based physicists on the project that finding a driver circuit and modifying it would be the best option.

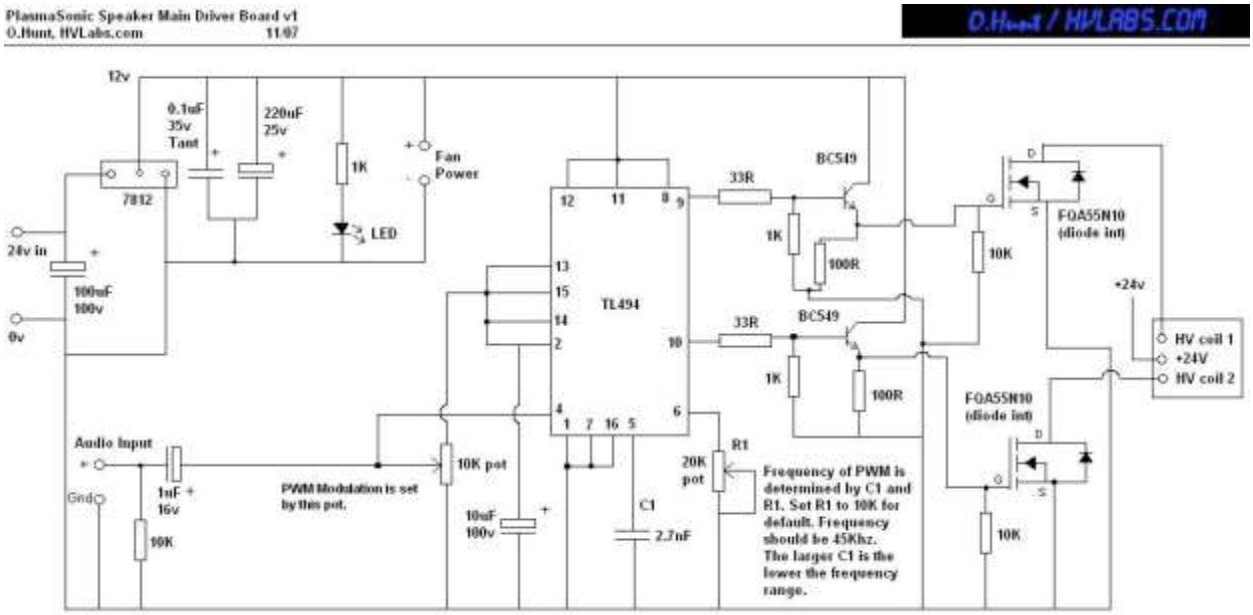

Figure 71: Base Schematic for the Solid State Driver from HV Labs (Hunt, Plasma Sonic Speaker Schematic)

Figure 71 shows the circuit that was chosen for its driver simplicity. This circuit employs the TL494, which is specifically a PWM chip. The 10 kΩ potentiometer sets the reference level for the pulse width modulation. During PWM, a saw tooth (triangle) wave is generated and the output is compared between the reference level and the saw tooth. By placing the reference in the middle, this will usually generate a 50% duty cycle. Duty cycle is how long a pulse is on versus how long it is off for the cycle.

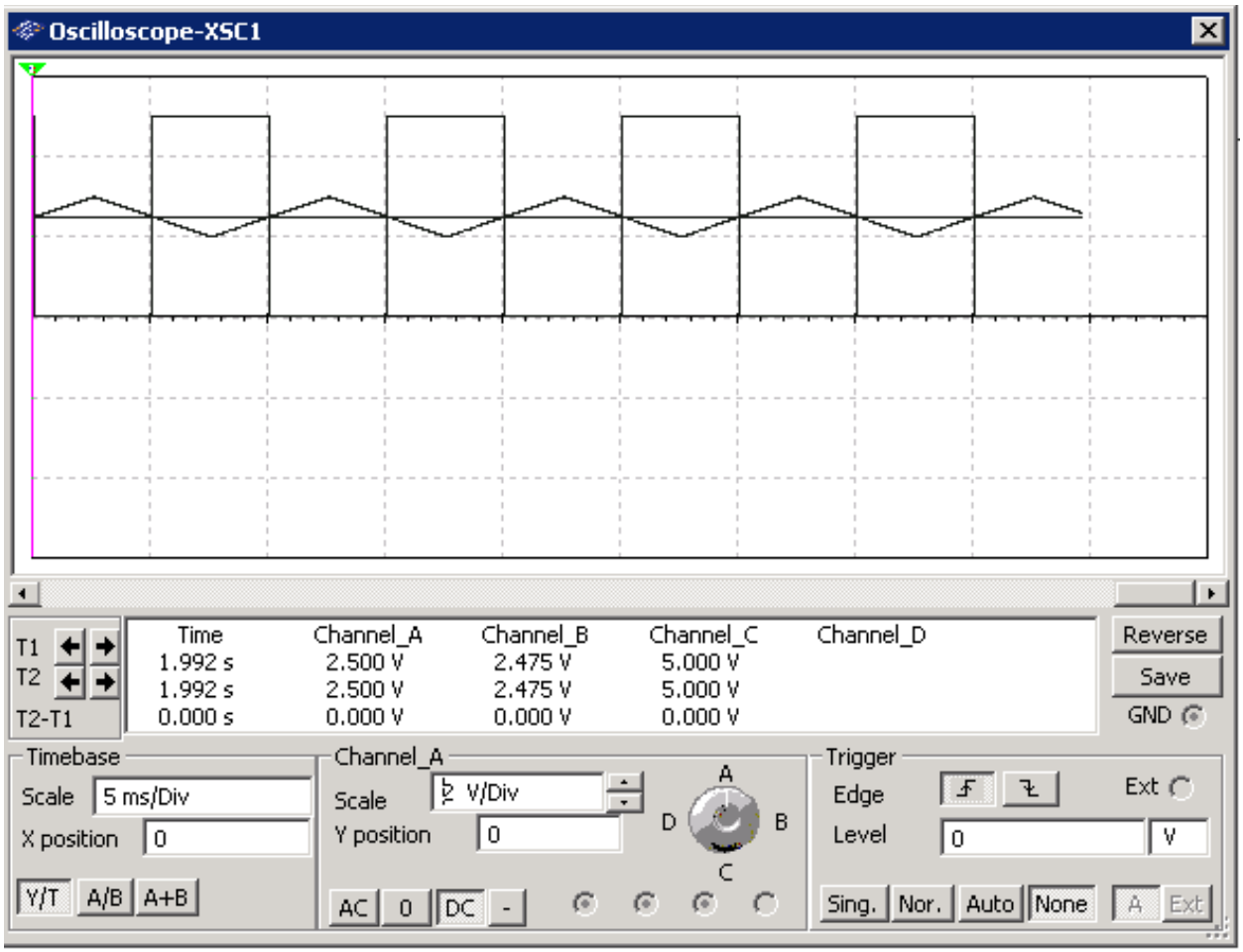

Figure 72: Multisim Simulation for Pulse Width Modulation

Figure 72 shows the resulting figure of pulse width modulation with the reference level properly set. This is just a visualization to help understand what happens with the Tesla coil driver by showing how an operational amplifier in a comparator configuration can create a PWM waveform.

Construction

The Secondary Coil and Primary

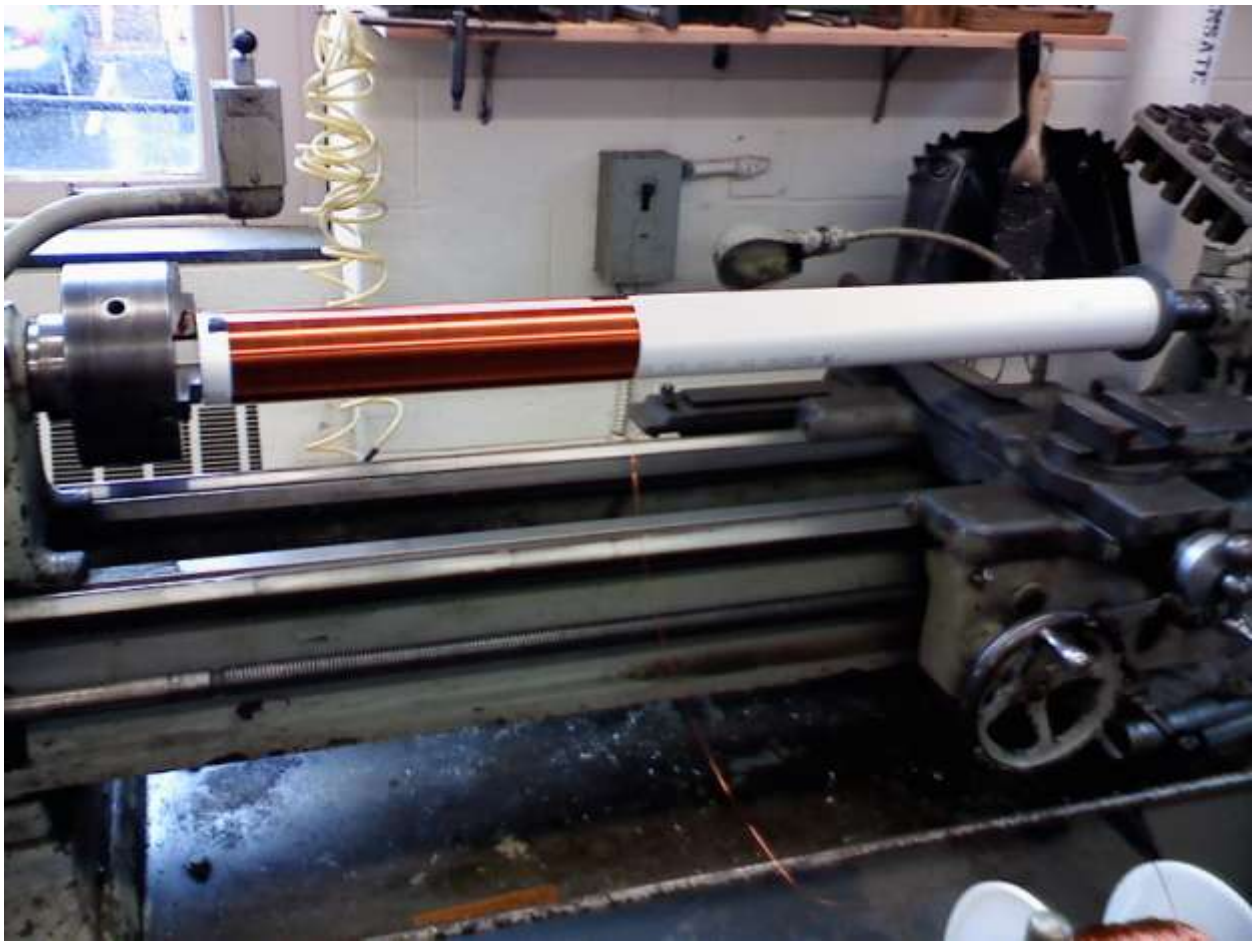

Figure 73: Coiling Apparatus

To wind the coil, a special piece was created to hold the PVC tube in place on a lathe. The first coil was wound using only a hand as a guide to help the wire along. The second coil found much success by using a ruler to feed the wire into the tight spiral. Tension has to be applied to the wire in order to get a tight fit on the PVC tube. As shown in the previous section, this was 22 AWG wire being wound.

The primary should be separated from the secondary by very little space as a high coupling coefficient. In this project, a Kapton film is used to isolate the primary from the secondary in addition to electrical tape. For future developments, it is important to note that

electric tape is rated for 600v. Thus if a higher voltage primary is used like in a standard Tesla coil, additional precautions will have to be taken.

The base for the Tesla coil is a 12 inch by 12 inch piece of wood. It is designed specifically to work with a 3.5 inch outer diameter PVC tube to be mounted inside. An important note is that when using screws on PVC, the screws should be hand tightened as PVC is prone to cracking when power tools are used if caution is not taken. For the top, elbow brackets are perfect to get the job done, however, the screws inside should be made of nylon instead of metal. This is to prevent another parasitic capacitance from forming. If another material can be used instead of metal for the elbow brackets, that would be ideal.

Instead of a spherical load, this project used a toroidal load that was made from dryer hose. However, alternative attempts to create toroids spawned from using straw wreaths and regular plastic tubing. The straw wreaths were created with a combination of aluminum strips and electrical tape. The electrical tape is put on the inside with the sticky side facing out. The aluminum strips are then placed on top of the electrical tape to make a nice aluminum wrap. For the plastic tubing, aluminum tape works very well to create a nice smooth shape and is very easy to work with.

Figure 74: Coil 2 (Left) and Coil 1 (Right)

As shown in Figure 73, the finished product of coil 1 and coil 2 without the base are sporting their toroidal loads. Coil 1 was originally wound using one source of wire until there was no more. At that point, Kapton film was applied behind the wire to isolate the end. At that point, a piece of plastic tubing was slid on and another wire was soldered onto the end of the other wire. Then the tubing was positioned to protect the wire from arcing.

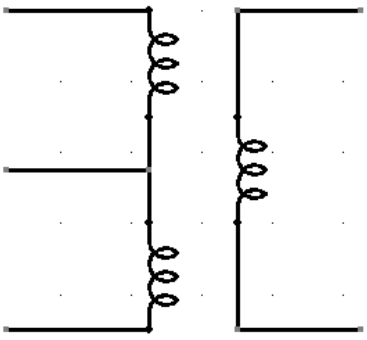

Figure 75: Center Tapped Primary (Left) with a Secondary (Right)

Figure 75 shows the premise for the primary of this Tesla coil design. The primary used in the project was wrapped around three times using 16 AWG wire clockwise then connected to a similar wire wrapped around counter clockwise. An important note is that there is a layer of electrical tape to provide added insulation to prevent arc over. This was in preparation for higher voltages than the original 25 volts used in the project. Note, that the center tap of this primary is given 25 volts DC, while the other ends are connected to the power MOSFETs.

Solid State Driver Construction

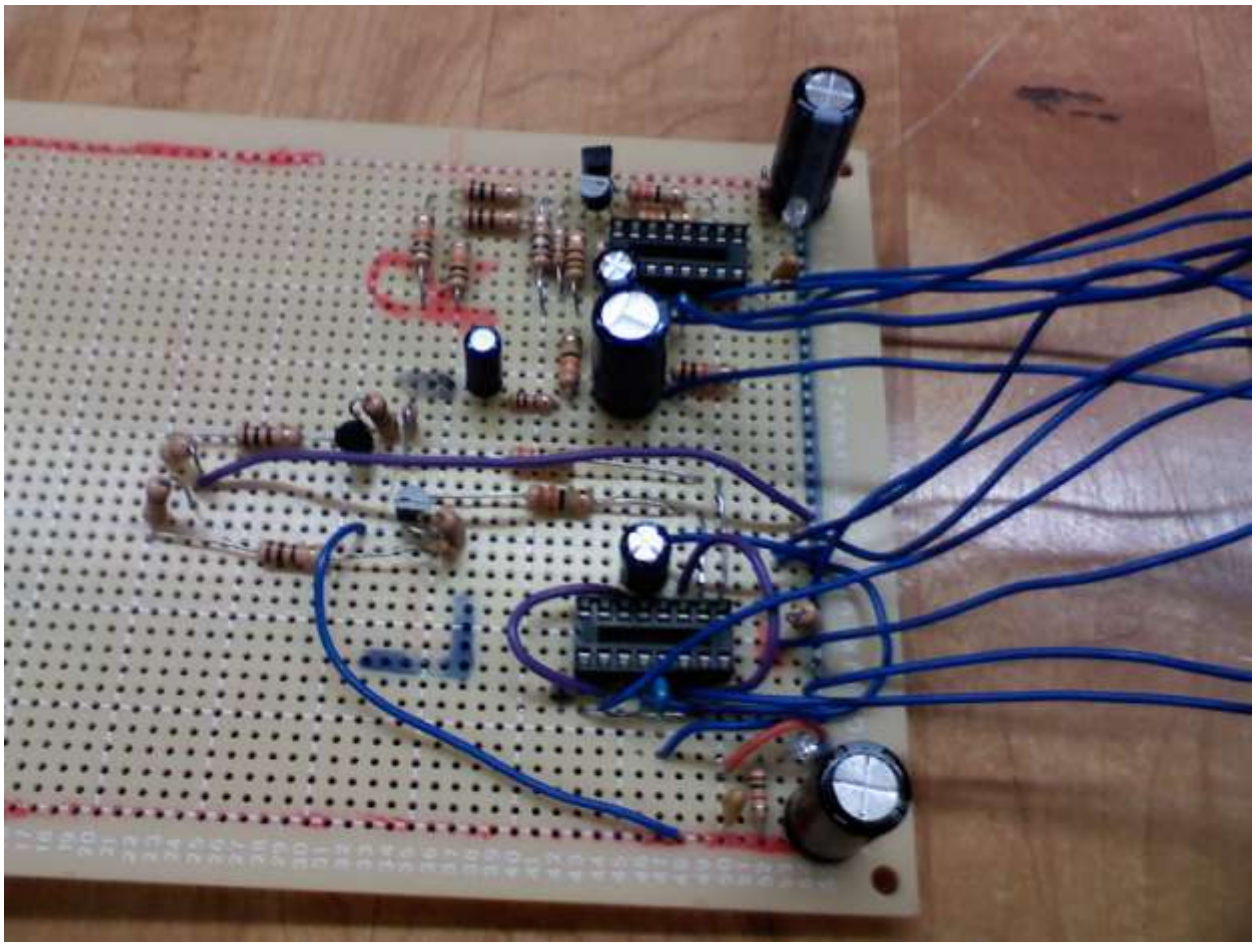

Figure 76: PWM Circuit Soldered onto a Perfboard

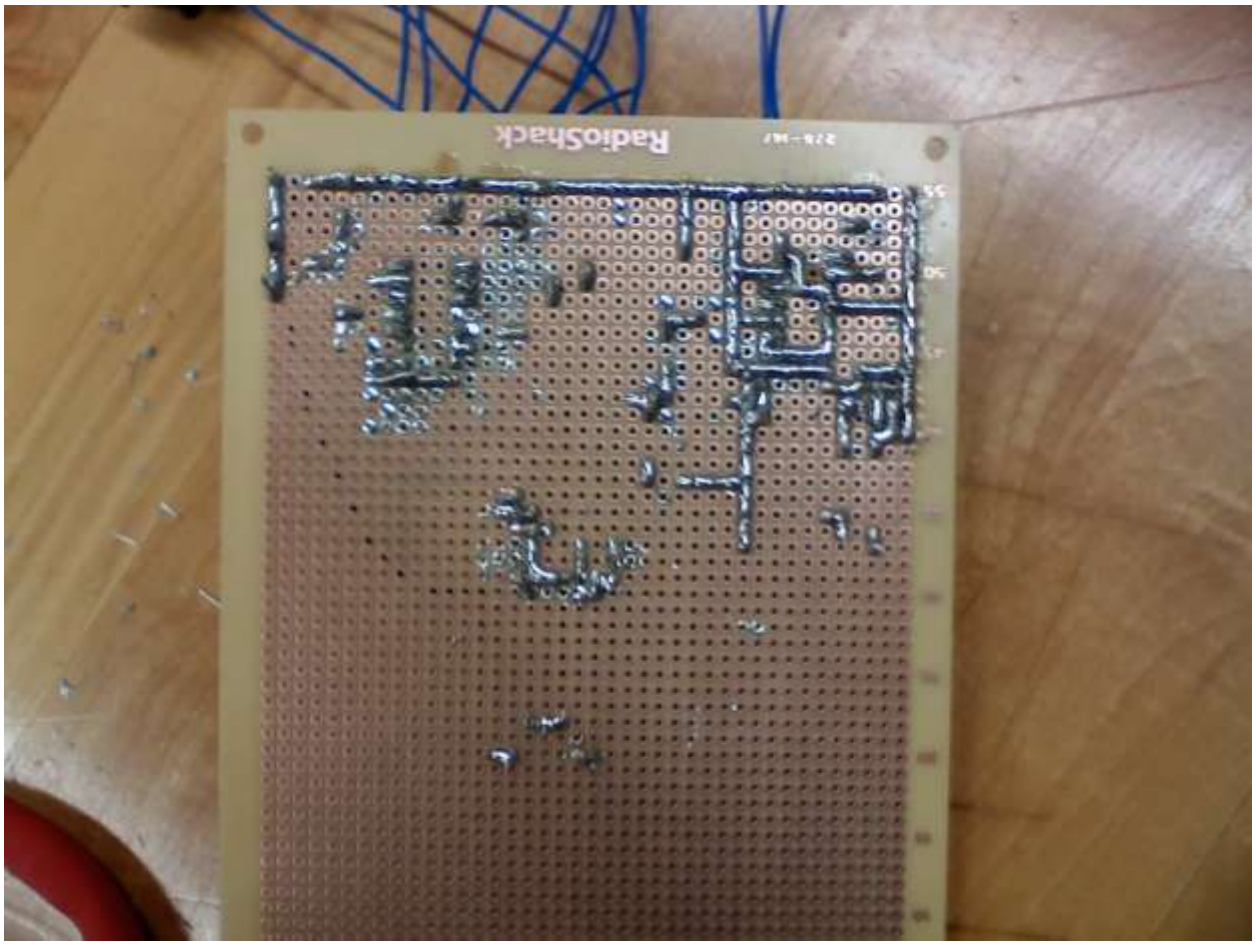

Figure 77: Bottom of the Soldered Circuit

Figure 76 and Figure 77 show the finished circuit. The bottom half of Figure 76 shows the left channel processing circuit while the top half is the right channel processing circuit. For all experiments, only the right side was used as the original intention was to have two Tesla coils running simultaneously. This requires two coils that are made out of resonance with one another to prevent any sort of interference. Figure 77 demonstrates the two tactics used for soldering. While the left side uses wires above to carry electricity, the right side relies heavily on solder traces to make the connections instead of wires. The result of this is seen clearly in Figure 76 as the top half is clearly missing any visible jumpers on top. The solder traces technique is much harder as it requires more planning.

Shown in the center of the board in Figure 76 are two dual-inline package sockets. This allows for a quick replacement of the TL494 chip if one is damaged during the testing. The power MOSFETS are connected the BJT driver portion of the circuit by wires that are not shown in the figure.

Item	Description	Quantity (One Coil)
TL494	PWM Controller	1
16 Pin	DIP Socket	1
2.7 nF @ 50V	Capacitor	1
0.33 µF @ 100V	Capacitor	1
1.0 µF @ 16V	Capacitor	1
10 µF @ 100V	Capacitor	1
100 µF @ 100V	Capacitor	1
330 µF @ 100V	Capacitor	1
2200 µF @ 10V	Capacitor	1
0.1 µF @ 35V	Capacitor / Tantalum	1
BC549	BJT Transistor	2
511-STP60NF10	Power MOSFET	2
CSD06060A-ND	Power Diodes	4
1.5T Red LED	Indicator	1
33 Ω	Resistor	2
100 Ω	Resistor	2
1 kΩ	Resistor	3
10 kΩ	Resistor	3
10 kΩ	Potentiometer	1
20 kΩ	Potentiometer	1
Heat sink	Heat Dissipation	2
Thermal Compound	Heat Transfer	1 Tube
12V Fan	Fan	2

Table 15: List of Materials

Table 15 gives the list of materials used in my rendition of the solid state Tesla coil. There are very few changes from the original parts list presented by Hunt's work. The differences that do exist were made for cost benefits and some of the parts being much harder to find than others. Such is the case as with the power MOSFET. The 511-STP60NF10 was used

because of its price point being $2.80 per FET instead of the $3.50 at the time. However, the FQA555N10 can now be bought for $0.99 through Newark.

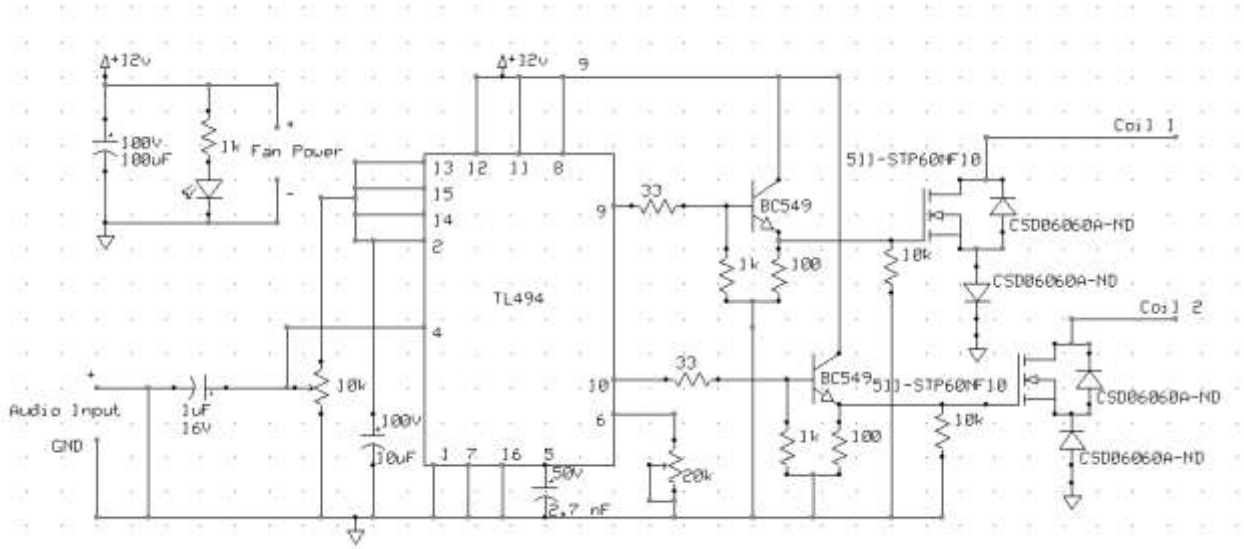

Figure 78: Modified Circuit (Hunt, Plasma Sonic Speaker Schematic) (Hunt, Solid State Tesla Coil Schematic)

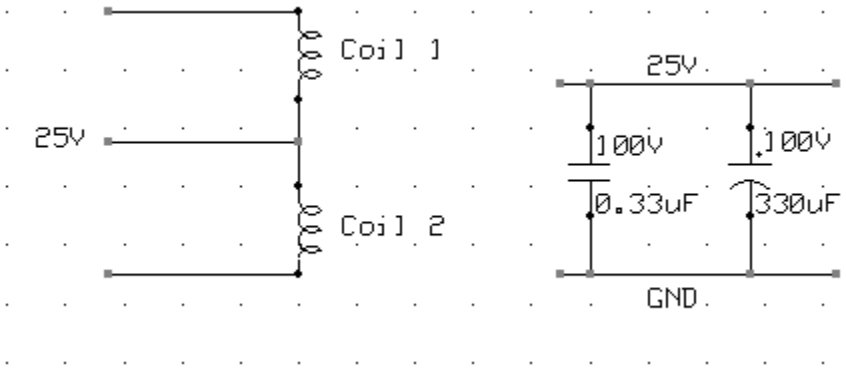

Figure 79: Tesla Primary Power Set Up and Filter

Figure 78 and Figure 79 document the modified circuit that is based off Hunt's schematics. The changes are minor for cost effectiveness and some parts have been switched. The Tesla coil driver in this case operates on a 12 volt source that is separated from the Tesla coil's power supply. This offers a superior design aspect as the voltage can be varied on the Tesla coil over a wide spectrum while the 12 volt supply keeps the TL494 at a constant level.

Analysis – Tesla Coil

Figure 80: Test Set Up

Shown in Figure 80 is the main test set up for the Tesla coil. Since this Tesla coil has a controlled discharge that can be focused between an electrode and the breakout point of the coil, this proved to be a robust testing environment with consistent results. After ten different trials, each placed the resonant frequency of the Tesla coil at 125 kHz.

To find the resonant frequency, the solid state driver was swept from 0 Hz to approximately 200 kHz reliably. The frequency range extended to approximately 500 kHz but

beyond 200 kHz the output signal was unstable. A separate power supply was devoted to supplying the primary with the current needed. This power supply was set to 25.0 ± 0.1 volts while the pulse duration for each MOSFET was set to a 50% duty cycle. At this setting, the Tesla coil would consistently draw 2.1 ± 0.1 amps. In order to aid in the search for resonance, the elements to look for are an arcing spark gap or a lit fluorescent bulb.

Figure 81: Spark Gap Active

Figure 81 demonstrates the constant arcing effect when the system is at its experimentally determined resonant frequency. Another tool used is the fluorescent bulb, which is often used by high voltage enthusiasts to detect large electromagnetic fields being created by their test set ups. In this exercise, the bulb lit up at multiple frequencies. However, there was only one frequency

that consistently lit the light bulb at full brightness and this was 125 kHz. This frequency was also when the spark gap would become active. The spark gap was set to 1 centimeter as it was very consistent in arcing. The multiple frequencies that were detected to light the fluorescent bulb wirelessly lend to the construction of a square wave.

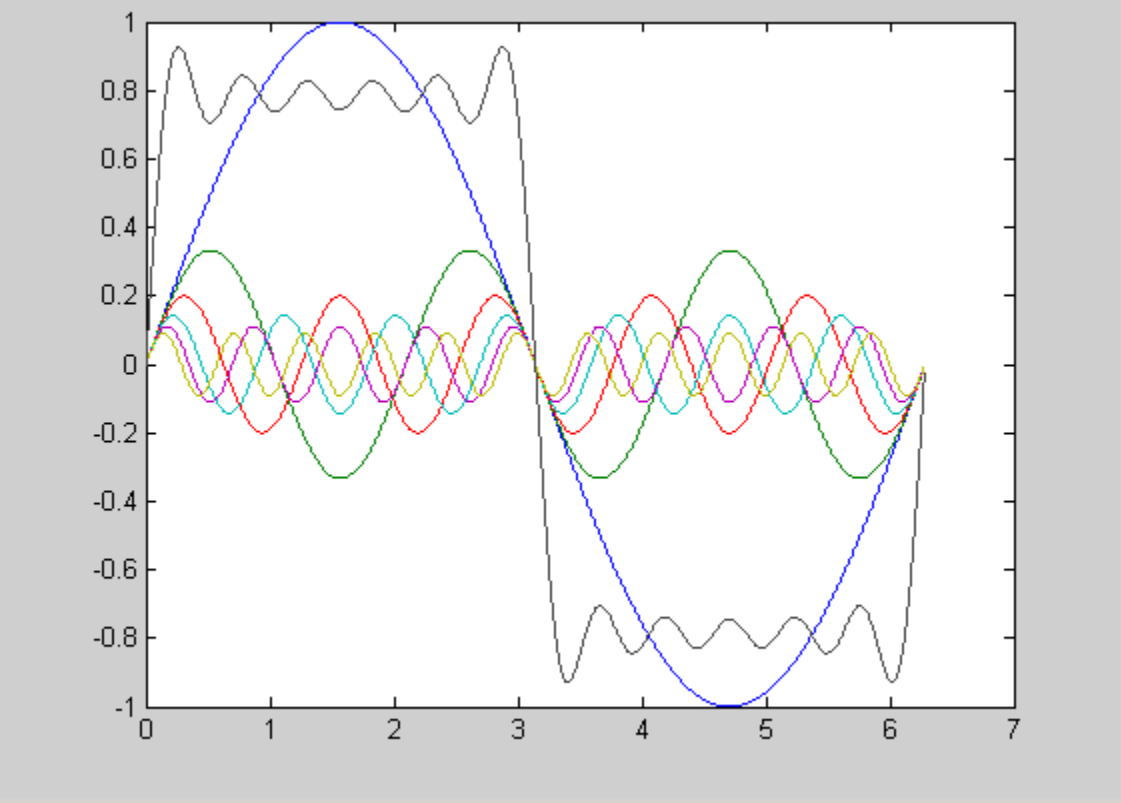

Figure 82: Square Wave Construction with Sine Waves

```
>> x = 0:0.001:6.28;
>> y = sin(x);
>> z = 1/3*sin(x*3);
>> u = 1/5*sin(x*5);
>> v = 1/7*sin(x*7);
>> t = 1/9*sin(x*9);
>> s = 1/11*sin(x*11);
>> plot(x,y,x,z,x,u,x,v,x,t,x,s,x,z+y+u+v+t+s);
```

Equation 30: Matlab Code for Basic Square Wave Construction

$$f(x) = \sum_{n=1,3,5\ldots}^{\infty} \frac{1}{n} \sin\left(\frac{n\pi x}{L}\right)$$

Equation 31: Fourier Series of a Square Wave

Figure 82 and its accompanying code displayed in Equation 30 shows the construction of a square wave using only sine waves. Equation 31 is the explicit equation for the Fourier series of a square wave. This shows that the 125 kHz could actually not be the resonant frequency as found through experimentation. The resonant frequency could be 375 kHz harmonic from the initial 125 kHz square wave. That harmonic differs from the calculated 345 kHz by 40 kHz, a ratio of 1.09. The 125 kHz differs by 220 kHz and yields a ratio of 0.36.

The second test set up used LabView 8.5 combined with an oscilloscope and signal generator instead of using the solid state driver. Before connecting the primary to a signal generator, the secondary was directly connected to the oscilloscope to set up a control for the experiment.

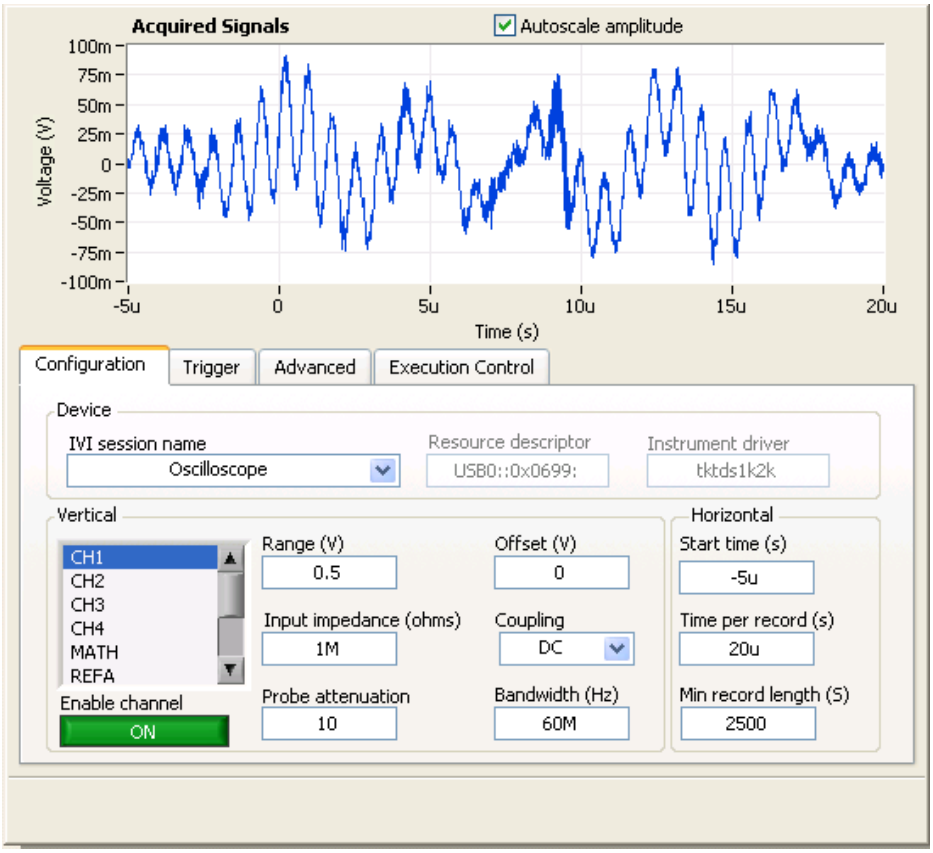

Figure 83: Initial Oscilloscope Reading from the Secondary / Primary Not Stimulated

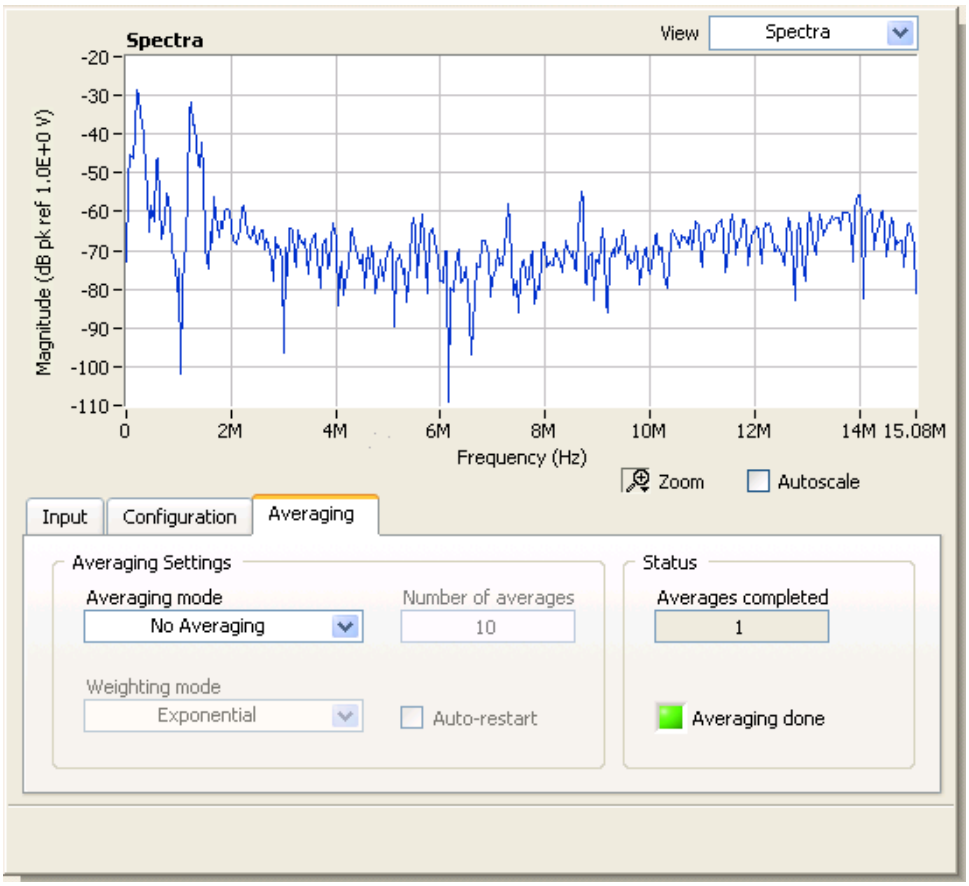

Figure 84: Power Spectrum of the Secondary / Primary Not Driven

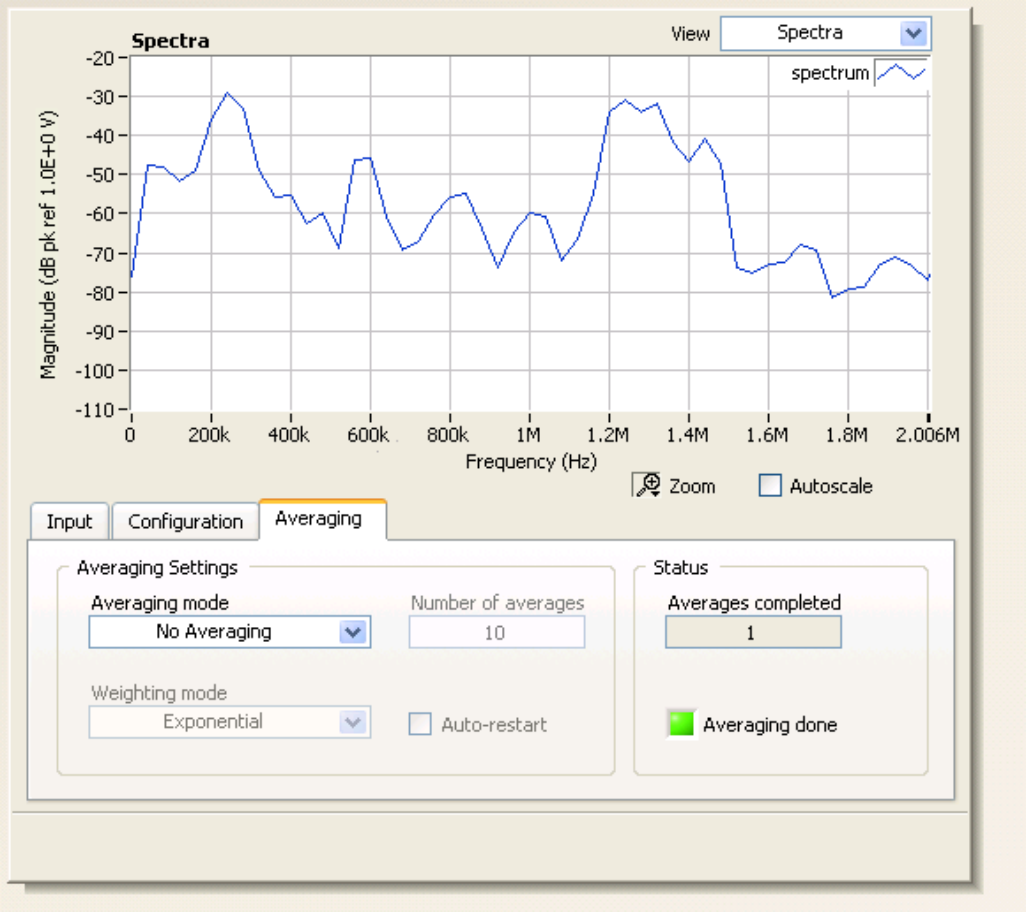

Figure 85: Close Up of the Highest Peaks of the Power Spectrum

Shown in Figure 83 is the waveform coming from the secondary. Figure 84 is the initial power spectrum taken from the secondary. Two peaks can be easily seen at approximately 220 kHz and 1.2 MHz. The rest of the spectrum is far lower than the two peaks of interest. This gave the starting point for the signal generator.

Using the signal generator, a 20mV peak to peak signal is fed into the primary using the center tap and then clockwise wound coil's connection. The frequency sweep starts at 1 Hz and went through to 1.4 MHz. The sweeping at 1.2 MHz to 1.4 MHz revealed that this was not a resonant frequency and was instead being stimulated by radio frequency waves in that region. The amount of wire used in the coil is approximately 418 meters, which is slightly less than half the 1 kilometer wavelength of a 1 MHz wave. However, this could lend to the power spectrum

peak since the medium wave band is 520 kHz to 1,610 kHz and is the AM radio band that most people are accustomed to.

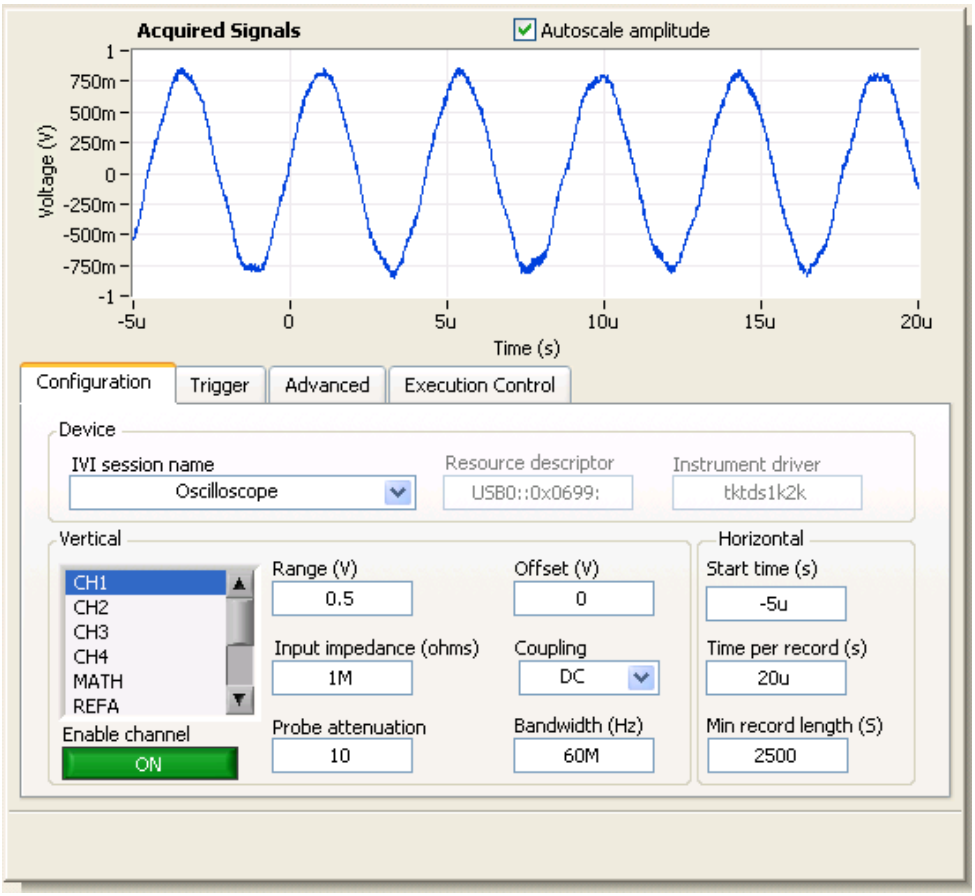

Figure 86: Secondary Waveform While Being Stimulated

Exploration of the 200-250 kHz band yielded one frequency that stood out among the rest and that is 226 kHz . Shown in Figure 86 is the output waveform that yielded the maximum output of 1.5 V peak to peak. That equates to a gain of 75 when it's being driven by a 20 mV peak to peak. The resonant frequency differs from the calculated resonant frequency by 119 kHz yielding a ratio of 0.655. However, assuming that the oscilloscope probe has 10 pF of capacitance, this yields a new resonant frequency of 258,857.3 Hz, which is 1.142 kHz different from the new expected value resulting in a ratio of 1.004.

Recommendations for the Future – Tesla Coil

Due to the nature of this project, it would be best to have at least two students working on something similar to this. An area that could be greatly improved is the power supply. The research presented in this report was limited by a 25 volt, 8 amp power supply. When running properly, the system operated at 25 volts with 2.12 amps being drawn. One solution for this power supply could take the 120 volts from the wall outlet and run it through the variable step down transformers that are owned by the Physics department. This can then go into a full bridge rectifier that has a large capacitance on the output. This will allow for approximately 170 volts if designed properly, which will allow for larger sparks. The variable transformer can limit the output voltage to make the overall product safer.

Using thinner wire, approximately 30 AWG, will also allow for more turns over the entirety of the area. This will allow for a larger secondary to primary ratio and allow for larger voltages on the secondary. The primary can be changed into any of the other Tesla coil shapes. These include the flat coil and the cone shape coil. These primaries are usually kept away from the base and make arcing to them incredibly difficult. They can also be made by taking copper tubing and bending them into the proper shape.

The solid state driver should include MOSFET drivers instead of the BJTs. During the course of testing, it was seen that the gates on the MOSFETs see a capacitive charging cycle. By using a MOSFET driver and a small input resistance to the gate, this will dramatically lower the RC time constant and allow for the gate's voltage to change faster. Another aspect of the MOSFETs that should be looked into is allowing for higher voltages across the drain and source. The current does not seem to be a huge issue with the MOSFETs when the pulse width modulation is set to approximately a 50% duty cycle.

The areas that need the most attention to further drive the research into solid state Tesla coils are the MOSFETs, overall construction, and the power supply feeding the Tesla coil. If each of these is addressed, then the limitations experienced in this project will be dealt with and allow for more dramatic results such as longer sparks.

Conclusion – Tesla Coil

Overall, this portion of the project continues the search for expanding knowledge based on physical phenomena that have been observed. While the visible results were not as spectacular as Tesla coils usually are; the valuable look into resonance and understanding how something that should be well defined is lacking. As shown in the analysis, the resonant frequency is not in line with what was predicted by the model when dealing directly with the solid state driver. When stimulating the input with a sine wave at the resonant frequency instead, does in fact line up very well with the simple series RLC model.

Overall Conclusion

We began this project wanting to answer our questions about catapults, corked bats, and tesla coils. We started with this initial idea, theorized an experimentation process, perfected that process, and finally came to conclusions about our initial question. In the end, we have satisfied our curiosity and more. For the future, we hope this MQP has stimulated further interest in not only these areas, but that it has inspired others to question and test even the simple concepts in life.

Works Cited

Adair, Robert K. The Physics of Baseball. New York: HarperCollins, 2002.

Associated Press. Sports Illustrate - Unsplendid Splinter. 03 June 2003. March 2009 <http://sportsillustrated.cnn.com/baseball/news/2003/06/03/sosa_ejected_ap>.

Blinder, S. Series RLC Circuits. 16 March 2009 <http://demonstrations.wolfram.com/SeriesRLCCircuits/>.

Bressoud, Thomas C. How Sound Works: The Physics of Sound. 1 April 2009 <http://personal.denison.edu/~bressoud/cs171-f05/lectures/18_Sounds1.pdf>.

Catapult Definition. <http://dictionary.reference.com/browse/catapult>.

Catapult Picture. <http://www.ghsteched.com/catapult2.jpg>.

Choudhary, Rizwan. Frequency Range of Human Hearing. 2004. 1 April 2009 <http://hypertextbook.com/facts/2003/ChrisDAmbrose.shtml>.

Cotterel, Brian and Johan Kamminga. Mechanics of Pre-Inductrial Technology. Cambridge: Cambridge University Press, 1990. 191.

Cox, Amanda, Samantha McGill and Michael Spremulli. South High Science and Engineering Club 2007-08. IQP. Worcester: Worcester Polytechnic Institute, 2008.

Falstad, Paul. Circuit Simulator Applet. 23 March 2009 <http://www.falstad.com/circuit/>.

Hunt, Oliver. HV Labs. 24 March 2009 <http://www.hvlabs.com/sstc.html>.

—. Plasma Sonic Speaker Schematic. 10 April 2009 <http://www.hvlabs.com/Images/plasmasonic.JPG>.

—. Solid State Tesla Coil Schematic. 16 April 2009 <http://www.hvlabs.com/Images/sstcv1.JPG>.

Information Unlimited. Neon Transformers, Neon Power Supplies. 17 March 2009 <http://www.amazing1.com/profneon.htm>.

Jermanis, Branko. Nikola Tesla and My Thoughts. 12 March 2009 <http://free-ri.htnet.hr/Branko/07d2.html>.

Johnson, Garry. Dr. Garry Johnson's Renewable Energy and Tesla Coils. 11 March 2009 <http://www.eece.ksu.edu/~gjohnson/TeslaCoilImpedance.pdf>.

Jones, Keith. AC Resistance of a Conducting Wire. 11 October 1999. 6 April 2009 <http://www.physics.uq.edu.au/people/jones/ph348/sols/sol12/node1.html>.

Ludwig, Reinhold and Gene Bogdanov. RF Circuit Design. Upper Saddle River: Pearson Prentice Hall, 2008.

Lux, Jim. Medhurst Formulas for self capacitance of air-core coil. 24 January 1998. 12 March 2009 <http://home.earthlink.net/~jimlux/hv/medhurst.htm>.

Nave, R. Increasing Current in a Coil. 11 March 2009 <http://hyperphysics.phy-astr.gsu.edu/hbase/magnetic/indcur.html>.

—. Spherical Capacitor. 16 March 2009 <http://hyperphysics.phy-astr.gsu.edu/Hbase/electric/capsph.html>.

Nicholson, Paul. Secondary Miscellanae. 18 July 2008. 12 March 2009 <http://abelian.org/tssp/misc.html>.

Nyack, Cuthbert. RLC Differential Equation. 1996. 16 March 2009 <http://circuitscan.homestead.com/files/ancircp/rlcdiff1.htm>.

P. Gamache, A. Galante, G. Seben, A.J. Elbirt. "Validating Baseball Bat Compliance." Sports Engineering (2007): 157 - 164.

PowerStream Technology. American Wire Gauge Table and AWG Electrical Current Load Limits. 1 April 2009 <http://www.powerstream.com/Wire_Size.htm>.

Resnick, Halliday and Krane. Physics. New York: John Wiley and Sons Inc, 2002. 23.

Results Definition. <http://dictionary.reference.com/browse/results>.

Russel, Daniel A. Physics and Acoustics of Baseball and Softball Bats. web page. Kettering University. Flint, MI, 2008.

Sears, Francis Weston. Mechanics, Wave Motion, Heat. Massachusetts: Addison-Weasley Publishing Company Inc, 1958. 36.

Shaw, Rebecca H. Laboratory and Field Experimental Investigation of The Relationship of Baseball Bat Properties on Batted-Ball Speed. Thesis. University of Massachusetts Lowell. Lowell, 2006.

Sweet Spot. 2007. March 2009 <http://en.wikipedia.org/wiki/Sweet_spot>.

Taylor, John. Classical Mechanics. California: University Science Books, 2005. 43.

Taylor, John. An Introduction to Error Analysis: The study of uncertainties in physical measurements. California: University Science Books, 1997. 72.

Torsion Spring. <http://en.wikipedia.org/wiki/Torsion_spring>.

Trebuchet Picture. <http://gottatopic.com/wp-content/uploads/2008/03/trebuchet_copy.jpg>.

Young and Freeman. University Physics. San Francisco: Pearson, 2004. 107.

Appendix – Constants and List of Variables for Tesla Coils

Constants

$$\mu_0 = 4\pi * 10^{-7} \left[\frac{H}{m}\right]$$

$$\varepsilon_0 = 8.854 * 10^{-12} \left[\frac{F}{m}\right]$$

$$\sigma_{Copper} \approx 58 * 10^{6} \left[\frac{S}{m}\right]$$

$$i = j = \sqrt{-1}$$

Variables

Symbol	Description	Unit Symbol	Unit Explicitly
F	Capacitance	[F]	Farads
Hz	Frequency	$\left[\frac{1}{s}\right]$ or s^{-1}	Inverse Seconds
I	Current	[A]	Amps
ℓ	Length	[m]	Meters
L	Inductance	[H]	Henries
N	Number of Turns	-	-
q	Charge	[C]	Coulombs
r	Radius	[m]	Meters
R	Resistance	[Ω]	Ohms
V	Voltage	[V]	Volts
X_L	Inductive Reactance	[Ω]	Ohms
δ	Skin Depth	[m]	Meters
σ	Conductance	$\left[\frac{1}{\Omega}\right]$	Mhos or Siemens
ω	Angular Frequency	$\left[\frac{rad}{s}\right]$	Radians per second